Towards Sustainable Landscape Development
Case Study of Using Remote Sensing as an Unconventional Tool for Environmental Observation

Der Fakultät Nachhaltigkeit
der Leuphana Universität Lüneburg
zur Erlangung des Grades Doktorin der Naturwissenschaften
-Dr. rer. nat.-
-

Vorgelegte Dissertation

von

Dalia Mostafa Amer Farghaly

geboren am 06. Mai 1972

in: Giza, Ägypten

Eingereicht am: 04.06.2019

Erstbetreuerin und -gutachterin: Prof. Dr. Brigitte Urban
Zweitgutachter: Prof. Dr. Uwe Sörgel
Drittgutachter: Prof. Dr. Henrik von Wehrden

Tag der Disputation: 20.07.2020

„The sustainable development is the key to our future"

-UN Agenda 21-

Dedicated to my great country, Egypt

the memory of my beloved father

my kind mother

my kind uncle

my kind husband Emad

my lovely children

Mona and Abdelrahman

PREFACE

This dissertation is based on the results and conclusions of the papers listed below. These papers are described and cited in the framework paper as follows:

Paper I

Farghaly, D., Elba, E., Urban, B. (2014): Observing the Middle Elbe Biosphere in Germany by Means of TerraSAR-X Images. International Journal of Geosciences, 5, 196-205.
DOI:10.4236/ijg.2014.52021.

Paper II

Farghaly, D., Elba, E. Urban, B. (2016): Towards Sustainable Land Uses within the Elbe River Biosphere Reserve in Lower Saxony, Germany by Means of TerraSAR-X Images. Journal of Geoscience and Environment Protection, 04, 97-121.
DOI: 10.4236/gep.2016.43009.

Paper III

Farghaly, D., Urban, B., Sörgel, U., Elba, E. (2019): Differentiating forest types using TerraSAR–X spotlight images based on inferential statistics and multivariate analysis.
In Remote Sensing Applications: Society and Environment 15, p. 100238.
DOI: 10.1016/j.rsase.2019.100238.

COPYRIGHT NOTICE

DECLARATION OF ORIGINALITY

I hereby certify that this dissertation entitled:" **Towards Sustainable Landscape Development - Case Study of Using Remote Sensing as an Unconventional Tool for Environmental Observation**'' is:

- written by me without using unauthorised aids,
- the result of my own work and includes nothing which is the outcome of work done in collaboration except as declared in Appendix A, specified in the text and acknowledged in citations,
- neither as a whole nor in parts been submitted to any other degree assessments and purposes at Leuphana University of Lüneburg or at other universities and institutions.

Lüneburg,
04.06.2019

Dalia Farghaly

ACKNOWLEDGEMENTS

*All praise is due to **Allah**, the lord of all creatures. It is HE who provided me with the resources and the ability that made this research possible.*

*I would like to express my deepest gratitude and appreciation to my supervisor, **Prof. Dr. Brigitte Urban**, for her excellent scientific advice and guidance, constructive suggestions, endless caring, extraordinary patience, and providing me with an excellent atmosphere for performing this research. During the work period, I found her a true academician. So, many thanks to her for everything she did to bring me to this level, and I will always remember her with respect.*

*I am deeply grateful to **Prof. Dr Uwe Sörgel** from Institute for Photogrammetry at Stuttgart University for his precious time reading my thesis and for his constructive comments, technical guidance, and providing me with new ideas.*

*I also want to express my sincere thanks to **Prof. Dr. Henrik von Wehrden** for his precious time reading my thesis and accepting to be an advisor of the examination board.*

*Special thanks for **Dr. Peter Lohmann** from Institute for Photogrammetry and Geoinformation (IPI) at Leibniz University in Hanover for his guidance and sharing his valuable recommendations and suggestions to me.*

*I am deeply thankful to **Prof. Dr. Peter Kershaw** from the school of earth, atmosphere and environment in faculty of Science at Monash University in Australia for his support and English revision.*

*I am greatly thankful for the staff of the Leuphana Graduate school in particular **Mrs. Susanne Wenzel**. The Graduate school granted me a scoloarship for four years in addition to finacial support to share my research in several internationl conferences and exchange experiences and konlowdeges.*

*I am greatly indebted to the administration of the Biosphere Reserve "Niedersächsische Elbtalaue" (Lower Saxonian Elbe Valley Biosphere Reserve) particularly to **Tobias Keienburg** and **Dr. Johannes Prüter**, the Institute of Photogrammetry and Geoinformation (IPI) at Leibniz University in Hanover and to the German Aerospace Centre (Deutsches Zentrum für Luft-und Raumfahrt, DLR) for providing the satellite images used in this study.*

ACKNOWLEDGEMENTS

Special thanks goes to my German, Egyptian and Arabic friends in Germany for their kind inspiration supports and most important their friendship.

Finally, I would like to thank my ***mother****, for bringing me up to value science and for coping with my long absence away from her. Special thanks go to my uncle* ***Dr. Eng. Salah Salam****,* ***Elba family, Farghaly family and Salam Family****. My deep gratitude is due to my dear husband* ***Dr.rer. nat. Eng. Emad Elba*** *for his continuous support and perseverance during these years. I would like also to express my thanks to my children,* ***Mona and Abd Elrahman*** *who, despite their young ages, understood that I needed to be the absent present mother while working on this research.*

I send it with love and gratitude.

Bad Bevensen, Germany,

Dalia Farghaly

06 May 2019

TABLE OF CONTENTS

LIST OF FIGURES

LIST OF TABLES

LIST OF ABBREVIATIONS

AMSL	Above Mean Sea Level
ATKIS	Amtliches Topographisch-Kartographisches Informationssystem
BfG	Bundesanstalt für Gewässerkunde
BKG	The Federal Agency for Cartography and Geodesy - Das Bundesamt für Kartographie und Geodäsie
dB	decibels
DGM5	Digitales Geländemodell Gitterweite 5 m
DLR	German Aerospace Centre - Deutsches Zentrum für Luft- und Raumfahrt
DTC	Decision Tree Classifier
FA	Factor Analysis
GIS	Geographical InformationSsystems
HH	Horizontal transmit and Horizontal receive
HS	High resolution Spotlight
LULC	Land Use / Land Cover
MGD	Multi-look Ground-range Detected
MLC	Supervised Maximum Likelihood Classifier
P-Value	Probability Value
RS	Remote Sensing
σ_0	Backscatter coefficient
SAR	Synthetic Aperture Radar
SE	Spatially Enhanced
TSX	TerraSAR-X imagery
TZT	Two sample Z-Test
UN	United Nations
UNCED	United Nations Conference on Environment and Development
VV	Vertical transmit and Vertical receive
Werder	Oxbow
WSV	Wasser - und Schifffahrtsverwaltung des Bundes

SUMMARY

"Sustainable development: enough for everyone, forever" is the definition of sustainability. Sustainable landscape development is the main goal of decision makers worldwide. Achieving this goal in the long term leads to achieving social, economic and environmental sustainability. Remote sensing has been playing an essential role in monitoring remote areas. This study has employed part of the role of remote sensing in supporting the direction of decision makers towards sustainable landscape development. The study has focused on some of the main elements affecting sustainable environment as stated in Agenda 21. These elements are land uses, specifically agricultural land uses, water quality, forests, and water hazards such as floods.

Three research programs were undertaken to investigate the role of Terrasar-x imagery, as a source of remote sensing data, in monitoring the environment and achieving the previous stated elements. The investigation was intended to investigate the effectiveness of TSX imagery in identifying the cropping pattern of selected study areas by employing a pixel-based supervised maximum likelihood classifier, as published in Paper I, assessment of the efficiency of using TSX imagery in determining land use and the flood risk maps by applying an object-based decision tree classifier as published in Paper II, and determination of the potential of inferential statistics tests such as the two samples Z-test and multivariate analysis, for example Factor Analysis, for identifying the kind of forest canopy, based on the backscattering coefficient of TSX imagery of forest plots, as presented in Paper III. Papers I and II covered two pilot areas in the Lower Saxonian Elbe Valley Biosphere Reserve “das Biosphärenreservat „Niedersächsische Elbtalaue„ around Walmsburger Werder between Elbe-Kilometer 533 - 543 and Wehninger Werder between Elbe-Kilometer 505 - 520. Paper III focused on the Fuhrberger Feld water protection area near Hanover in Germany. The inputs for this research were mainly SAR Imagery and the ground truth data collected from field surveys, in addition to databases, geo-databases and maps.

The study presented in Paper I used two filters to decrease speckle noise namely De-Grandi as multi-temporal speckle filter, and Lee as an adaptive filter. A multi-temporal classification method was used to identify the different crops using a pixel-based maximum likelihood classifier. The classification accuracy was assessed based on the external user accuracy for each crop, the external producer accuracy for each crop, the Kappa index and the external total accuracy for the entire classification. Three cropping pattern maps were produced namely the cropping pattern map of

Wehninger Werder in 2011 and the cropping pattern maps of Walmsburger Werder in 2010 and in 2011. The study showed that image filtering was essential for enhancing the accuracy of crop classification. The multi-temporal filter De-Grandi enhanced the producer accuracy by about 10% compared to the Lee filter. Furthermore, gathering and utilizing large ground truth data greatly enhanced the accuracy of the classification. The research verified that using sequence images covering the growing season usually improved the classification results. The results exposed the effect of the polarization, where using VV-polarized data enabled on average 5% higher classification accuracy than the HH-polarized data, however using dual polarized data enhanced the classification accuracy by 3%. The study demonstrated that the majority of the classifications produced according to the crop calendar had higher total producer accuracy than using all acquisitions.

The study demonstrated undertaken in Paper II applied the decision tree object-based classifier in determining the major land uses and the inundation extent areas in 2011 and 2013 using the Lee-filtered imagery. Based on the maps produced for the land uses and inundation areas, the hazard areas due to the floods in 2011 and 2013 were identified. The study illustrated that 95% of the inundated area was classified correctly, that 90% of vegetated lands were accurately determined, and around 80% of the forest and the residential areas were correctly recognized. The study demonstrated that the residential areas did not experience any hazards in both pilot areas, however some cultivated lands were fully or partially submerged in 2011. These fields are in the high flood zone and therefore are expected to be entirely submerged during future high floods. Although, these fields were flooded in January 2011, they were cultivated with maize and potatoes in summer 2011 and in subsequent years and consequently were inundated in June 2013 with high economic losses to the owners of these fields.

The research undertaken in Paper III statistically analyzed the backscattering coefficient of the Lee-filtered TSX in some forest plots by the Factor Analysis and two sample Z-test. The study showed that Factor analysis tools succeeded in differentiating between the coniferous forest and the deciduous forest and mixed forest, but failed to discriminate between the deciduous and the mixed forest. On one hand, only one factor was extracted for each sample plot of the coniferous forest with approximately equal loadings during the whole acquisition period from March 2008 to January 2009. On the other hand, two factors were extracted for each deciduous or mixed forest sample plot, where one factor had high loadings during the leaf-on period from May to October,

and the other one had high loadings during the leaf-off period from November to April. Furthermore, the research revealed that the two sample Z-test enabled not only differentiation between the deciduous and the mixed forest against the coniferous forest, but also discrimination between deciduous forest and the mixed forest. Statistically significant differences were observed between the mean backscatter values of the HH-polarized acquisitions for the deciduous forest and the mixed forest during the leaf-off period, but no statistically significant difference was found during the leaf-on period. Moreover, plot samples for the deciduous forest had slightly higher mean backscattering coefficients than those for the mixed forest during the leaf-off period.

The outputs from the three research studies were land-use maps, flood risk maps, forest canopy maps and cropping pattern maps. If these outputs are produced and used by stakeholders and decision makers as they are designed to be, this can lead to facilitation of sustainable development in landscapes in the long-term. For example, these maps can be used in monitoring crop phenological phases and crop distribution, which can lead to enhance crop economics, protect ground water quality and with the aid of them to protect the Biosphere Reserve. The flood risk maps can be used to find out appropriate measures for flood protection and flood prevention and to set up to date proper land-use policies and regulations to protect the residential areas and enhance crop economics. Distinction of forest types, track changes in forest patterns, and estimation of the extent of environmental disasters in forest regions can be used in sustainable forest management, which plays an important role in preserving groundwater quality and achieving climate change adaptation goals.

To conclude, the results of this study emphasize the role of remote sensing in sustainable development of landscapes, as stated in Agenda 21, through the use of output maps in planning and monitoring of investigated areas in a sustainable manner. For each pilot area, the data of some surveyed fields was processed as training data, while the data of the remaining fields was used in testing the effectiveness of the applied methods. It is determined that the adopted methods can be applied to any accessible or remote landscape area. Last century, several new optical and RADAR satellite imagery were launched. In addition, photos acquired by unmanned aerial vehicles are starting to be widely used. Thus, the enlargement of the role of remote sensing in ecology and sustainable research to enable accessing remote areas and extensive large areas by a cost and time effective method in order to achieve the goal of sustainable landscape development, is endorsed.

Frame Paper

1. INTRODUCTION

1.1. Global History of Sustainable development

In 1972 the United Nations (UN) Conference on the Human Environment was held in Stockholm, Sweden. The Conference focused on human interactions with the environment and agreed upon a declaration enclosing 26 principles to motivate and guide the people of the world in the preservation and enhancement of the human environment (UN 1972). Since the 1980s, sustainability as a term has been used and the topic of sustainable development gained more importance in the last two decades of the 20th century to become a focal discussion point at the 1987 world commission on environment and development. It was held in Geneva, Switzerland where the concept of sustainable development was introduced for the first time (WCED 1987). The commission report, also named Our Common Future, addressed the need for the integration of economic development, natural resources management and protection, social equity and involvement. The report defined the sustainable development as "development that meets the needs of the present without compromising the ability of future generations to meet their own needs" (WCED 1987).

Five years later, the United Nations Conference on Environment and Development (UNCED) also known as the Earth Summit was held in Rio De Janeiro, Brazil in 1992. The conference declaration proclaimed 27 principles initiating that human beings have to be at the center of concerns for sustainable development; the right to promote development must be fulfilled so that developmental and environmental needs of present and future generations can be met; and that environmental protection must constitute an integral part of the development process to achieve sustainable development (UN 1992). In addition, a dynamic program was launched; called Agenda 21 which was an action agenda for the UN, other multilateral organizations, and individual governments around the world that can be executed at local, national, and global levels. The agenda included four sections. Section I included the social and economic dimensions and aimed for combating poverty, promoting health and achieving a more sustainable population. Section II considered conservation and management of resources for development, including atmospheric protection,

combating deforestation, protecting fragile environments, conservation of biodiversity, control of pollution and the management of biotechnology, as well as radioactive wastes. Section III emphasized the strengthening of the role of major groups including children and youth, women, NGOs, local authorities, business and industry, and workers. Section IV stated the means of implementation including science, technology transfer, education, international institutions and financial mechanisms (UN 1993).

In 2002, the world summit on sustainable development (Earth Summit 2002) was held in Johannesburg, South Africa. The Johannesburg declaration on sustainable development was a more general statement than the Rio Declaration. It mainly considered "the worldwide conditions that pose severe threats to the sustainable development of our people, which include: chronic hunger, malnutrition, foreign occupation, armed conflict, illicit drug problems, organized crime, corruption, natural disasters, illicit arms trafficking, trafficking of persons, terrorism, intolerance and incitement to racial, ethnic, religious and other forms of hatred, xenophobia, and endemic, communicable and chronic diseases" (UN 2002b, UN 2002a).

Ten years later, the United Nation Conference on Sustainable Development (UNCSD or “Rio+20”) was held in Rio De Janeiro, Brazil. It was held to review the progress of implementation of agreements taken during the first Rio Earth Summit in 1992. They decided to establish a high-level political forum on sustainable development to subsequently replace the Commission on Sustainable Development (UN 2012b). In addition, they presented the results of the project of sustainable development in the 21st Century” (SD21) as a summary for the policymakers (UN 2012a). In 2015, the United Nations General Assembly officially approved the universal, integrated and transformative 2030 Agenda for Sustainable Development, officially known as Transforming Our World: the 2030 Agenda for Sustainable Development, along with a set of 17 Sustainable Development Goals and 169 associated targets. The agenda covers a broad range of sustainable development issues, including ending poverty and hunger, improving health and education, making cities more sustainable, adapting climate change, and protecting oceans and forests (UN 2015b).

1.2. Sustainable development

The definition of sustainability given by Murray (2012) is "Sustainable development: enough for everyone, forever". Sustainable development is an approach to development which considers

integrating economic activity with environmental protection and social concerns (Bell and Cheung 2009, Elliott 2013, Auty and Brown 1997). For a particular process to be sustainable, it should not cause irreversible change to the environment, should be economically viable, and should benefit society as shown in Figure 1 (Bell and Cheung 2009). The Figure shows the interaction between three spheres: society, economics, and environment. Sustainability incorporates all three of them. The social aspects incorporate standards of living, accessibility of education and jobs, and equal opportunities for all members of society. The economic aspects comprise drivers for growth, enhancing profit, reducing costs, and investing in research and development. The environmental aspects take account of fair use of natural resources, pollution prevention, biodiversity, ecosystem and ecological health (Auty and Brown 1997, Archibugi and Nijkamp 1989, Bell and Cheung 2009).

Wellbeing and quality of life are main aspects of many people's lives. In a poor economy, people are more likely to suffer from a poor quality of life. In a poor environment, the impacts on the quality of life are not always clear and observable. However, problems such as polluted surface water runoff, over-development of floodplains, polluted groundwater, and the poor management of limited water resources can have an impact on the everyday quality of life. This means that the interaction between these three spheres plays an essential role in achieving sustainability (Azapagic and Perdan 2011, Becker 2012, Murray 2012). The intersection of social and economic spheres initiates social-economic aspects, including business ethics, fair trade, and worker's benefits. The intersection of economic and environmental spheres leads to environmental-economic aspects taking account of increasing energy efficiency, development of renewable fuels, green technologies, as well as the establishment of special incentives and funding for environmentally oriented businesses. The intersection of social and environmental spheres brings about social-environmental aspects incorporating conservation and environmental protection policies, the establishment of environmental justice, along with global stewardship for the sustainable use of natural resources (Bell and Cheung 2009, Elliott 2013, Murray 2012, Rodríguez et al. 2002, Auty and Brown 1997, Sachs and Nijkamp 1989, Becker 2012). Sustainable landscape management includes various practices that have developed according to environmental issues such as air, water, land and other natural resources. These practices are used in all phases of landscaping, including planning, construction, implementation and management of residential, commercial, and environmental landscapes (Cook and Van Der Zanden 2011).

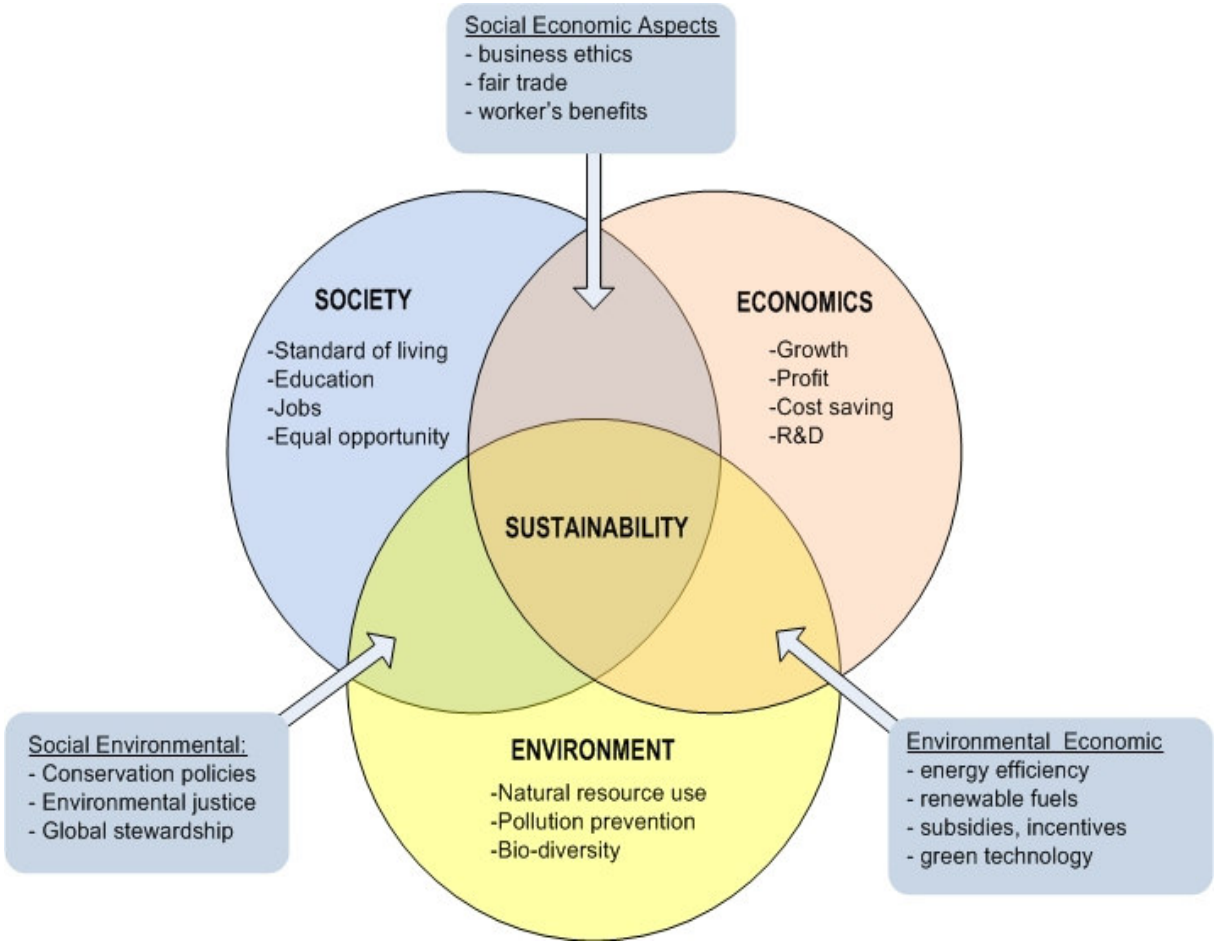

Figure 1: The interaction of the environmental, economic, and social aspects of sustainable development (Becker 2012).

1.3. Sustainable environment

In a sustainable environment, an ecosystem should conserve population and biodiversity, and incorporate their actions for a long period of time, while keeping the balance between the conservation of natural resources, and avoiding environmental disturbances (Peacock 2008). Therefore, the environmental impact assessment plays an essential role in designing and evaluating any project (Vezzoli and Manzini 2008, Colby 1991). Proper management of the natural resources is one of the major concepts of environmental sustainability (Barrow 2006, Clini et al. 2008). On a global scale, sustainable environmental management entails managing influences that have an impact on water resources, land and atmosphere, according to sustainability principles (Barrow 2006, Clini et al. 2008, Morelli 2011). Natural resource management considers the interaction between people and natural landscapes, including land use planning, water management,

biodiversity conservation, and the future sustainability of industries like agriculture, mining, tourism, fisheries and forestry (Conroy and Peterson 2013, Pound 2003). The land use/cover including urban uses, industry, agriculture, forest, grassland and pasture has an obvious impact on the global water, carbon and nitrogen biogeochemical cycles. Therefore, land use planning and observation of land use changes are essential to manage the environment. The changes in the carbon cycle count for the human-induced change and its catastrophic effects on biodiversity and human communities (Morelli 2011, Peacock 2008).

Agricultural land uses have major impacts on the environment, such as topsoil depletion, erosion and conversion to desert land caused by the constant tillage of annual crops, overgrazing, salinization, sodification, water logging, high levels of fossil fuel use, reliance on inorganic fertilizers and synthetic organic pesticides, water resource depletion, pollution of water bodies by run-off and groundwater contamination (WRI 1998). These problems must be addressed to promote sustainable agriculture through the production of food, fiber, or other plant or animal products using farming techniques that protect the environment, public health, human communities, and animal welfare. Therefore, monitoring the agricultural and grass lands is needed for a sustainable development (Röling and Wagemakers 1998).

Water is the main source for life on the planet Earth. Three percent of the available water resources are made up of fresh water, with two percent confined in ice caps and glaciers. One-fifth of the available one percent fresh water is in remote, inaccessible areas and are found in seasonal rainfall during monsoonal floods, which cannot be gathered (WRI 1998, Simonović 2009). Many countries suffer from water scarcity, and limited access to clean, safe, drinking water. Therefore, optimizing the fresh water has been the major problem in several regions worldwide. Water resource management aims to optimize the water use and minimize the negative impacts of water uses on the environment. The observation of the quantity and the quality of the water resources facilitates integrated water resource management (Borchardt et al. 2016). Sufficient water supply of proper quality is a major feature in the health and well-being of humans and ecosystems, and for the social and economic development. Thus, water quality is as significant as water quantity for satisfying basic human and environmental needs. In addition to the negative impacts of the deteriorated water quality on the human health, it causes several economic costs, such as degradation of ecosystem services, higher water treatment costs, health-related expenses, and impacts on profitable activities such as agriculture, industrial production and tourism (Conroy and

Peterson 2013, Borchardt et al. 2016). Consequently, the use of sufficient clean water in a sustainable way is the major concern worldwide (Peacock 2008, Pound 2003).

Water-related hazards, including floods, mudslides, storms, ocean storm surge, heat waves, cold spells, droughts and waterborne diseases by contaminated resources, comprise 90% of the natural hazards. Usually, these disasters are caused by a combination of water related hazards, and other hazards related to geological and biological causes, such as earthquakes, tsunamis, landslides, glacier lake eruptions, etc... (UN 2015a). The water-related disasters have a direct impact on buildings, infrastructure and crops, and increase the loss of lives and property. Moreover, they also have a negative effect on human health, production and profits, and cause higher investment risks (Střelcovà 2008). Therefore, further considerations are set on the awareness, prevention and monitoring of the major causes of the water related disasters to promote local and global sustainability (Barrow 2006, Clini et al. 2008, Peacock 2008).

47% of the world's forests were removed by humans. The current forest cover stands for 25% of the land with approximately 50% in the tropics (Coulston et al. 2013, Watson et al. 2000, WRI 1998). Therefore, deforestation in the tropics is of major global concern. Locally, forests maintain the climate. Globally, they conserve biodiversity, protect water quality, pReserve soil and soil quality, sustain water cycles through their light reflectance and evapotranspiration, provide fuel and pharmaceuticals, and purify the air. In contrast, deforestation causes soil degradation and organic decomposition that returns carbon dioxide to the atmosphere. Approximately 90% of the carbon stored in vegetated areas is confined in trees and increases the carbon in the atmosphere by approximately 50%, causing global climate change (FAO 2010). Approximately 20% of total global carbon emissions are due to the changes in land use. Sustainable forest management aims to maintain the balance between the three main columns of sustainability: ecological, economic and social. This leads to the possibility of conserving local livelihoods to keep the biodiversity and ecosystems provided by forests, reducing rural poverty and mitigating some of the effects of climate change (Heinrichs et al. 2016).

1.4. Role of remote sensing towards sustainable landscape development

Remote sensing (RS) and geographical information systems (GIS) play an essential role in promoting sustainable development. In 1992, the United Nations Conference on Environment & Development emphasizes this role in several chapters of Agenda 21. Chapter 7 focused on promoting sustainable human settlement development through executing programs promoting sustainable land-use planning and management, and enlightened RS and GIS as components of the scientific and technological means of implementing this program. Agenda 21 stated in section 7.33 that "All countries, particularly developing countries, alone or in regional or sub-regional groupings, should be given access to modern techniques of land-resource management, such as geographical information systems, satellite photography/imagery and other remote-sensing technologies" (UN 1992).

Chapter 11 focused on combating deforestation through establishing and/or strengthening capacities for the planning, assessment and systematic observations of forests and related programs, projects and activities, including commercial trade and processes. In section 11.36, Agenda 21 described the programs for the activities of assessment and systematic observation involving major research efforts, statistical modeling and technological innovation. These activities can improve the technological and scientific content of assessment and periodical evaluations. Some of the activity components are: "a. Developing technical, ecological and economic methods and models related to periodical evaluations and evaluation; b. Developing data systems, data processing and statistical modeling; c. Remote sensing and ground surveys; d. Developing geographic information systems; e. Assessing and improving technology". To promote human resource development, section 11.38 stated that "The program activities foresee the need and include provision for human resource development in terms of specialization (e.g., the use of remote-sensing, mapping and statistical modeling), training, technology transfer, fellowships and field demonstrations" (UN 1992).

Chapter 12 focused on managing fragile ecosystems and combating desertification and drought via developing comprehensive drought preparedness and drought-relief schemes, including self-help arrangements for drought-prone areas, and designing programs to cope with environmental refugees. To execute these programs, the data and information related to the program activities are explained in section 12.49. This section encouraged the governments of affected countries to

support the relevant international and regional organizations to implement research on seasonal forecasts. The research can improve contingency planning and relief operations and can allow preventive measures to be taken at the farm level. The measures include strengthening national early-warning systems, with particular emphasis on the area of risk-mapping, remote-sensing, agro-meteorological modeling, integrated multidisciplinary crop-forecasting techniques and computerized food supply/demand analysis (UN 1992). Floods are considered the main source of risks worldwide. Flood maps are useful tools that provide information about hazards, vulnerabilities, and risks of a given area.

Chapter 18 focused on the protection of the quality and the supply of freshwater resources with respect to application of integrated approaches to the development, management and use of water resources. The activities of the program of water resource assessment were presented in section 18.27, which stated that „All States, according to their capacity and available resources, and through bilateral or multilateral cooperation, including the United Nations and other relevant organizations as appropriate, could undertake many activities for data systems including assimilating remotely sensed data and the use, where appropriate, of geographical information systems" (UN 1992).

Chapter 40 focused on the programs needed to be implemented to ensure that the decision makers made their decisions based on adequate information. Such programs are aimed at bridging the data gap, and improving information availability. In order to improve the data collection and use, section 40.8 endorsed the countries and international organizations to carry out inventories of environmental, resource and developmental data, based on national/global priorities for the management of sustainable development, and to make use of new techniques of data collection, including satellite-based remote sensing to strengthen these data-collection activities. These activities include those of Earth-Watch and World Weather Watch, especially in the areas of urban air, freshwater, land resources (including forests and rangelands), desertification, soil degradation, biodiversity, other habitats, the high seas and the upper atmosphere (UN 1992).

1.5. Previous studies

As stated in the above mentioned chapters of Agenda 2, remote sensing plays essential role in planning and accomplishes sustainable landscape development. This role can be implemented through using satellite images in producing various land uses maps, change deduction maps, and hazards maps. Land uses can be defined through field survey, aerial photos or satellite images. Surveying costs and time make it difficult to produce land use maps in the field (Makhanya 1992). As an alternative, satellite images can be used to provide the necessary information, especially RADAR imagery in European countries with heavy cloud covers. These images attest to be functional in generating land cover maps (Purkis and Klemas 2011).

Previous studies investigated crop production and land use maps using ENVISAT imagery. Some studies recommended the use of an appropriate range of images within a time series according to the crop-calendar, to achieve better classification results than using all of the images (Tavakkoli et al. 2008). Many fields are cultivated by more than one type of crop during the year. Thus, such succession is difficult to model because it is controlled by phenological and ecological courses. Tavakkoli et al. used ENVISAT images and showed that using all of the images without considering the crop calendar resulted in less producer accuracy, where the classification process identifies patterns of similar characteristics according to the corresponding observed backscattering response and their temporal progress (Tavakkoli et al. 2008). ENVISAT images have a C-band signal which passes partially through vegetation cover. This might lead to classification errors where the signals are influenced by the soil surface under the vegetation cover (Richards 2009). Thus some studies recommend using higher frequency signals such as X-band where the signals are more reflected by the vegetation cover (Tavakkoli 2011). Farghaly et al. showed the effectiveness of TSX images in distinguishing between aquatic weed types over Lake Kyoga (Farghaly et al. 2011). Lohmann et al. also demonstrated the efficiency of these images in determining the different types of crops within agricultural fields near Hanover, Lower Saxony (Lohmann et al 2009a, 2009b).

Lohmann et al. (2009b) investigated the multi-temporal classifications of dual polarized TSX imagery covering a time period from March to November 2008. The study used Factor Analysis to reduce the data required from satellite images for each surveyed area to determine the bands that must be considered to identify areas similar to the training areas, approach that improves the

results of the classification process. The study showed that even when not using all images of a given season, but only those that are indicated by the crop-calendar or those that show high loadings in the Factor Analysis, a classification accuracy of more than 90% can be achieved (Lohmann et al. 2009).

Generally, flood mapping is obtained using image classification, where each individual pixel is classified based on all existing information using the grey values and spatial information of an image (APFM 2014, Chenghu et al. 2000, Skakun et al. 2014). The satellite imagery can be classified on a pixel-based or object-based basis. Numerous studies have investigated the effectiveness of different SAR imagery polarization in identifying flooded areas (Chenghu et al 2000, Manjusree et al. 2012).

Several studies have also investigated the effect of the wavelength of SAR sensors on mapping water and the vegetation canopy (Sandro2010, Lillesand et al. 2015). Although many procedures have been studied in the literature, this research focuses on Decision-Tree methodology, which has not yet been comprehensively evaluated. The present research employs remote sensing tools in identifying the detection maps and land use/land cover LULC maps using TSX imagery for two study areas within the Elbe Biosphere Reserve in Lower Saxony “Niedersächsische Elbtalaue”. Both the LULC and flood-detection maps are generated using a Decision-Tree object-based classifier. The agricultural land use types were defined before in Paper I (Farghaly et al. 2014). These flood risk maps can be used to find out the appropriate measures for flood protection and flood prevention and to update the land-use policies and regulations in the study area in order to protect the residential areas and enhance crop economics in a proper way. Obtaining the pervious targets will initiate the economic, social and environmental sustainability, and finally will facilitate the landscape sustainability.

Forest mapping and monitoring surveys are often based on costly and time-consuming field work since forest areas are large and remote (Richards, 2009). These processes require satellite remote sensing data that facilitates the mapping of large forest areas (Purkis and Klemas 2011). The shorter wavelength bands (X and C) are sensitive to small twigs and leaves; therefore, it can provide information on the uppermost canopy level. Therefore, TerraSAR-x imagery with its x band can be used to distinguish between forest types.

Previous studies using satellite images were only able to clearly distinguish between different types of forests by integrating additional data such as DEMs (Ortiz et al 2012, Solberg et al 2018). They also did not explore the potential of statistical analysis tools such as two sample Z-test (TZT) and Factor Analysis (EFA) as a means to analyze the vast amount of information acquired by satellite imagery. Z-test was rarely used in analyzing the backscatter of SAR imagery; however it was applied on evaluating few classification results. For example, Kumar et al. (2017) used Kernel-based support vector machines, maximum likelihood and normalized difference vegetation index classification schemes to evaluate their crop classification effectiveness. The classifications results were statistically analyzed and compared using Z-test and χ^2-test (Kumar et al. 2017).

2. STUDY OBJECTIVES

This study aims to emphasize the role of remote sensing and geographic information systems in landscape sustainability studies, in order to promote sustainable development in landscapes. The study focused on some of the main factors affecting sustainable environment as stated in paragraph 1.3. These factors are land uses in particular agricultural land uses, water quality, forests, and water hazards such as floods. Three investigations were carried out concerning these factors. The three papers are already published in international journals. Paper I is titled "Observing the Middle Elbe Biosphere in Germany by Means of TerraSAR-X Images". This paper concentrated on the agricultural land uses specially how to produce cropping pattern maps. Paper II "Towards sustainable use of land uses within the Elbe River Biosphere Reserve in Lower Saxony, Germany by means of Terrasar-x images", focused on land uses and flood hazards. Paper III "Differentiating forest types using TerraSAR–X Spotlight Images based on inferential statistics and multivariate analysis", gave attention to ground water quality and forest distribution.

Figure 2 exposes the diagram of the conceptual design of the research and its result based management. The diagram shows the causal or logical relationships between what is needed as inputs, and what is derived and required as outputs, in order to achieve the outcomes, and reach the plausible short-term targets, accomplish the consequential medium-term goals, and lastly obtain the probable long-term impacts. The diagram shows the purpose of the three produced scientific papers, where each paper presented one or more outputs.

The inputs for this research were mainly the SAR Imagery and the ground truth data collected from the field survey, in addition to databases, geo-databases and maps. Based on these inputs, the outputs of the study were acquired. These outputs included land-use maps, flood risk maps, forest canopy maps and cropping pattern maps. If those outputs are produced and used by the direct stakeholders and decision makers as expected, then several outcomes could be obtained. The possible outcomes could be measures for flood prevention and protection in addition to land-use policy and regulations in flood plain if land-use maps and flood risk maps are employed. The outcomes could be monitoring forest as well based on the forest canopy maps and the land-use maps. Another probable outcome could be monitoring crop phenological phases and crop distribution if the cropping pattern maps and the land-use maps were utilized.

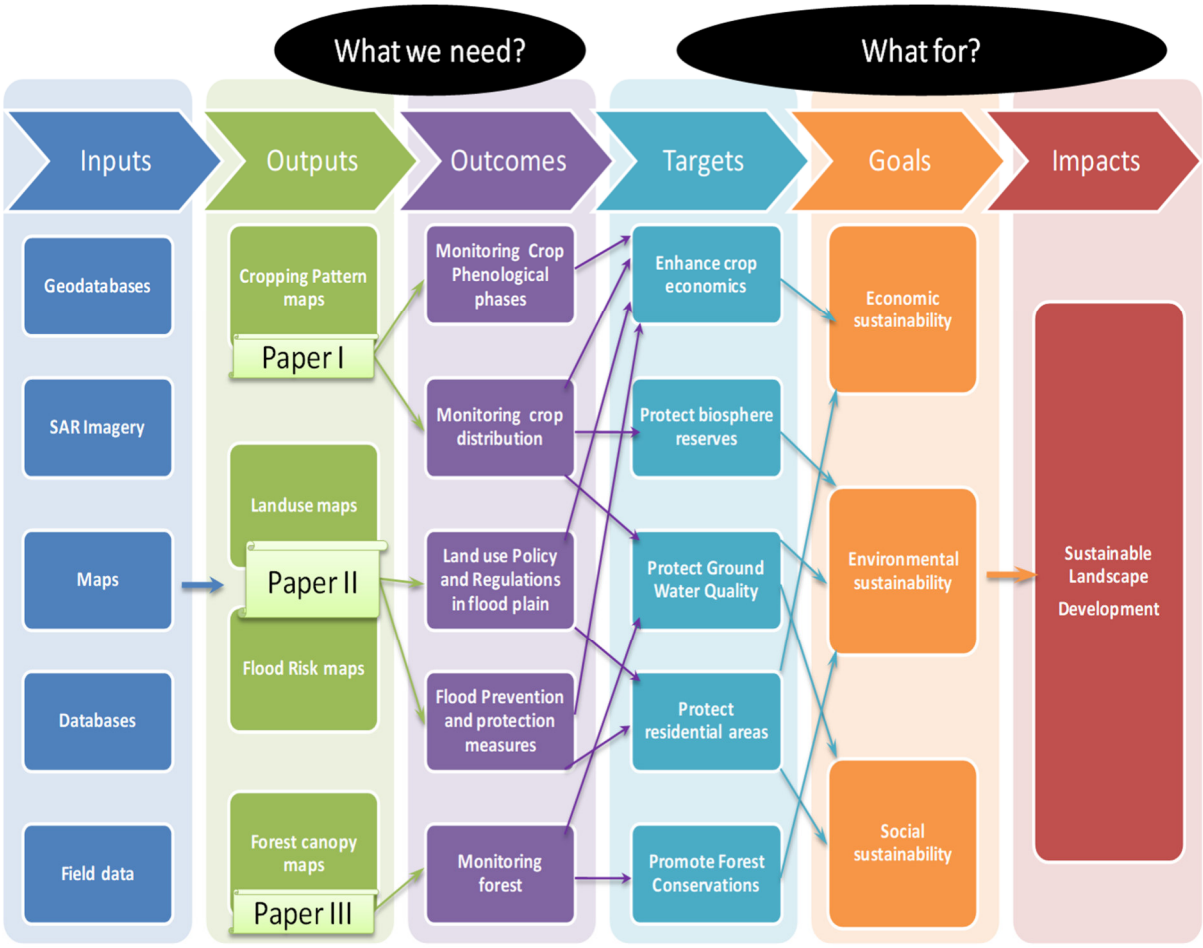

Figure 2: Diagram for the conceptual design of the research and its results-based management

Several short-term targets are expected to be gained if the previous outcomes are implemented. For example, if measures for flood prevention and protection in addition to land-use policy and regulations in flood plain were implemented, then protected residential areas can be available as short-term target. These two previous outcomes as well as monitoring crop phenological phases and crop distribution can enhance crop economics in the short-term. Forest monitoring by remote sensing tools provides additional and actual information of the current status of the forests and can be used for proper conversation measures. Protected Biosphere Reserve is a further target that can be attained in the short term if the crop distribution is observed. An added target can be the protection of ground water quality, which can be realized if programs for monitoring forest and crop distribution are applied.

STUDY OBJECTIVES

If the short-term targets are achieved, then three medium-term goals will be accomplished. For instance, Economic sustainability can be attained in the medium term if residential areas are protected and the crop economics are enhanced. In the medium term, the goal of social sustainability can be obtained as well if the residential areas and the groundwater quality are protected. Further medium-term goal can be environmental sustainability, if the programs of forest conservation are promoted as well as the programs for protecting the groundwater quality and Biosphere Reserves. Those medium-term goals can finally lead to facilitate the sustainable development of landscapes with a long-term impact.

This study exposed part of the remote sensing role in supporting the decision makers towards sustainable development in landscapes. The research investigated the use of TerraSAR-X imagery (TSX) in monitoring the environment in some pilot areas. The research aimed to study the following:

- the effectiveness of the TSX imagery in identifying the cropping pattern by employing pixel-based supervised maximum likely hood classifier, as published in Paper I,
- the efficiency of using TSX imagery in determining the land uses and the flood risk maps by applying object-based decision tree classifier, as published in Paper II, and
- the potential of inferential statistics tests such as two samples Z-test and the multivariate analysis, for example Factor Analysis for identifying the kind of forest canopy, based on the backscattering coefficient of TSX imagery of forest plots, as presented in Paper III.

3. METHODOLOGY

Several steps were implemented and several methods were carried out to reach the study objectives as shown in Figure 3. These steps and methods are described below.

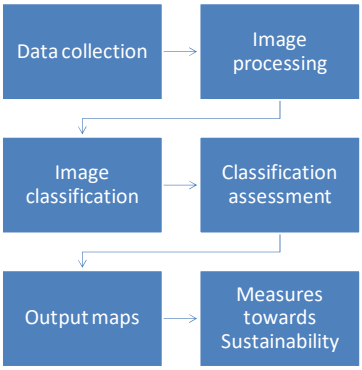

Figure 3: The implemented steps in order to achieve the objective of the study.

3.1. Study areas

Three pilot areas were selected in Lower Saxony in Germany to carry out the research questions. Two test areas are located in the Biosphere Reserve Lower Saxonian Elbe Valley (das Biosphärenreservat „Niedersächsische Elbtalaue“), while the third one the Fuhrberger Feld is located in a groundwater protection area near Hanover. The pilot areas are exposed in Figure 4. Details for each pilot area are given below.

3.1.1. Lower Saxonian Elbe Valley Biosphere Reserve

The Elbe River Biosphere Reserve in Lower Saxony reaches from Schnackenburg in the south-east at Elbe-km 472.5 to Hohnstorf in the north-west at Elbe-km 569. The Elbe River kilometrage starts with zero at the Czech-German state border, the numbers grow in the upstream direction on the Czech side, as well as in the downstream direction on the German side (Mangi 2016). The terrain of the Reserve ranges from 5 m to 109 m above mean sea level. It covers a total area of about 570 square kilometers. As a historically cultural landscape the floodplains are used in various ways with a predominance of agricultural land use (Härdtle et al. 2006, Urban 2003, Prüter et al. 2014). A big division of 68% is covered with agricultural fields and grassland areas (Härdtle et al. 2006).

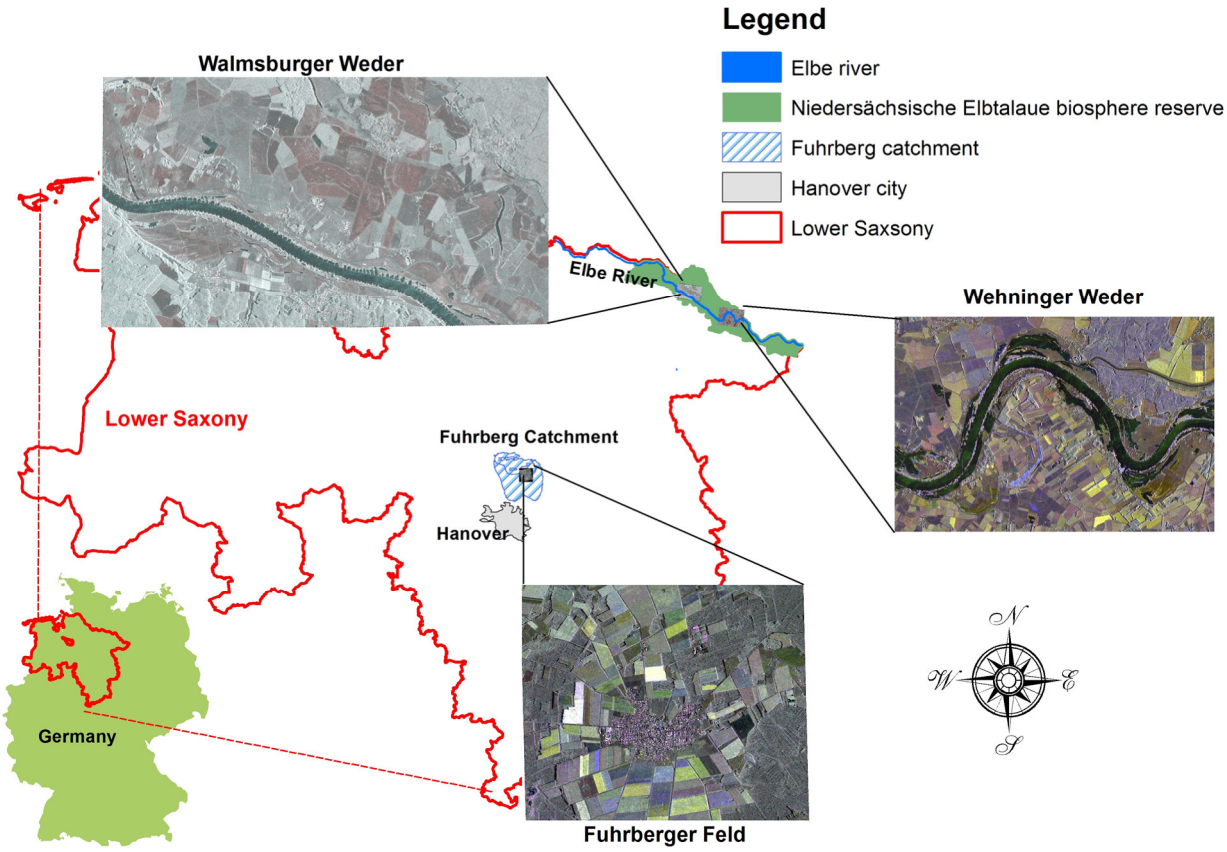

Figure 4: Location of the study areas in Lower Saxony

It is divided into three protection zones: Zone A (16,540 ha), Zone B (20,100 ha) and Zone C (20,120 ha) as shown in Figure 5 (Prüter et al. 2014, UNESCO 2007, UNESCO 2011). Zone A generally covers the urban areas together with other areas which are particularly subject to human influence, where the people live and spend most of their live. Moreover, the areas of this zone function as connecting elements between the zones B and C. Zone B includes areas which are mainly part of the cultivated landscape, and yet the habitats involved also have characteristic associations with the natural site conditions. This terrain is to be conserved and developed with the aim of achieving a functioning, natural balance which serves both people seeking recreation and the countryside itself. Zone B fulfils the criteria which apply to a landscape protection area. Zone C is Reserved for those areas of the Biosphere Reserve which are especially worthy of preservation and care. The criteria involved correspond to those which apply to German nature Reserves, and all previous nature Reserves of the region have been adopted into zone C. Zone C contains 'natural' habitats in the sense that they represent conditions close to those which would exist in the complete

absence of human intervention. However, there are many areas which need to be tended regularly so that they can continue to fulfill their function as a refuge for individual species or ecological communities of wild plants and animals. Other habitats such as water bodies, wetlands, moors and forests are predominantly characterized by their own natural momentum (Prüter et al. 2014, UNESCO 2007, UNESCO 2011, Urban 2003). As a UNESCO Biosphere Reserve it is a model region for sustainable development, which aims to achieve a balance between the interests of environmental protection and of social and economic development. It promotes environmentally-friendly agriculture, regional marketing, low-impact tourism, and an educational program for sustainable development (ESD), including research and monitoring activities. It represents vital habitats, the diversity of fauna and flora, typical landscapes including mainly farmland located in the rural areas and cultivated at different levels (UNESCO 2007, UNESCO 2011).

Numerous researchers have reflected on land use effects on the environment. Regions around rivers in the Biosphere areas must be monitored to avoid environmental problems that might affect the multiple ecological, economic and social functions of those areas (Tevi 2012). Pasture land situated in the recent flood plain is affected by contaminated suspended sediment loads deposited during flooding which can cause soil, crop, and fodder pollution (Koppe et al. 2008). On the other hand arable land is a possible source for groundwater and soil pollution. This floodplain has suffered from major flooding such as the 2002 flood, which caused huge damage in hazardous areas of the Elbe catchment. Thus many studies have been conducted to improve flood risk management schemes for the Elbe basin (Urban et al. 2011). Therefore, the Biosphere Reserve Administration requires updated, comprehensive land use maps for planning the development of sustainable forms of land use there.

Two pilot areas were studied around the Wehninger oxbow (Wehninger Werder) between Elbe-Kilometer (505-520), and Walmsburger oxbow (Walmsburger Werder) between Elbe-Kilometer (533-543) within the Lower Saxonian Elbe valley Biosphere Reserve (Figure 4). Both areas are bearing several types of land use including urban and rural regions with agricultural land use dominant. 30% of this area is covered by forests, which must be maintained to ensure the sustainability of the flood plain environment. Over 65% of this area is covered by agricultural fields and grasslands, which are considered the main possible sources of environmental pollution as well as they are possible sinks for flood borne contaminations (UNESCO 2005). The majority of both areas is situated in Protection Zones B and C emphasizing the importance of an in-depth

study of both pilot areas. Paper I and Paper II studied the two described pilot areas to investigate the possibility of applying the research methods on any other remote area.

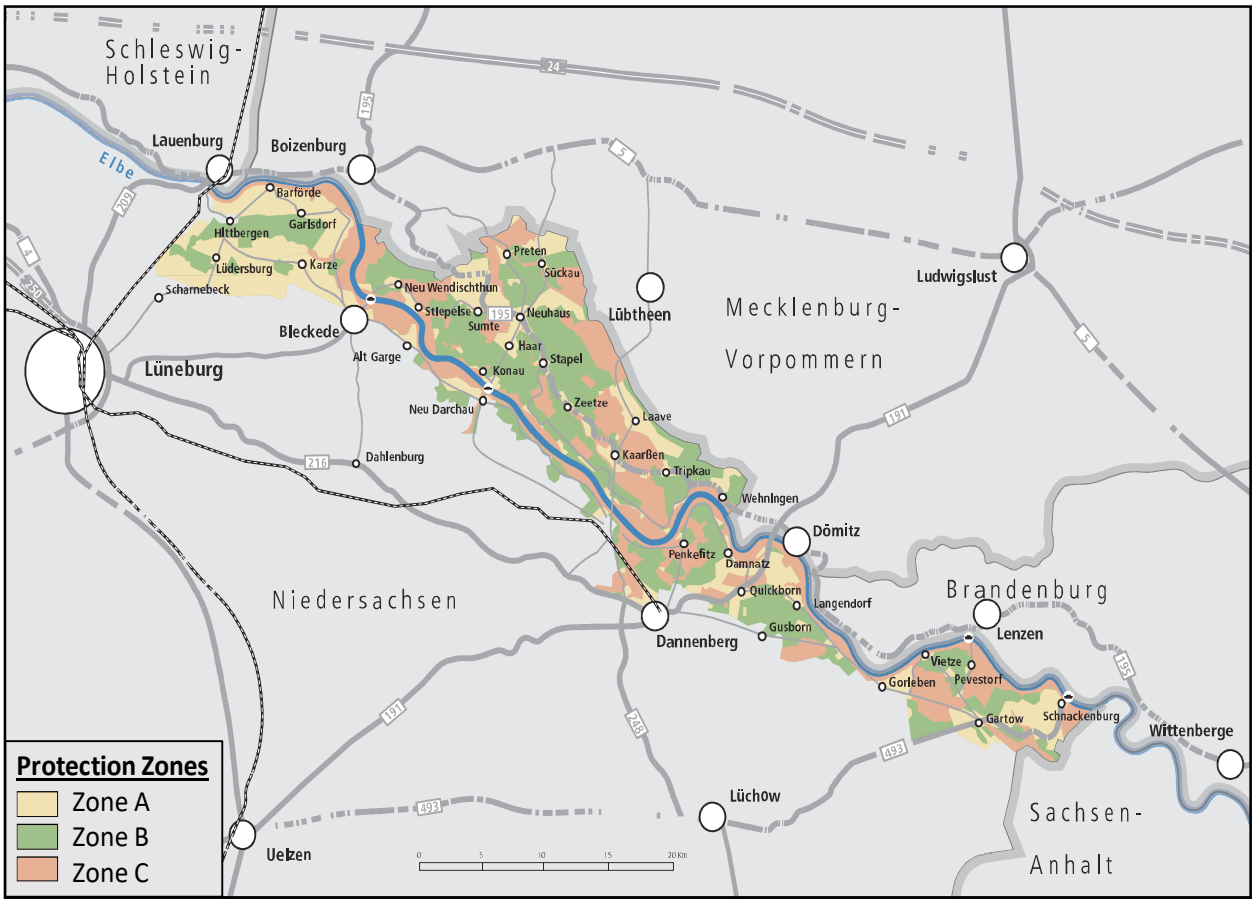

Figure 5: Main Protection zones of Lower Saxonian Elbe Valley Biosphere Reserve (Prüter et al. 2014)

The Elbe River suffered from many severe floods during the last decades (Kundzewicz et al. 2013). The century flood of Elbe River occurred during summer 2002, beside other less intensely floods occurred in 2006, followed by two extreme wide scale floods in 2011 and 2013 (Geller et al. 2004, Balthasar et al . 2011, Schröter et al. 2014, LHW 2014). At Walmsburger Werder, the maximum water level of 13.16 m above mean sea level (AMSL) was measured on 23rd January 2011, while it reached 13.58 m AMSL on 11th June 2013. At Wehninger Werder, the maximum water level of 16.57 m AMSL was measured on 23rd January 2011, while it reached 17.02 m AMSL on 11th June 2013.

3.1.2. Fuhrberger Feld

The Fuhrberger Feld groundwater catchment area is situated approximately 30 km north of the city of Hanover in northwestern Germany, the capital of state of Lower Saxony (Figure 4). This catchment area serves as an aquifer supplying about 90% of the municipal water for the 650.000 inhabitants living in Hanover region (Wolf 2013). With an area of approx. 300 km², the Fuhrberger Feld is the largest protected drinking water catchment area in northern Germany, with 50 Million cubic meters being extracted annually. According to national guidelines that define groundwater protection zones, Fuhrberger Feld consists of 3 protection zones as shown in Figure 6. Zone I, 'Well Field Protection Zone,' which is designed to protect individual wells and their immediate environment against any contamination and interference with a buffer zone with a fixed diameter of 10 meters. Zone II, 'Narrow Protection Zone,' which is meant to provide protection against contamination by pathogenic bacteria and viruses within a 50-day travel time, is largely forested, and can be used for limited development, for example road construction or agriculture. Zone III, 'Wide Protection Zone,' which is designed to protect wells against long-range impairments, especially against contamination by non-degradable or less readily degradable chemical or radioactive substances and which covers the entire subsurface catchment area. If the catchment area is very large, i.e., if it has a boundary more than 2 km from the well, it may be subdivided into Zone III A and Zone III B with different levels of land use restrictions(WHO 2005).

In this groundwater catchment area, the land uses are classified into approximately 45% of agricultural fields and grassland, 40% of forests, 7% for settlements, and 8% for other uses. The forest areas include 75% coniferous trees and 5% deciduous trees, and the rest of the area is mixed forest (Wolf 2013). A pilot area around Fuhrberg city in Zone III was studied as shown in Figure 3. Since agriculture is the dominant use in this area, groundwater protection is a major priority. Therefore, several measures have been taken to avoid the negative impacts of agricultural land use on groundwater quality by Stadtwerke Hannover "Enercity". These include the following:

- voluntary agreements with farmers to minimize the use of fertilizer,
- initiatives to increase the percentage of deciduous forests in the catchment area, and
- setting aside arable land to reduce nitrate leaching from soils (WHO 2005, Enercity 2015).

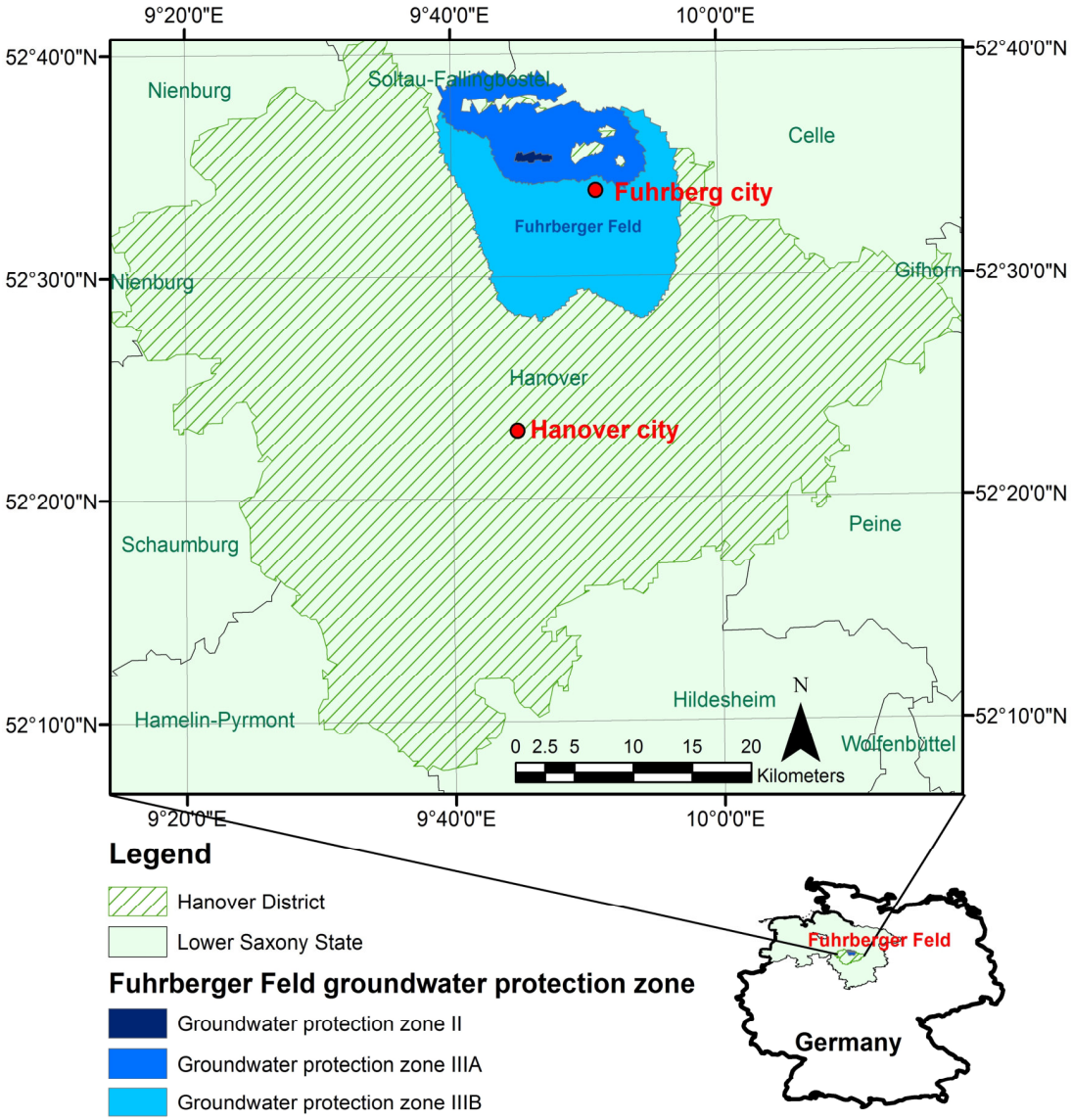

Figure 6: Location of Fuhrberger Feld catchment area and the groundwater protection zones in Lower Saxony, Germany- Shape files source for Lower Saxony ATKIS (Amtliches Topographisch-Kartographisches Informationssystem)

Since 1996, Lower Saxony has worked on projects for forest conversion in general and the reconstruction of coniferous forests into mixed deciduous forests in particular to achieve, to use the name of the related projects, Tree by Tree sustainability. This approach not only positively affects the climate, but also the groundwater balance. This is due to the fact that conifers are characterized by high evaporation rates during the entire year, have rough bark that reduces water runoff, and have strong grass cover. As a result, seepage is also limited. In contrast, deciduous

trees, especially when they are leafless, contribute to the replenishment of groundwater. Their smooth bark optimizes water drainage, they have less grass cover, and as a consequence, seepage is optimized. One hectare site rebuilt with mixed forest produces annually in federal grants 800,000 liters more additional groundwater and drinking water than pure coniferous forest monocultures (Enercity 2015, UNEP 2011, KIM 2010, Becker 2013, Becker et al. 2014). In the water Reserve Fuhrberger Feld alone, 650,000 deciduous trees have been planted annually since 1996 to gradually replace the coniferous trees. By 2015, 3500 hectares had been converted from coniferous into mixed deciduous forest in this protection zone, and 14 million deciduous trees had been planted (Enercity 2015). Hence, it is essential to monitor the forests in Zone 3 to certify that the percentages of the area coverage of deciduous and the mixed forests in this catchment area are increasing. Paper III was applied to this described pilot area.

3.2. Data Collection

As shown in Figure 2 and Figure 7, the input data for this research included satellite images, field survey to obtain ground truth data, maps, databases and geo-databases. These inputs are described below.

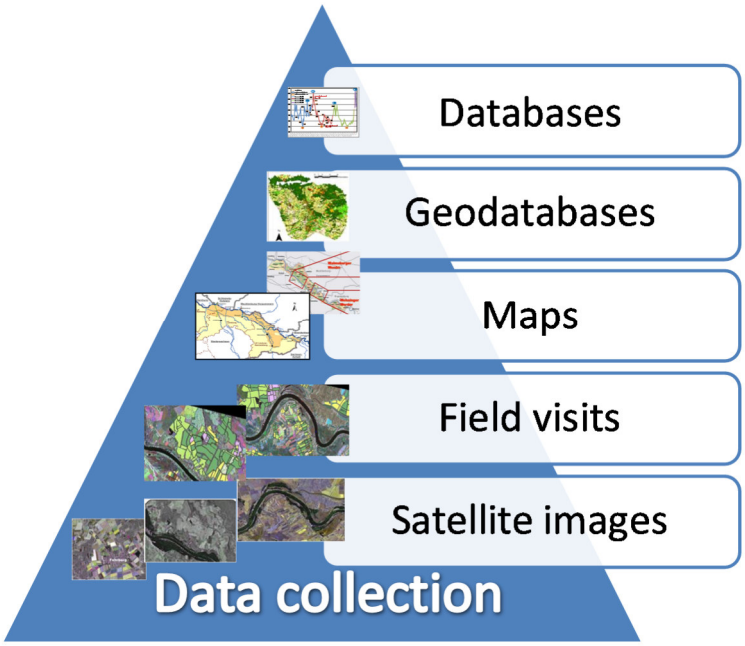

Figure 7: Input data of the Study

3.2.1. Satellite images

The study areas are located in Germany which is often characterized by heavy rains and dense cloud cover with limited annual sunshine hours. For this reason, optical satellite images can rarely be used. Active remote sensing systems, for instance synthetic aperture radar (SAR), are slightly influenced by weather conditions, and therefore SAR imagery was used in this research, in particularly TerraSAR–X images (TSX). TSX imagery is a very recent and effective source of information, which was generated by the German Aerospace Centre (DLR) since June 2007 (Soergel 2010). Its orbit passes over the same location every 11 days. It uses an X-band SAR, with a 31 mm wavelength and 9.6 GHz frequency, providing high-quality topographic information for commercial and scientific applications (Ochs and Pitz 2007). The shorter wavelength bands (X and C) are sensitive to small twigs and leaves; therefore, it can provide information on the uppermost canopy level. In contrast, long wavelength bands (L and P) are sensitive to boles and branches; as a result, it can provide information on the woody structure and underlying ground surface (Richards 2009, Purkis and Klemas 2011).

The images used for this research are dual-co-polarized TerraSAR-X (HH/VV) High resolution Spotlight (HS) products, generated by DLR as Multi-look Ground-range Detected (MGD) products with Spatially Enhanced (SE) processing. MGD has reduced speckle and approximately square resolution cells on the ground. Each scene size was 10 km x 5 km (width x length). The co-polarized refers to identical transmit and receive polarization states. HH refers to horizontal transmit and horizontal receive, and VV refers to vertical transmit and vertical receive (Soergel 2010, Richards 2009, Balz et al. 2018). The image coordinates are oriented along the flight direction and the ground range. Geometric projection is in the azimuth-ground range without terrain correction. The images are high resolution, with an azimuth pixel spacing of 1m. The TSX imagery for Paper I and Paper II were granted by DLR to the administration of the Lower Saxonian Elbe Valley Biosphere Reserve according to the agreement between UNESCO and DLR. The proposal number is HYD0677. The TSX imagery for Paper III was granted by DLR during a pilot project of DLR TerraSAR Science proposal LAN0011 to the Institute for Photogrammetry and Geoinformation (IPI) at Leibniz University in Hanover, Germany. Details about each pilot area are given in chapter 4.1, 4.2 and 4.3

3.2.2. Field Survey

The accessible fields covered by the TSX images were surveyed to identify the crops cultivated there, and the type of forest. Field visits were conducted almost monthly to several reachable and representative areas on similar dates to the acquisition times. More than 150 individual fields were visited around Walmsburger Werder, about 300 fields were investigated around Wehninger Werder which were used in Paper I, in addition to about 120 fields were visited in Fuhrberger catchment area data of which were used in Paper III. The fields were divided into training fields group which was used as reference data, and a testing field group which was used for assessing the accuracy of the produced classifications as shown in Figure 7.

3.2.3. Databases

Water level data are essential in studying the characteristics of the floods. To study the flood problems around Elbe River, the water levels measured at the Neu Darchau gauge at Walmsburger Werder and at the Damnatz gauge at Wehninger Werder were collected for the periods from January 2010 until December 2012 and during June 2013. The readings of both gauges were converted to real water levels above mean sea level. A database was created for the water level during the stated periods and was used in the research. The data were provided from the administration of the Lower Saxonian Elbe Valley Biosphere Reserve.

3.2.4. Geodatabases

Several geodatabases and shape files were used for the three pilot areas. To study the areas around Elbe river, a shape file for the river was taken from the Lower Saxony ATKIS (Amtliches Topographisch-Kartographisches Informationssystem) produced by the Federal Agency for Cartography and Geodesy (BKG). The boundary of the Biosphere Reserve (Grenze des Biosphaerenreservats), the official boundary of the flood extent around Elbe River (Amtliche Überschwemmungsgebiete), a digital elevation model for the Elbe Biosphere Reserve in five meters spatial resolution (DGM5) produced by BKG, and the postion of the gauges along Elbe River were provided by the administration of the Lower Saxonian Elbe Valley Biosphere Reserve. For the pilot area of the Fuhrberger Feld catchment, feature classes from the ATKIS were used for both the Fuhrberger Feld catchment area and the groundwater protection zones, beside the land-uses, and the forest canopy. The geo-databases were provided in form of different projections,

therefore the feature classes in the geodatabases were transformed into UTM zone 32 projection to avoid the problems of different projection types.

3.2.5. Maps

Some maps were used in the study to show the study areas. These maps included a map for the major rivers in Europe, a map of the Elbe River basin, a map of the gauges location along Elbe River, a map of the Lower Saxonian Elbe River Biosphere Reserve. Besides, a map of the flood extent of the flood in 2013, created by DLR, was used to get the flooded areas in 2013 around Walmsburger Werder and Wehninger Werder.

3.3. Image Processing

Processing of TSX images was required to use the images in producing the outputs of the research. A scheme of the steps of image processing is presented in Figure 8. For each acquired date, one image for the HH-polarization and one more for the VV polarization were delivered in Tiff format. As shown in Figure 6, initially the images were coregistered to correct for relative translational shift and rotational and scale differences by performing spatial registration and potential resampling. This was done using the SARSCAPE module of the ENVI program after importing them in TerraSAR-X standard format. The resulting images were then geocoded to provide a radiometric calibration and a cartographic reference system. In a next step, the images were filtered to remove or decrease these noises to permit better discrimination of scene targets.

TSX images are known for speckle noise problems which affect the accuracy of classification results. These speckle noises are due to coherent superposition of multiple backscatter sources. For that reason, speckle reduction must be applied to the images in order to remove the speckle noise to allow better differentiation between different objects (Richards 2009). Lee filter is an adaptive filter which is based on the assumption that the mean and variance of the pixel of interest are equal to the local mean and variance of all pixels within the moving window. This pReserves image sharpness and details while suppressing noise (Lee et al. 2008). Many images of the same location are taken at different frequent dates. Thus, multi-temporal speckle filtering is applied to exploit the space varying temporal correlation of speckle between the images, which reduces the system inherent multiplicative noise (Richards 2009, De Grandi et al. 1997). The De-Grandi filter is an optimum weighting filter which was introduced to balance differences in reflectivity between

images at different times. This enhances the image sharpness and enables identifying more details (Lee et al. 1997, De Grandi et al. 1997).

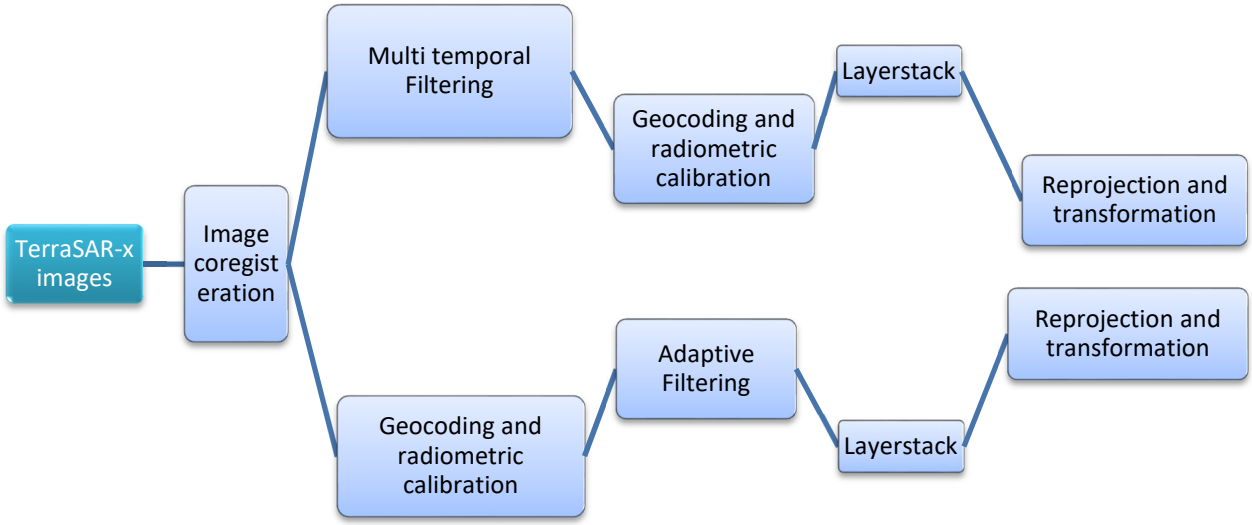

Figure 8: Scheme of the steps of image processing in the research

The images were filtered using Lee and Degrandi filter as mentioned before. An example of the effect of these filters is exposed in Figure 9. The De-Grandi Filter was carried out using SARSCAPE Module under ENVI program on the coregistered images. The lee filter was performed using ERDAS imagine software through the Speckle Suppression option under Radar Interpreter menu. The coefficient of variation for the subset of the geocoded images was calculated for each image. The Lee filter was selected from the list of available filters and the coefficient of variation value was inserted. The window size was set to 7 pixels. The De-Grandi-filtered images were non-pixilated, more homogenous and similar to the optical ones other than the Lee-filter images.

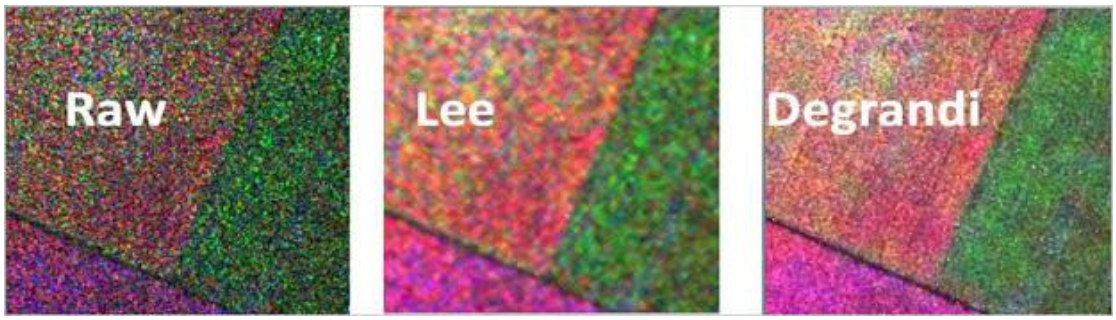

Figure 9: Effect of using Lee and De Grandi filters on removing the speckle noises.

The images for HH and VV polarization acquired on the same date were stacked together to create an image with 2 bands for each date and each study area. Image rectification and geo-reference transformation were then applied to the stacked images using ERDAS Imagine software. The TSX images were geometrically transformed to Universal Transverse Mercator (UTM) projection with spheroid WGS 84 and Zone 32 North and resampled into one meter pixel size using the projective transform model provided by the Geocorrect image tool. Finally, for each study area, the filtered images were stacked together to have one image consisting of several layers presenting the different acquired dates in both VV and HH polarization.

3.4. Image classification

Four essential outputs were required in this research to facilitate the expected outcomes and impacts of the study. These outputs included land-use maps, cropping pattern maps, flood risk maps, and forest canopy maps. In order to get the proposed outputs, image classification was needed. Due to the limitation of the possible polarizations (HH, VV) of the TSX sensor data, using only unique date images for establishing the required agricultural classification is unlikely to achieve accurate results. Therefore, multi-temporal approaches were used to increase the classification accuracy through enabling mapping of temporal changes due to plant growth, especially for mapping cropping pattern and forest canopy. Therefore, the images for each study area were stacked together into individual imagery. Each imagery had many bands representing the different acquisition dates in both polarizations. A scheme of the classification steps and the role of field survey in it is exposed in Figure 10.

Supervised Maximum Likelihood Classifier (MLC) and Decision Tree Classifier (DTC) were used to generate the classifications. The MLC uses image pixels representing regions of known, homogenous surface composition in the training areas to classify unknown pixels based on the probability that a pixel falls within a certain class (Fröhlich et al. 2013, Richards 2009). The DTC builds classification in the form of a tree structure. It performs multistage classifications by using a series of binary decisions to place pixels or objects into classes. Each decision divides the pixels in a set of images into two classes based on an expression. Each new class can be divided into two more classes based on another expression. As many decision nodes as needed, can be utilized. The results of the decisions are classes. The Decision Tree classification method can be applied to pixel-based classification in the same way as traditional classification algorithms would be applied.

It can also be used to generate rules for knowledge-based and possibly object-based classification with different types of attributes (Fröhlich et al. 2013, Richards 2009, Lillesand et al. 2015).

Beside the conventional pixel-based classification method, the object-based classification method and the plot-based statistical analysis method were carried out to acquire the outputs of the research.

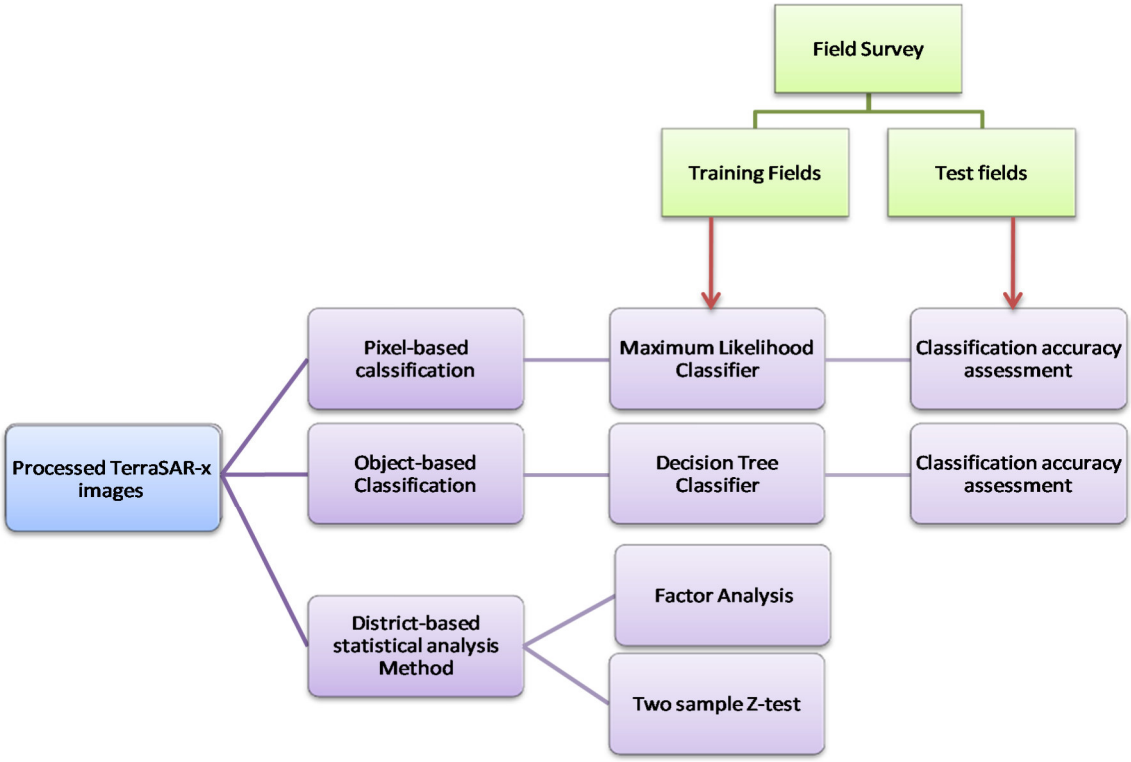

Figure 10: Scheme of the steps of image classification of this research

3.4.1. Pixel-based classification Method

Pixel-based image processing classifies single pixels according to their spectral reflectance (Richards 2009, Lillesand et al. 2015). The classifications were produced using the classifier tools in ERDAS Imagine software. Supervised classifications were generated using the MLC. The fields surveyed in each pilot area were divided into a training fields group which was used as reference data, and a testing fields group which was used for assessing the accuracy of the produced classifications. These test fields were assumed as remote inaccessible areas to test the possibility of considering the classification of the real remote areas. The classifications were carried out based on several attempts using all available acquired dates, besides attempts representing partial periods

based on crop calendar or leaf-cycle, in addition to attempts using single polarization. The Model Maker of ERDAS imagine was used to combine the individual crop classifications together to produce crop calendar classifications. This classification process was implemented in Paper I and Paper III.

3.4.2. Object-based classification Method

Object-based image processing classifies the objects, which it segmented. It divides an image into a network of homogeneous image objects by grouping together neighboring pixels with similar feature values such as brightness, texture, color, etc. Image texture provides information about the spatial arrangement of color or intensities in an image or selected region of an image. Homogeneous objects have additional information relevant to classification, such as shape, texture and relationships to neighboring objects. The classification of image objects is carried out after segmentation. Thus, contextual classification is based not only on spectral statistics, but also on the additional information including shape, texture and network relationship, and this enables the segmented image objects to be related to land cover classes. This classification provides usually better results since it reduces salt-and-pepper noise in the classification results (Richards 2009, Lillesand et al. 2015).

The object-based classification method was processed by the Rule-based classifier in the ENVI EX program. Envi EX has a tool that utilizes object-based processing named Feature Extraction. Feature Extraction is a tool for extracting information from high-resolution panchromatic or multispectral imagery based on spatial, spectral, and texture characteristics. It uses an object-based approach to classify imagery through segmenting the image into regions of pixels, computing attributes for each region to create objects, and classifying the objects based on those attributes (ITT Visual Information Solutions 2008). In this research, a DTC algorithm was applied using the rule-based classifier to generate the land-use/land-cover maps (LULC). The LULC maps included four features, namely water, forest, vegetated lands and residential areas, where each feature has different roughness and texture characteristics. Initially, the water class and land class were defined. Then, the land class was isolated and classified as either flat terrain, such as vegetated lands, or uneven terrain, including forests and residential areas. Lastly, the uneven terrain class was detached and further classified as either forest class or residential class.

This classification method was carried out in Paper II.

3.4.3. Classification accuracy assessment

The produced classifications were analyzed using the spatial module under ARCGIS to estimate the distribution of the classification with respect to the class distribution within the test fields. The distribution results were exported into dBase format and thus transformed into excel files to calculate accuracy assessment parameters including the user accuracy for each class, the producer accuracy for each class, the Kappa index for the whole classification, and the total accuracy for the entire classification (Kumar et al. 2016).

3.5. District-based statistical analysis Method

Due to the inadequate classification accuracy, statistical analysis tests on the imagery backscattering can be used to distinguish between the classes in different districts.

In this research, Factor Analysis as a multivariate statistical technique, and Two sample Z-test as an inferential statistical test were carried out on the districts examined in this study. Subsets of these districts were created in ERDAS imagine using the stacked imagery, to analyze the backscattering coefficient (σ_0) for each pixel in decibels (dB). The σ_0 values of these districts were transferred to ASCII files using the tools available under ERDAS imagine. The ASCII files were then used as input for the statistical analysis software SPSS. The variables were the values of σ_0 for each acquisition date in both HH and VV polarization. Boxplots were employed to visualize the data distribution. A boxplot shows five statistical parameters (minimum, first quartile, median, third quartile, and maximum); this approach is useful when different variables represent a single characteristic measured at different times (King and Mody 2011).

3.5.1. Factor Analysis

Multivariate statistical techniques such as Factor Analysis (FA) offer a more integrated approach to multi-element analysis, in which the interrelationships of all the elements in a data set are modeled concurrently. FA is a statistical method for determining the regularity and order of phenomena and as such can be applied to identify the underlying structure in data. In other words, it explains multivariate relationships (correlations) between observations (indicators) by a smaller number of not directly observable variables (factors), while these factors are responsible for the correlations between the observable variables (Gorsuch 1983, Mulaik 2009, Klovan 1972).

Four main stages were applied in the FA analysis of the ASCII files. At first, initial solutions were produced to determine the inter-correlation matrix among all of the variables. Then, an appropriate number of components (factors) was extracted from the correlation matrix based on the initial solutions for factors with eigenvalues greater than or equal to 1.0. In some cases, one or more variables may load about the same on more than one factor, and for this reason, it is difficult to clearly identify factors. Therefore, factors were rotated in order to clarify the relationship between the variables and the factors. The Orthogonal Varimax method was used as rotation method since it can produce factor structures that are uncorrelated (Mulaik 2009, Syvitski 2007, Kaplunovsky 2005). Finally, results were derived by analyzing the factor load of each variable to identify the different factors. The FA was carried out for each polarization individually.

3.5.2. Two sample Z-test

Two sample Z-test is an inferential statistical test that determines whether there is a statistically significant difference between the means of two independent groups (Syvitski 2007, Fisher 1987, Markowski and Markowski 1990). The Two sample Z-test was used to test whether the mean backscatter coefficient of a district is a statistically significant difference from the mean backscatter coefficient of another district. New SPSS file was generated with four variables including the acquisition dates, the polarization type, the district class, and the backscatter coefficient. This file was used to check if the values of the backscatter coefficient were normally distributed and to calculate the number of records (n_i), the mean ($\overline{x_i}$) and the standard division ($ó_i$) of each examined group. The Z-score (Z) was calculated according to equation (1) (Syvitski 2007, Fisher 1987, King and Mody 2011, Markowski and Markowski 1990).

$$Z = \frac{(\overline{x_1} - \overline{x_2})}{\sqrt{\frac{ó_1^2}{n_1} + \frac{ó_2^2}{n_2}}}$$ ---------- Equation (1)

Where:

$\overline{x_1}$ and $\overline{x_2}$ are sample average of group1 and group2,

$ó_1$ and $ó_2$ are the standard deviations of both populations

and n_1 and n_2 are the number of samples in each group

Two tailed Probability Value (P-Value) was estimated based on Z-score tables for two tailed hypothesis. Finally the P-value was evaluated at a confidence level of 95%. If the P-Value was less than 0.05, then there was significant difference between the two groups. If the P-Value was greater than 0.05, then there was likely no significant difference between the two groups (Syvitski 2007, Fisher 1987, Markowski and Markowski 1990).

The above stated statistical analysis methods were applied in Paper III.

4. RESULTS

The results of the study were published in three papers. The title of these papers and a comprehensive summary of each of them are given below.

4.1. Paper 1

TITLE:

"Observing the Middle Elbe Biosphere in Germany by Means of TerraSAR-X Images"

AUTHORS:

Dalia Farghaly, Emad Elba, Brigitte Urban

4.1.1. Background

Paper I focused on the agricultural land-uses in the Lower Saxonian Elbe Valley Biosphere Reserve, which are considered the major land-use there (Urban 2003, Urban et al. 2011, Krüger and Gröngröft 2003).

One of tasks of the Biosphere Reserve Administration is to develop sustainable forms of land uses which requires comprehensive updated land cover maps, especially of the agricultural land-uses (Urban 2003, Urban et al. 2011, Krüger and Gröngröft 2003).

In this paper, the TerraSAR-X images were processed and classified to produce cropping pattern maps for two pilot areas in the Biosphere Reserve of Elbe River in Lower Saxony.

4.1.2. Study objective

This paper aimed to study the factors affecting the crop classification in order to achieve better crop classification results, where the classification process identifies patterns of similar characteristics according to the corresponding observed backscattering response and their temporal progress.

The paper investigated several parameters that influenced the accuracy of the agricultural land uses classifications produced using the TSX images, namely:

- the effect of the number of used images,
- the effect of using speckle noise filters,
- the necessity of using single or dual polarization,
- the consequences of some missing images within the crop calendar, and
- the importance of considering the cultivation period of each crop (crop calendar)

4.1.3. Methodology

The study was applied to two pilot areas in the Elbe Biosphere Reserve. These areas are situated around the oxbows Wehninger Werder and Walmsburger Werder as shown in Figure 11.The inputs of this research paper included the following:

- location maps of the Elbe Biosphere Reserve and the two oxbows,
- 24 High resolution spot TSX co-dual-polarized imagery including:
  - eight images over Wehninger Werder in 2011,
  - seven images in 2010 over Walmsburger Werder, and
  - nine images in 2011 over Walmsburger Werder,
- five times field survey in 2011 including:
  - 150 fields around Walmsburger Werder covering 1550 hectares (80% of arable lands),
  - 300 fields around Wehninger Werder covering 1860 hectares (70% of arable lands),
- two geodatabases for the survey results of both study areas.

Two filters were applied to decrease speckle noise namely De-Grandi as multi-temporal speckle filtering, and Lee as an adaptive filter (Gagnon 1999, Lee et al. 1997, Lee et al. 2008, DeGrandi 1997). Multi temporal classification method was used to identify the different crops using pixel-based maximum likelihood classifier (Richards 2009, Lohmann et al. 2009b). The classification accuracy was assessed based on the external user accuracy for each crop, the external producer accuracy for each crop, the Kappa index and the external total accuracy for the entire classification (Rossiter 2004, Mansourpour et al. 2006). For each filter several classifications were generated including 16 classifications around the Wehninger Werder in 2011, 15 classifications in 2010 and 19 classifications in 2011around the Walmsburger Werder. Finally, the classifications with the

highest accuracy were selected to produce the cropping pattern maps. Three cropping pattern maps were produced namely:

- the cropping pattern map of Wehninger Werder in 2011,
- the cropping pattern map of Walmsburger Werder in 2010, and
- the cropping pattern map of Walmsburger Werder in 2011.

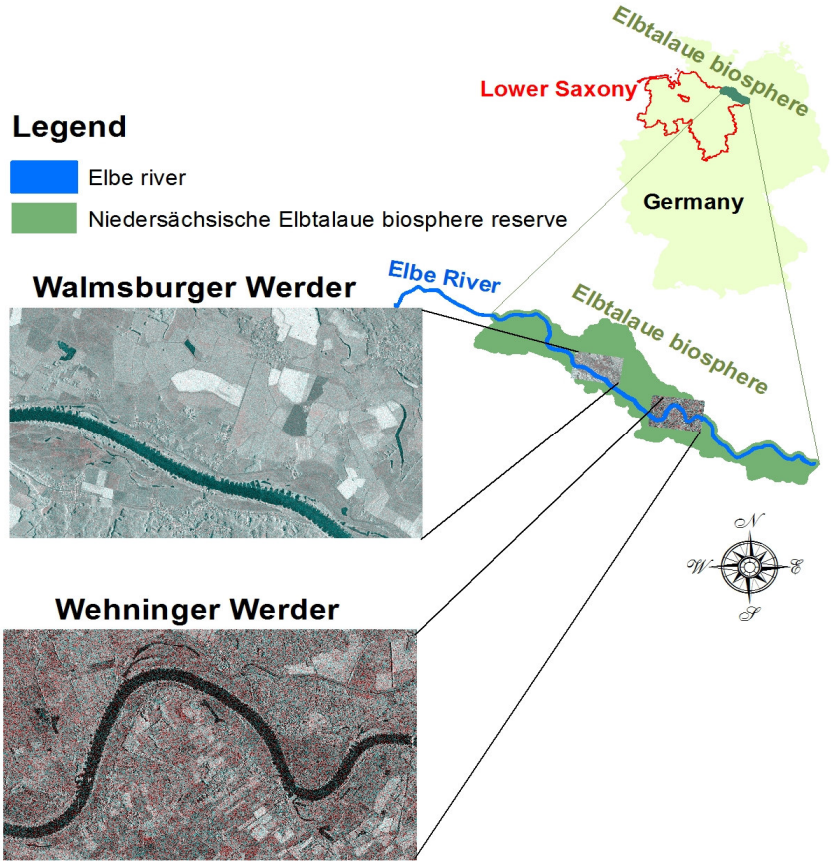

Figure 11: Location of the study areas in Lower Saxony Elbtalaue Biosphere Reserve and zoom into the TerraSAR-x images over the investigated areas around Wehninger and Walmsburger Werder in July 2011

4.1.4. Results and discussions

The producer accuracy was used to assess the accuracy of the classifications produced in this study. A comparison between the total producer accuracy of the classifications produced using all the images, and according to crop calendar, in addition to the HH-polarized imagery and VV-polarized images is given in Table 1. This table exposed that, the accuracy of the classifications produced using the HH-polarized imagery was less the one generated using the VV-polarized imagery.

However, using HH-polarized and VV-polarized imagery simultaneously lead to higher producer accuracy than using them individually as given in Table 1. Furthermore, using all the imagery in producing the classification enabled high producer accuracy almost equal to the one generated using imagery according to the crop calendar of each crop.

Table 1: Summary of the producer accuracy for the total accuracy using both Lee and De Grandi filtered imagery around Walmsburger Werder and Wehninger Werder in 2011 based on the crop calendar, all images, all VV-polarized images and all HH-polarized images

	Degrandi Filter			Lee Filter		
	Walmsburer	**Wahninger**	**Average**	**Walmsburer**	**Wahninger**	**Average**
HH	88	83	**85.5**	78	73	**75.5**
VV	90	90	**90**	82	79	**80.5**
CAL	93	91	**92**	86	81	**83.5**
All	92	93	**92.5**	86	84	**85**

A summary of the producer accuracy for each crop and total producer accuracy of the classifications produced using the imagery according to the crop calendar of each crop is exposed in Table 2. As shown in this table, using De-Grandi filter enhanced the producer accuracy of the classification by approximately 10% than these classifications produced using the Lee filtered imagery. The best result is attained for potato fields cultivated around the Wehninger Werder, where its external producer accuracy is 100%. On the other hand, the worst result is gained for the sugar-beet root fields cultivated around Walmsburger Werder in 2011 with only 40%. Most of the crops had high producer accuracy of over 85% especially these produced using the imagery processed with De-Grandi filter.

The study showed that image filtering was essential for enhancing crop classification results. The multi temporal filter De-Grandi enhanced the producer accuracy by about 10% compared to the Lee filter. Furthermore, gathering and utilizing large ground truth data of over 150 fields in 2011 greatly enhanced the accuracy of the classification with regards to the results of the classification acquired using just 50 fields as in 2010. The research verified that using sequence images covering the growing season usually improved the classification results, where missing acquisitions within the cultivation period decreased significantly the attained classification producer accuracy. The results exposed the effect of the polarization, where using VV-polarized data enabled on average 5% higher classification accuracy than the HH-polarized data, however using both polarization lead to about 3% better classification accuracy than the VV-polarized imagery. The study

demonstrated that the majority of the classifications produced according to the crop calendar had higher total producer accuracy than using all acquisitions.

Table 2: Summary of the producer accuracy for the different crops and the total accuracy using both Lee and De Grandi filtered imagery according to the crop calendar around Walmsburger Werder and Wehninger Werder in 2011

Crop	2011						2010	
	De- grandi filtered imagery			Lee-filtered imagery			Degrandi	Lee
	Walmsburer	Wahninger	Average	Walmsburer	Wahninger	Average	Walmsburer	
Cereals	97	92	**94.5**	90	79	**84.5**	74	70
Grassland	89	91	**90**	80	85	**82.5**	78	94
Maize	90	91	**90.5**	81	84	**82.5**	62	52
Potato	94	100	**97**	89	95	**92**	94	94
Sugarbeat	40	96	**68**	77	96	**86.5**	76	60
Sun Flower	73	95	**84**	61	92	**76.5**		
Rapeseed,	93	89	**91**	92	68	**80**	89	79
Rye-Grass	95	50	**72.5**	93	57	**75**		
Total	**93**	**91**	**92**	**86**	**81**	**83.5**	81	75

4.1.5. Conclusion and Recommendations

This study was conducted on accessible fields. Over 50% of these fields were used as testing fields for evaluating the external producer accuracy for the generated classifications. The classification result showed high external producer accuracy. Thus this method can be applied to other remote areas. These agricultural land uses maps produced in this study can be used in monitoring crop phenological phases and crop distribution, which can lead to enhance crop economics, protect ground water quality and protect the Biosphere Reserve. Obtaining the previous targets will promote the economic, social and environmental sustainability, and finally will enable the sustainable landscape development. It is recommended to generally monitor the whole Biosphere Reserve using TerraSAR-X images, according to the role of remote sensing in sustainable development stated in chapter 1.4, in order to prevent any environmental problems due to misuse of these protected areas, and to protect ground water quality ofthem, which can enable sustainable landscape on the long term.

4.2. Paper 2

TITLE:

'Towards Sustainable Land Uses within the Elbe River Biosphere Reserve in Lower Saxony, Germany by Means of TerraSAR-X Images'

AUTHORS:

Dalia Farghaly, Emad Elba, Brigitte Urban

4.2.1. Background

Paper II focused on the flood hazards in both rural and urban regions in the Lower Saxonian Elbe Valley Biosphere Reserve. Floods considered the source for huge risks mainly in urban areas, resulting in severe impacts on people, industry and economy (Besselet al. 2013, Kienzler et al. 2014, Mudersbuch et al. 2013). The extreme flood of 2013 and the consequent damages demonstrate that new flood risk management plans are required (Gremli et al. 2014). Several land uses can be found in this area including many cities, roads, industrial areas, forests and arable lands in and around the flood zone (Prüter et al. 2014, Urban 2003, Urban et al. 2011). These various land uses promote the need of investigating the present and the future flood hazards.

4.2.2. Study objective

The paper investigated the possibility of using the decision tree object-based classifier in determining the major land uses and the inundation extent areas in 2011 and 2013. Based on the maps produced for the land uses and inundation areas, the hazard areas due to the floods in 2011 and 2013 were identified. The study was applied to two pilot areas in the Lower Saxonian Elbe Valley Biosphere Reserve. These areas are situated around the oxbows Wehninger Weder and Walmsburger Weder as shown in Figure 12.

The inputs of this research paper included the following:

- location maps of the Elbe River and the main gauges along it,
- location map of the Biosphere Reserve and the two oxbows investigated in this research,
- the flood extent maps in June 2013 as represented by DLR,
- four High resolution Spot TSX co-dual-polarized imagery including:

- two images over Wehninger Weder in 2011 for pre-flood and post-flood periods, and
- two images over Walmsburger Weder in 2011 for pre-flood and post-flood periods,

- two databases for the water levels measured by Wasser - und Schifffahrtsverwaltung des Bundes (WSV), and provided by Bundesanstalt für Gewässerkunde (BfG) during the period from January 2010 till December 2012 and in June 2013 at two gauges along Elbe River, as shown in Figure 9, namely :
  - Neu Darchau gauge on Walmsburg Werder, and
  - Damnatz gauge on Wehningen Werder,
- digital elevation model (DEM) in one meter spatial resolution for the floodplain of both study areas, and
- geo-databases for the gauge locations along Elbe River, the Elbe River, and the Lower Saxonian Elbe Valley Biosphere Reserve.

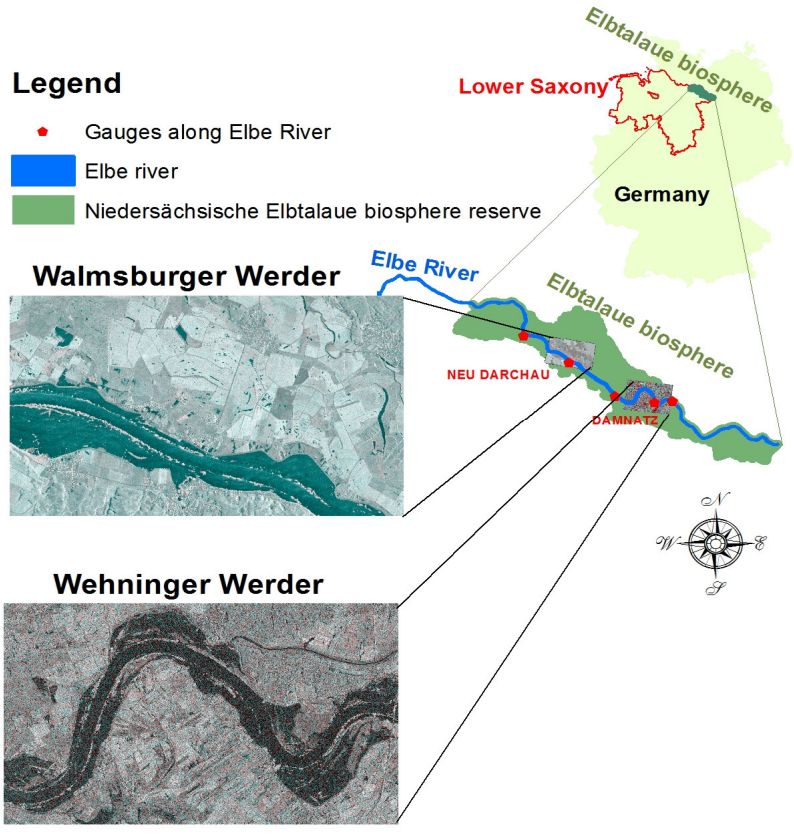

Figure 12: Location of the study areas and the main gauges on Elbe River in the Lower Saxonian Elbe Valley Biosphere Reserve and zoom into the flooded areas in January 2011

4.2.3. Methodology

For the post flood period, at Walmsburger Werder, the TSX imagery acquired on 19th January 2011 was used, where the average water level was 12.35 m AMSL. At Wehninger Werder, the TSX imagery acquired on 25th January was used, where the mean water level was 16.17 m AMSL. For the pre flood period, TSX imagery acquired on 22nd June 2011 with average water level of 7.24 m AMSL at Walmsburger Werder were used, while the one on 28th June 2011 with average water level of 11.05 m AMSL at Wehninger Werder was considered. All post and pre flood images were taken in descending orbit direction. Both pre flood imagery were used to define the land uses while the post flood images were used in mapping the flooded areas. The land use maps and the detection maps were used in evaluating the hazards due to January 2011 flood and to identify the risk zones.

The adaptive filter Lee was applied to the TSX images for both pre and post flood periods (Lee et al. 1997, Lee et al. 2008). A Decision-Tree classification algorithm was applied using the rule-based classifier on both non-filtered and lee-filtered images, as shown in Figure 13 (Burt et al. 2009, Senthilnath et al. 2013, Lillesand et al. 2015, Manjusree et al. 2012). The pre-flood images in both study areas were used to identify the land uses. The radar signals returned from water bodies, such as rivers and lakes, have low backscatter. These areas, therefore, are mostly dark on the TSX imagery (Townsend 2001, Giustarini et al. 2013). The backscatter from forests and residential areas is mainly volume scattering. The back-scatter from vegetation-covered areas, such as grasslands, croplands and bare soil fields, depends on the crop types and their distribution on the fields. The scattering from roads is affected by the trees on either side, so they show up as bright lines on radar imagery. In contrast, roads not lined with trees are less visible and may be mistaken for water. Generally, the land cover types in both study areas are complex or mixed, so that different features may show similar physical scattering mechanisms (Lillesand et al. 2015, Manjusree et al. 2012, Richards 2009).

Therefore, the water class and land class were defined in a first step. Then, the land class was isolated and classified as either flat terrain, such as vegetated lands, or uneven terrain, including forests and residential areas. Lastly, the uneven terrain class was detached and further classified as either forest class or residential class. The concepts of natural breaks and clustering were used to define the decision boundaries. Finally, land classified as vegetated was also subdivided as either crop land or grass; this classification was imported here from previously performed and reported

work, which is described in chapter 4.1 for Paper I (Farghaly et al. 2014). The study investigated several parameters that can affect the classification accuracy such as:

- the effect of classifying the Lee-filtered and the non-filtered images,
- the effect of using single and/or dual-polarization, and
- the effect of using the spatial attributes and/or the spectral attributes for defining the decision tree rules and the effective attributes to be considered.

Similarly, based on the investigated parameters, the optimum classification methods with respect to the LULC classification results were applied for mapping the flood extent areas for both study locations. The flood extent maps initially produced were corrected using the digital elevation model (DEM) for this area and the resulting LULC maps. The DEM was used to remove the regions misclassified as water within the area around the river that had a land level higher than the water level measured at the gauges. The LULC maps produced in this study were used to remove the forest and residential areas which were misclassified as water due to the limitations of x-band imagery in mapping the water areas beneath forest and urban coverage.

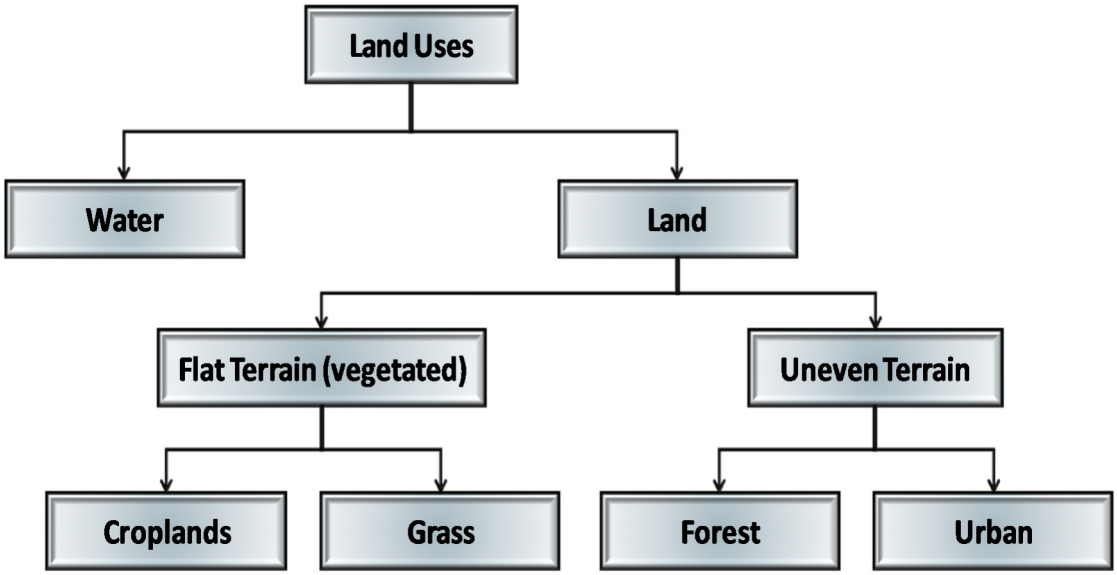

Figure 13: Decision tree classification algorithm for mapping land uses using the pre flood images

4.2.4. Results and Discussions

The study showed that the merging of similar pixels into objects diminishes the problem of speckle noise in the TSX imagery and, thus, enables high producer accuracies from the non-filtered images similar or even better results than the Lee-filtered images. Further, the use of dual-polarized images

enhances the classification results and leads to higher producer accuracies than the single-polarized data. The classification accuracy assessment verified that the Decision-Tree procedure applied in this study resulted in considerably better total producer accuracies, such that about 95% of the water area was accurately defined, as well as about 90% of vegetated lands being correctly determined, and around 80% of the forest and the residential area classes recognized. The 20% misclassified areas within the forest and residential areas were due to the existence of vegetated areas and trees within the residential areas around the buildings.

Furthermore, the research exposed that the use of texture and spatial attributes with the spectral attributes enhanced the classification results. Applying rules based on the band-average, as a spectral attribute, and the texture-mean facilitated correct identification of about 95% of the flood extent for post-flood imagery. Furthermore, the use of the texture-entropy attribute enabled recognition of about 90% of the vegetated lands. The texture-mean attribute enabled efficient distinguishing of residential areas and forest classes. On one hand, correcting areas misclassified as water within the residential areas enhanced the total producer accuracy by about 0.1%, while correcting areas misclassified as water within the forest resulted in an increase in the land producer accuracy of about 1.5%, and thus increase the total producer accuracy by about 1%. On the other hand, the DEM did not improve the classification results.

The flood detection maps produced for January 2011 were compared to the flood extent areas in June 2013 as represented by DLR, and to the high flood zone maps. The flood extent areas were approximately identical for 2011 and 2013 floods. Thus, the flooded areas as exposed in the maps produced for 2011 were used in defining the hazard areas for the winter flood in January 2011 and the summer flood in June 2013. The reference LULC maps, and the agricultural land use maps during the summer of 2011, produced in Paper I, were overlaid onto the flooded areas identified for January 2011 in order to determine the hazard areas.

The paper revealed that the residential areas did not experience any hazards in the pilot area around Walmsburger Werder, however four large cultivated fields were fully or partially submerged in 2011 as shown in Figure 14. These fields may be expected to be entirely submerged in future high floods since they are located within the high flood zone. Although, these four fields were flooded in January 2011, they were cultivated with maize and potatoes in summer 2011. These fields were again cultivated in summer 2013 and thus inundated in June 2013 with high economic losses to the owners of these fields. On the other hand, the cultivated area around Wehninger Werder was

not submerged and did not endure any hazards, however part of the residential area in the Strachauer Rad, in the city of Dannenberg, Lower Saxony, is located within the high flood zone as shown in Figure 15.

4.2.5. Conclusion and Recommendations

To achieve sustainable development in landscapes in this area, the fields inundated in 2011 and 2013 must be included in the flood hazard maps. The submerged areas around the Walmsburger Werder are located in Zone C of the Biosphere Reserve. This Zone is Reserved for those areas of the Biosphere Reserve which are especially worthy of preservation and care. Therefore, more regulations must be established to prevent cultivation in these areas, permitting the fields to be used only as grassland, in order to avoid economic losses. Although, the residential areas were not submerged during the most recent high floods, in 2011 and 2013, the areas located in the high flood zone and in Zone C of the Biosphere Reserve should be added to the hazard and risk maps to avoid the possible human and economic losses that may occur due to higher floods.

To conclude, the results show that similar rule sets can be used for the Decision-Tree procedure on two remote study areas in the Elbe River flood plains to achieve higher classification producer accuracies. Thus, the suggested Decision-Tree in Paper II should be applicable to other remote areas. Therefore, it is recommended to continuously monitor the entire Biosphere Reserve using TSX imagery, according to the role of remote sensing in sustainable development stated in chapter 1.4, in order to monitor new constructions such as residential building, in addition to the areas cultivated in the flood zone. Construction and cultivation in flood plains should be carefully planned according to the flood risk maps to ensure sustainable landscape development.

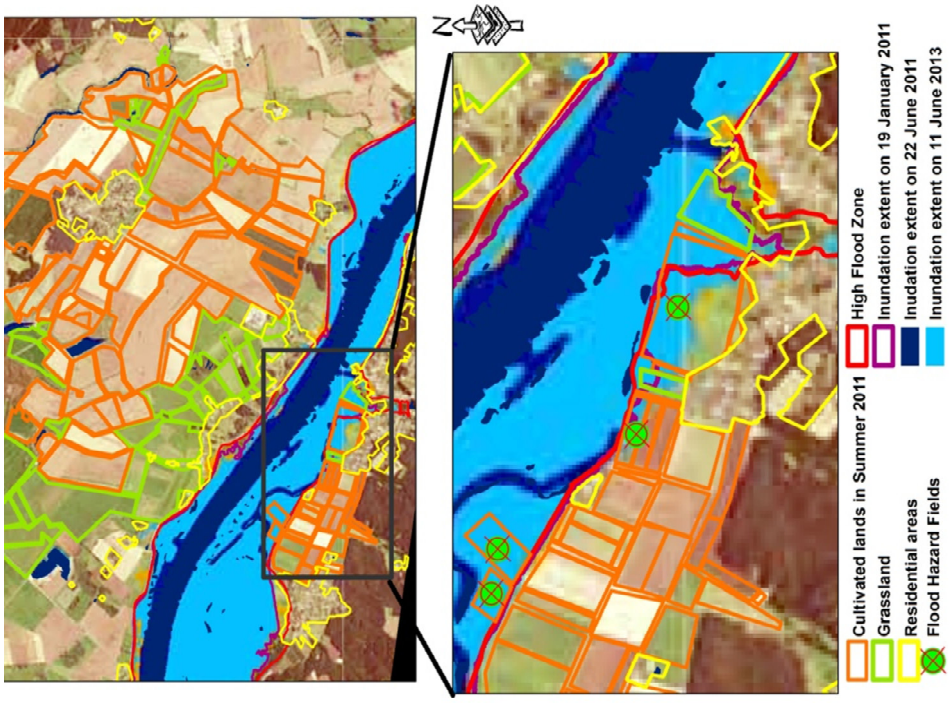

Figure 14: The flood extent of the flood in 2013 created by DLR overlaid with the flood extent in June and January 2011, the residential areas and agricultural land use in Summer 2011 at Walmsburger Werder.

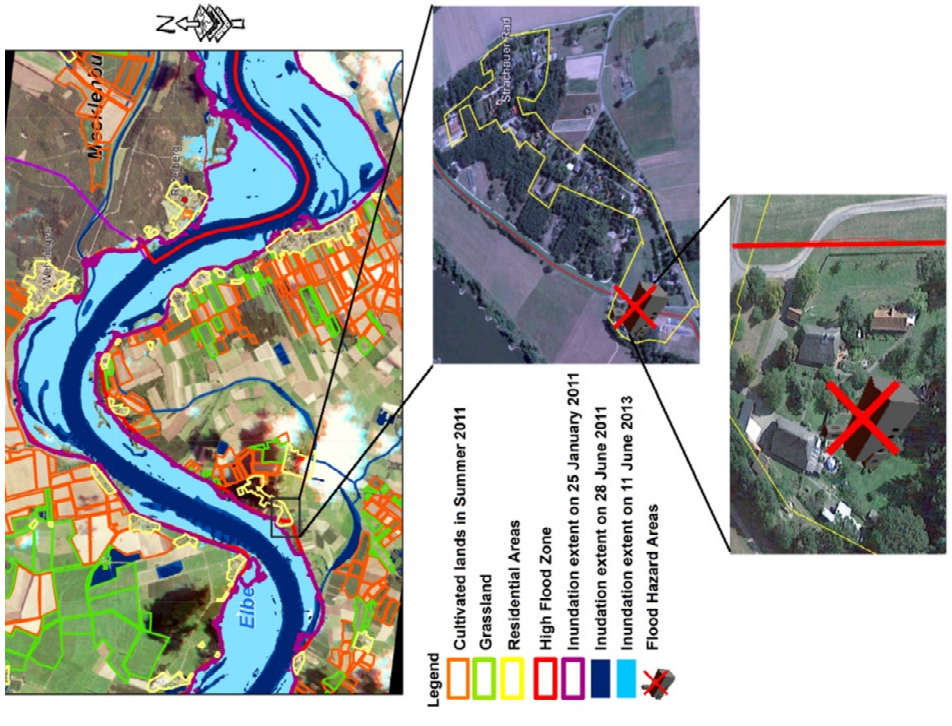

Figure 15: The flood extent due to the floods in 2013 produced by DLR overlaid with the flood extent in June 2011 and January 2011, the residential areas and the agricultural land use in summer 2011 at Wehninger Werder.

4.3. Paper 3

TITLE:

"Differentiating forest types using TerraSAR–X Spotlight Images based on inferential statistics and multivariate analysis"

AUTHORS:

Dalia Farghaly, Brigitte Urban, Uwe Sörgel, Emad Elba

4.3.1. Background

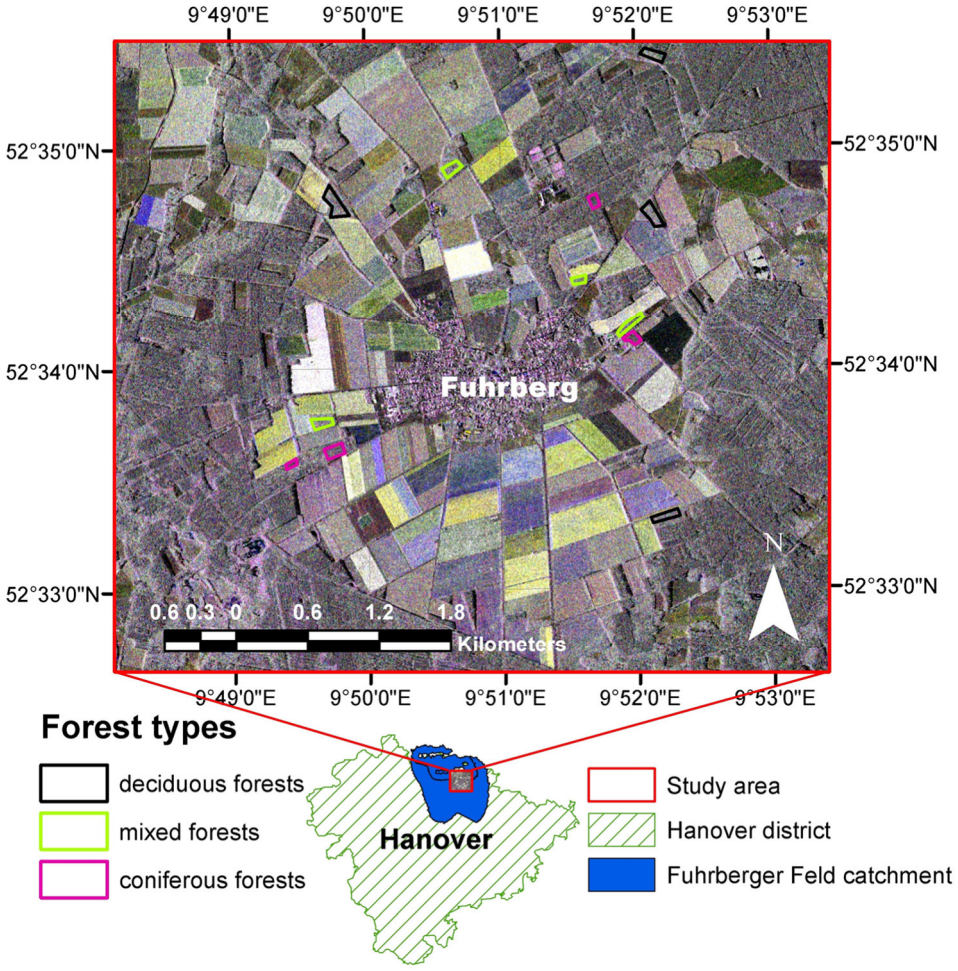

Figure 16: Location of study area overlaid by RGB color composite of TerraSAR-X images taken on 18 May 2008, 09 June 2008 and 01 July 2008 showing the investigated plots of the Fuhrberger Feld catchment area around the city of Fuhrberg: - Shape files source of Hanover district boundary and Fuhrberger Feld catchment boundary- ATKIS (Amtliche Topographisch-Kartographische Informationssystem)

Paper III focused on monitoring the types of the forests and their extension in a ground water protection area, where coniferous trees are replaced by deciduous trees to maintain groundwater quality and increase quantity. The study was applied to the water protection catchment area around Fuhrberg City near Hanover, Germany, as shown in Figure 16.

4.3.2. Study objective

This study investigated the forest classification based on maximum likelihood classifier MLK, beside the potential of applying statistical analysis tests, for example, two sample Z-test and the Factor Analysis (FA) tool, on the TerraSAR-X backscattering coefficient, in distinguishing between different types of forests and detecting the changes in distribution and extension of them. 12 pilot plots of forests were selected to cover the different types of forests in the Protection Zone Cas shown in Figure 16. These pilot areas were investigated in this study the input data of this research paper included the following:

- location maps of Fuhrberger groundwater catchment area,
- geo-database of Fuhrberger Feld catchment area and its groundwater protection zones ,
- geo-databases of the land-use type in the Fuhrberger Feld catchment area,
- field survey of the forest areas in the 12 pilot areas, and
- 14 high resolution spot TSX co-dual-polarized imagery in the period between March 2008 to January 2009.

4.3.3. Methodology

The images were coregistered, geocoded and processed using Lee filter. Using the Lee-filtered imagery, 18 supervised MLK classifications were generated for the pilot area around Fuhrberger Feld. Two types of classification were produced nine times to distinguish between coniferous forest and the deciduous and mixed trees forest, to test the use of each polarization individually and simultaneously during leaf-on, leaf-off and the whole acquisition period. Similarly, three types classifications were produced nine times to discriminate between coniferous deciduous and mixed forest. The produced classifications were assessed and the external producer accuracy for forest type and the overall total accuracy were estimated for each classification. The 12 surveyed forest plots were used as reference data, and half of them were used as training samples in producing the supervised classifications. The produced classifications were analyzed using the spatial module

under ARCGIS to estimate the distribution of the classification with respect to the forest type within the 12 test plots. The distribution results were exported into dBase format and thus transformed into excel files to calculate accuracy assessment parameters including, for example, the producer accuracy for each forest, and the total accuracy for the entire classification.

For the study area, the non-filtered imagery and those processed with the Lee filter were interpreted. The boxplots of the backscatter coefficient (σ_0) in (dB)on sample plots dominated by coniferous, deciduous, or mixed forest in the non-filtered imagery and the one preprocessed with the Lee filter were created to represent the minimum, first quartile, median, third quartile, and maximum σ0. These boxplots were used for a comparison of the multi-temporal behavior of the backscattered coefficient in a year during the leaf-off and leaf-on periods obtained from VV and HH acquisitions.

To describe the covariance structure among many variables in terms of a few underlying factors that are not directly observable, Factor Analysis was applied. In this study, this analysis was conducted by grouping the backscattering coefficient of the 14 acquisition times in a way that within-group correlations were large and between-group correlations were small. This step was accomplished by applying principal component analysis to the correlation matrix. The number of these groups was chosen based on the eigenvalues associated with each group, the plot of eigenvalue versus component number, and the cumulative proportion of variance by including additional groups, where every group stands for one axis in metric state space. The axes were interpreted by identifying the common characteristics of metrics. These metrics were computed to discern groups along individual axes and with similar loadings.

The two sample Z-test was carried out to compare the mean backscattering coefficient of coniferous, deciduous and mixed trees forest, obtained from Lee-filtered dual-co-polarized TSX data that were acquired from March 2008 to January 2009. The Kolmogorov-Smirnov test was run at first, and showed that σ0 values for both HH-, and VV-polarized data were normally distributed, and thus two sample Z-test can be carried out. The TZT was run on the entire acquisition period from March 2008 to January 2009, to compare the variation between forest types with respect to leaf-cycle, acquisition date and acquisition polarization.

4.3.4. Results and discussion

Studying the rotated factor loadings of $\sigma_0$of the coniferous, mixed and deciduous trees showed that the rotated factors were accounting for approximately 57% on average for the total variance in the data set for each examined polarization. For HH-polarized imagery, Factor 1 included significant loadings for σ_0 of the coniferous forest for the whole time series. Factor 2 and Factor 3 included significant loadings for σ_0 of the deciduous and mixed trees forest for the acquisition dates during the leaf-on period from May to October. On the contrary, Factor 4 and Factor 5 had significant loadings for σ_0 of the deciduous and mixed trees forest for the acquisition dates during the leaf-off period from November to April. For VV-polarized imagery, Factor 3 incorporated significant loadings for σ_0 of the coniferous forest for the 14 acquisition times. Factor 1 and Factor 2 included significant loadings σ_0 of the deciduous and mixed forest during the leaf-on period from May to October. Meanwhile, Factor 4 and Factor 5 included significant loadings for σ_0 of the deciduous and mixed forest during the leaf-off period from November to April. For both HH-, VV-polarized imagery, the loadings values of all the rotated Factors were higher than 0.5 with an average of more than 0.65.

The results of the TZT in comparison with the mean backscattering coefficient of deciduous and mixed tree forest of different acquisition dates during leaf-off and leaf-on periods demonstrated that mean σ0 of the deciduous forest was not significantly different from the mixed tree one during the leaf-on period from May to October ($p > 0.05$). However, means of these two forest types during the leaf-off period from November to April were statistically different ($p < 0.001$) for the HH- acquisition. For the VV- polarized acquisition, the TZT revealed that mean σ0 of the deciduous forest was not significantly different from the mixed tree forest during part of the leaf-on period from August to September at 95% confidence interval. ($p > 0.05$), and from May to July at 90% confidence interval ($0.05 > p > 0.01$). Nevertheless, means of these two forest types during the rest of the acquisition dates from October to April were statistically different ($p < 0.001$).

The classification results based on the multi temporal approaches for almost one year from March 2008 to January 2009 showed that the use of HH- and VV-polarized imagery acquired during the entire period could effectively distinguish between the class of coniferous forest and the combined class of deciduous and mixed forests. Nevertheless, poor classification results were obtained from the three-types classifications, since they failed to distinguish between the class of deciduous forest and the class of mixed tree. Therefore, we could not count on the classical classification methods in estimating the area of the mixed forest.

The study showed that Factor analysis tools succeeded in differentiating between the coniferous forest and both the deciduous forest and the mixed forest, and failed in discriminating between the

deciduous and the mixed forest. On one hand, only one factor was extracted for each sample plot of the coniferous forest with approximately equal loadings during the whole acquisition period from March 2008 to January 2009. On the other hand, two factors were extracted for each deciduous or mixed forest sample plot, where one factor had high loadings during the leaf-on period from May to October, and the other one had high loadings during the leaf-off period from November to April.

Furthermore, the research revealed that the two sample Z-test enabled not only the differentiating between the deciduous and the mixed forest against the coniferous forest, but also the discrimination between deciduous forest and the mixed tree one. Statistically significant differences were observed between the mean backscatter values of the HH-polarized acquisitions for the deciduous forest and the mixed tree one during the leaf-off period from November to April, meanwhile no statistically significant difference was found during the Leaf-on period from May to October. Moreover, plot samples for the deciduous forest had slightly higher mean backscattering coefficient than those for the mixed forest during the leaf-off period.

4.3.5. Conclusion and Recommendations

Applying the Factor Analysis and the two sample Z-test on the backscattering coefficient of multi-temporal TerraSAR-X data facilitates distinction of forest types, track changes in forest patterns, and estimate the extent of environmental disasters in forest regions. This accomplishes sustainable forest management, which can play an important role not only in preserving groundwater quality but also in achieving climate change adaptation goals.

While the emphasis in this study was on the identification of type of forests in the context of managing a ground water protection area, the analysis of σ_0 values obtained from multi-temporal TerraSAR-X by EFA and TZT can also be applied to monitoring forest areas, to track ecological processes, and to measure the extent of the damage caused by events such as fires or earthquakes. As this research explained, Factor Analysis and two sample Z-test could be an important tool for researchers and forest managers to monitor and protect the forest environment using remote sensing and to develop sustainable forest management and land use practices.

Therefore, it is recommended to continuously monitor the forest areas around groundwater protection areas using TSX imagery, according to the role of remote sensing in sustainable development stated in chapter 1.4, in order to monitor the replacement of coniferous forest into

mixed forest, which lead to enhanced groundwater quality. Obtaining the previous targets will initiate the economic, social and environmental sustainability, and finally will facilitate the sustainable development in landscapes.

5. CONCLUSION AND RECOMMENDATIONS

This study exposed part of the role of remote sensing in supporting the decision makers towards sustainable landscape development, as stated in chapter 1.4. The research investigated the use of TerraSAR-X imagery in monitoring three sites in Lower Saxony. Paper I and Paper II invested two pilot areas in the Lower Saxonian Elbe Valley Biosphere Reserve around Walmsburger Werder and Wehninger Werder. Paper III focused on a water protection area near Hanover.

Paper I showed the effectiveness of the TSX imagery in identifying the cropping pattern by employing pixel-based supervised maximum likely hood classifier. The study verified that the multi temporal filter De-Grandi enhanced the producer accuracy by about 10% compared to the Lee filter. Furthermore, gathering and utilizing large ground truth data enhanced the accuracy of the classification with regards to the results of the classification acquired using fewer ground truth data. It showed that using set of sequence images covering the growing season usually improved the classification accuracy in comparison to processing set with missing acquisitions within the cultivation period. Furthermore, the VV-polarized data enhanced the classification accuracy by 5% with respect to the HH-polarized data. The dual polarization data increased the classification accuracy by approximately 3%. Generally, the accuracy of the classifications produced according to the crop calendar was better than these produced using all acquisitions.

Paper II exposed the efficiency of using TSX imagery in determining the land uses and the flood risk maps by applying object-based decision tree classifier. The Decision-Tree procedure applied to the texture, spatial attributes and the spectral attributes enabled high producer accuracies. For example, 95% of the water area was accurately defined, 90% of vegetated lands being correctly determined, and 80% of the forest and the residential area classes were recognized. The study revealed that few cultivated fields were fully or partially submerged due to floods in 2011 and 2013. In addition part of the residential area is located in a high flood zone and did not exposed flood risk in 2011 and 2013.

Paper III demonstrated the potential of inferential statistics tests such as two samples Z-test and the multivariate analysis, for example Factor Analysis for identifying the kind of forest canopy, based on the backscattering coefficient of TSX imagery of forest plots. The results of the FA showed that one factor included significant loadings for σ_0 of the coniferous forest for the whole

time series, and two factors had significant loadings for σ_0 of the deciduous and mixed trees forest for the acquisition dates during the leaf-on period from May to October, in addition to two other factors with significant loadings for σ_0 of the deciduous and mixed trees forest for the acquisition dates during the leaf-off period from November to April. The results of the TZT demonstrated that mean σ_0 of the deciduous forest was significantly different from the coniferous forest all over the year, however it was not significantly different from the mixed tree one during the leaf-on period from May to October and statistically different during the leaf-off period from November to April.

The results of this study emphasizes the role of remote sensing in sustainable landscape development, through using the output maps in planning and monitoring the investigated areas in a sustainable approach. For each study area part of the surveyed area was used as training data and the other part was used in testing the effectiveness of the applied methods. Thus, the methods of this study can be applied to any accessible or remote landscape areas. During the last century, numerous number of optical and RADAR satellite imagery were launched. Furthermore, the images taken by the unmanned aerial vehicle start to be widely used. Therefore, it is recommended to enlarge the role of remote sensing in ecology and sustainable research to facilitate reaching remote areas and enable investigating huge study area by a cost and time effective method and help in achieving our main goal of sustainable development in landscapes.

PUBLICATION BIBLIOGRAPHY

Auty, R. M. & Brown, K. (1997): Approaches to sustainable development. Global development and the environment. London: Pinter. ISBN: 9781855674394.

Azapagic, Adisa & Perdan, Slobodan (2011): Sustainable development in practice - Case studies for engineers and scientists. Chichester, Hoboken: Wiley-Blackwell, 2ed. ISBN: 9780470718728.

Balz, T., Soergel, U., Crespi, M. & Osmanoglu, B. (Eds) (2018): Advances in SAR. Sensors, methodologies, and applications. Basel: Remote Sensing, MDPI. ISBN: 9783038971825.

Barrow, C.J. (2006): Environmental management for sustainable development. London: Routledge, 2ed. ISBN: 9780415365345.

Becker, C. U. (2012): Sustainability ethics and sustainability research. Dordrecht: Springer. ISBN: 9789400722842.

Becker, N. (2013): Water policy in Israel- Context, issues and options. Global Issues in Water Policy, vol 4, Dordrecht: Springer. ISBN: 9789400759107.

Becker, J., Keienburg, T., Kittel, A., Kretschmann, N., Kruse, E., Mersch, I., Nehlsen, E., Prüter, J., Urban., B.& Zimmermann, T. (2014): KLIMZUG-NORD - Klimaanpassung in der Metropolregion Hamburg. Beispiele für inter- und transdisziplinäre Forschung in Modellgebieten. In: Wege zur Anpassung an den Klimawandel, Biebeler, H., Bardt, H., Chrischilles, Mahammadzadeh, M., Striebeck, J. (eds), pp. 85–103. Köln: Institut der deutschen Wirtschaft, Medien GmbH. ISBN: 9783602149322.

Bell, V. J., Cheung, Y-K. A. (2009): Introduction to Sustainable Development. Oxford: EOLSS Publishers. ISBN: 9781848262225.

Bessel, T., Möhrle, S., Dittrich, A., Schröter, K., Mühr, B., Elmer, F., Kunz-Plapp, F., Trieselmann, W. & Kunz, M. (2013): Flood in Central Europe - Focus Germany Report 2 - Update 1: Impact and Management. Karlsruhe: Center for Disaster Management and Risk Reduction Technology (CEDIM). https://www.cedim.kit.edu/download/FDA-Juni-Hochwasser-Bericht2-ENG.pdf

Borchardt, D., Bogardi, J. J., Ibisch, R. B. (Eds.) (2016): Integrated Water Resources Management: Concept - Research and Implementation. s.l: Springer. ISBN: 9783319250694.

Burt, J.E., Barber, G.M. & Rigby, D.L. (2009): Elementary Statistics for Geographers. New York: The Guilford Press, 3ed. ISBN: 9781572304840

Chenghu, Z., Luo, J., Zang, C., Li, B. & Wang, S. (2000): Flood Monitoring Using Multi-Temporal AVHRR and RADARSAT Imagery. Photogrammetric Engineering & Remote Sensing 66 (5): 633–638.

Clini, C., Musu, I., Gullino, M. L. (2008): Sustainable development and environmental management - Experiences and case studies. Dordrecht: Springer. ISBN: 9781402065989.

Colby, Michael E. (1991): Environmental management in development – the evolution of paradigms. Ecological Economics 3 (3): 193–213. DOI: 10.1016/0921-8009(91)90032-A.

Conroy, Michael J.; Peterson, James T. (2013): Decision making in natural resource management: a structured, adaptive approach. Hoboken: Wiley. ISBN: 978 0470671740.

Cook, T. W.; Van Der Zanden, A. (2011): Sustainable landscape management – Design, construction, and maintenance. Hoboken: Wiley. ISBN: 9780470480939

Coulston, J. W., Reams, G. A., Wear, D. N. & Brewer, C. K. (2013): An analysis of forest land use, forest land cover and change at policy-relevant scales. Forestry 87 (2): 267–276. DOI: 10.1093/forestry/cpt056.

De Grandi, G. F., Leysen, M. , Lee, J. S. & Schuler, D. (1997): Radar Reflectivity Estimation Using Multiplicative SAR Scenes of the Same Target–Technique and Applications In: IGARSS'97. 1997 IEEE International Geoscience and Remote Sensing Symposium Proceedings. Remote Sensing - A Scientific Vision for Sustainable Development, Vol. 2, pp 1047–1050. DOI: 10.1109/IGARSS.1997.615338

Elliott, J. A. (2013): An introduction to sustainable development. New York: Routledge, 4ed. ISBN: 9780415590723

Enercity (2015): Enercity Wasser – Natürlich aus der Region – Seit über 100 Jahren. Hanover: Enercity Hannover. https://www.enercity.de/infothek/downloads/broschueren/wasser/trinkwasser-enercity.pdf.

FAO (2010): Global forest resources assessment 2010– Main report. Rome: FOOD AND AGRICULTURE ORGANIZATION OF THE UNITED NATIONS (FAO forestry paper, 163). http://www.fao.org/docrep/013/i1757e/i1757e.pdf.

Farghaly, D., Urban, B., Lohmann, P. & Elba, E. (2011): Differentiation and Extend of Aquatic Weeds over Lake Kyoga, Uganda by Multiple Remote Sensing Technology. In 4th TerraSAR-X Science Team Meeting, Oberpfaffenhofen: Deutschen Zentrum für Luft- und Raumfaht (DLR). http://sss.terrasar-x.dlr.de/papers_sci_meet_4/oral/LAN0499_Farghaly.pdf

Farghaly, D., Elba, E. & Urban, B. (2014): Observing the Middle Elbe Biosphere in Germany by Means of TerraSAR-X Images. International Journal of Geosciences 5:196–205. DOI:10.4236/ijg.2014.52021.

Farghaly, D., Elba, E. & Urban, B. (2016): Towards Sustainable Land Uses within the Elbe River Biosphere Reserve in Lower Saxony, Germany by Means of TerraSAR-X Images. Journal of Geoscience and Environment Protection 4: 97-121. DOI: 10.4236/gep.2016.43009.

Fisher Box, J. (1987): Guinness, Gosset, Fisher, and Small Samples. Statistical Science, 2 (1): 45–52. DOI:10.1214/ss/1177013437. JSTOR 2245613

Fröhlich, H. L., Schreinemachers, P., Stahr, K. & Clemens, Gerhard (Eds.) (2013): Sustainable land use and rural development in Southeast Asia – Innovations and policies for mountainous areas. Heidelberg: Springer. ISBN: 9783642333767

Gagnon, L. (1999): Wavelet Filtering of Speckle Noise – Some Numerical Results, Proceedings 12th Conference on Vision Interface (VI'99) Trois-Rivières, Québec, pp.336-343.

Geller, W. (2004): Schadstoffbelastung nach dem Elbe Hochwasser 2002 Endbericht des Ad-hoc-Projekts "Schad-stoffuntersuchungen nach dem Hochwasser vom August 2002 – Ermittlung der Gefährdungspotentiale an Elbe und Mulde. BMBF- PTJ 0330492, Leipzig: Kompetenzzenrum Digitaldr

Giustarini, L., Hostache, R., Matgen, P., Schumann, G.-P., Bates, P.D. & Mason, D.C. (2013): A Change Detection Approach to Flood Mapping in Urban Areas Using TerraSAR-X. IEEE Transactions on Geoscience and Remote Sensing 51: 2417-2430. DOI: 10.1109/TGRS.2012.2210901.

Gorsuch, R. L. (1983): Factor analysis, Hillsdale: Lawrence Erlbaum Associates, 2ed. ISBN: 9780898592023.

Gremli, R., Keller, B., Sepp, T. and Szönyi, M. (2014): European Floods - Using Lessons Learned to Reduce Risks. Zurich: Zurich Insurance Group Ltd.
https://www.zurich.com/_/media/dbe/corporate/docs/corporate-responsibility/european-floods-using-lessions-learned.pdf

Härdtle, W., Redecker, B., Assmann, T. & Meyer, H. (2006): Vegetation responses to environmental conditions in floodplain grasslands - Prerequisites for preserving plant species diversity. Basic and Applied Ecology 7 (3): 280–288. DOI: 10.1016/j.baae.2005.09.003.

Heinrichs, H., Martens, P., Michelsen, G.& Wiek, A. (Eds.) (2016): Sustainability Science. Dordrecht: Springer. ISBN: 9789401772419

Kienzler, S., Pech, I., Kreibich, H., Müller, M. & Thieken, A.H. (2014): After the extreme flood in 2002-Changes in preparedness, response and recovery of flood-Affected Residents in Germany between 2005 and 2011. Natural Hazards and Earth System Sciences 2: 6397-6451. DOI: 10.5194/nhessd-2-6397-2014.

Kim, S. J., Kim, J. & Kim, K. (2010): Organic carbon efflux from a deciduous forest catchment in Korea. Biogeosciences 7 (4), 1323–1334. DOI: 10.5194/bg-7-1323-201.

King, M. R. & Mody, N. A. (2011): Numerical and statistical methods for bioengineering. Applications in MATLAB. Cambridge: Cambridge University Press. ISBN: 978-0521871587.

Klovan, J. E. (1975): R- and Q-Mode Factor Analysis. In: McCammon RB (Ed) Concepts in Geostatistics. pp. 21–69. Berlin, Heidelberg: Springer. DOI: 10.1007/978-3-642-85976-2_2

Koppe, B., Lacay, B. & Peffer, G. (2008): RAMWASS Decision Support System (DSS) for the Risk Assessment of Water-Sediment-Soil Systems—Application of a DSS Prototype to a Test Site in the Lower Part of the Elbe River Valley, Germany. In: Samuels, P., Huntington, S., Allsop, W. & Harrop, J. (Eds). Flood Risk Management—Research and Practice. London: CRC Press, pp 385–395. DOI: 10.1201/9780203883020.ch45

Krüger, F. & Gröngröft, A. (2003): The Difficult Assessment of Heavy Metal Contamination of Soils and Plants in Elbe River Floodplains. Acta Hydrochimica et Hydrobiologic 31(4-5): 436-443. DOI: 10.1002/aheh.200300495

Kumar, P., Prasad, R., Choudhary, A., Mishra, V. N., Gupta, D. K. & Srivastava, P. K., (2017): A statistical significance of differences in classification accuracy of crop types using different classification algorithms. Geocarto International 32(2): 206-224. DOI: 10.1080/10106049.2015.1132483

Kundzewicz, Z.W., Pińskwar, I. & Brakenridge, G.R. (2013): Large Floods in Europe, 1985-2009. Hydrological Sciences Journal 58: 1-7. DOI: 10.1080/02626667.2012.745082

Lee, J. S., Grunes, M. R. & De Grandi, G. (1999): Polarimetric SAR speckle filtering and its implication for classification. IEEE Trans. Geosci. Remote Sensing 37(5): 2363–2373. DOI: 10.1109/36.789635

Lee, J., Ainsworth, T. L. & Chen, K. (2008): Speckle Filtering of Dual-Polarization and Polarimetric SAR Data based on Improved Sigma Filter. In: IGARSS 2008 - 2008 IEEE International Geoscience and Remote Sensing Symposium, Vol. 4: pp 21- 24. DOI: 10.1109/IGARSS.2008.4779646.

Lillesand, T. M., Kiefer, R. W. & Chipman, J. W. (2015): Remote sensing and image interpretation. Hoboken: Wiley, 7. ed. ISBN: 9781118343289.

LHW (2014): Bericht über das Hochwasser im Juni 2013 in Sachsen-Anhalt Entstehung, Ablauf, Management und statistische Einordnung. Magdeburg: Landesbetrieb für Hockwasserschutz und Wasserwirtscaft Sachsen-Anhalt (LHW).

https://docplayer.org/21786723-Bericht-ueber-das-hochwasser-im-juni-2013-in-sachsen-anhalt-entstehung-ablauf-management-und-statistische-einordnung.html

Lohmann, P., Soergel, U., Tavakkoli, M. & Farghaly, D. (2009a): Multi-Temporal Classification for Crop Discrimination Using TerraSAR-X Spotlight Images, In ISPRS Hanover 2009 – High Resolution Earth Imaging for Geospatial Information, Vol. 38 (1-4-7).

http://www.isprs.org/proceedings/XXXVIII/1_4_7-W5/p aper/Lohmann-129.pdf

Lohmann, P., Soergel, U. & Farghaly, D. (2009b): Classification of Agricultural Sites Using Time-Series of High Resolution Dual-Polarisation TerraSAR-X Spotlight Images. In the 29th Symposium of the European Association of Remote Sensing Laboratories, Chania, Greece - Imaging Europe. Amersterdam: IOS Press, pp 249-260. ISBN: 1607504936.

Manjusree, P., Prasanna K.L., Bhatt, C.M., Rao, G.S. & Bhanumurthy, V. (2012): Optimization of Threshold Ranges for Rapid Flood Inundation Mapping by Evaluating Backscatter Profiles of High Incidence Angle SAR Images. International Journal of Disaster Risk Science 3: 113–122. DOI: 10.1007/s13753-012-0011-5

Mansourpour, M., Rajabi, M. A. & Blais, J. A. R. (2006): Effects and Performance of Speckle Noise Reduction Filters on Active Radar and SAR Images. In ISPRS Topographic Mapping from Space, Ankara. Vol. 37(1/ W41). http://www.isprs.org/proceedings/XXXVI/1-W41/makaleler/Rajabi_Specle_Noise.pdf

Mangi, H. O. (2016): Tide Management in the Elbe River and Changes in Ecosystem Services. Advances in Ecology 2016(1): 1–13. DOI: 10.1155/2016/9519637.

Makhanya, E. M., Piper S. E. & Townsend, M.(1992): Mapping Rural Land Use in Selected Subsistence Farming Areas of South Africa Using Remote Sensing Products: In ISPRS Congress

Technical Commission VII: Interpretation of Photographic and Remote Sensing Data. Vol. 29(7): pp 675-682. http://www.isprs.org/proceedings/xxix/congress/part7/675_XXIX-part7.pdf

Markowski, C. A & Markowski, E. P. (1990): Conditions for the Effectiveness of a Preliminary Test of Variance. The American Statistician 44 (4): 322–326. DOI: 10.2307/2684360. JSTOR 2684360.

Marco, J.B. (1994): Flood risk mapping. In: Rossi G., Harmancioğlu N., Yevjevich V. (Eds) Coping with Floods. NATO ASI Series (Series E: Applied Sciences), vol 257: pp 353-373. Dordrecht: Springer. DOI: 10.1007/978-94-011-1098-3_20.

Morelli, J. (2011): Environmental Sustainability: A Definition for Environmental Professionals. JES 1 (1): 1–10. DOI: 10.14448/jes.01.0002.

Mulaik, S. A. (2010): Foundations of factor analysis. Statistics in the social and behavioral sciences series, Boca Raton: CRC Press - Taylor & Francis Group, 2 ed. ISBN: 9781420099614

Mudersbuch, M., Bender, J., Kelln, V. & Jensen, J. (Eds.) (2013): Analysis Flood Frequencies at the Elbe River—Do Recent Extreme Events Affect Design Levels? In the International Conference on Water Resources and Environment Research (ICWRER), Koblenz, pp 346-362.

Murray, J., Cawthorne, G., Dey, C. & Andrew, C. (Eds.) (2012): Enough for all forever - A hand book for learning about sustainability. Champaign, Ill: Common Ground. ISBN: 978-1612290140

Ochs, S., Pitz, W. (2007): The TerraSAR-X and TanDEM-X Satellites. In 2007 3rd International Conference on Recent Advances in Space Technologies, Istanbul, Turkey: IEEE, pp 294–298: DOI: 10.1109/RAST.2007.4283999

Ortiz, S. M., Breidenbach, J., Knuth, R. & Kändler, G. (2012): The Influence of DEM Quality on Mapping Accuracy of Coniferous- and Deciduous-Dominated Forest Using TerraSAR-X Images. Remote Sensing 4 (12): 661–681. DOI: 10.3390/rs4030661

Peacock, K. W. (2008): Natural resources and sustainable development. Global Issues, New York: Infobase Pub. ISBN: 9781438117454.

Pound, B., Braun, A., McDougall, C. & Snapp, S. (Eds.) (2003): Managing natural resources for sustainable livelihoods. Uniting science and participation, Routledge: Taylor & Francis Group: ISBN: 1844070263.

Prüter, J., Keienburg, T. & Schreck, C. (2014): Klimafolgenanpassung im Biosphärenreservat Niedersächsiche Elbtalaue - Modellregion für nachhaltige Entwicklung Berichte aus den Klimzug-Nord Modellgebieten - Band 5, neue Ausg, Hamburg: TuTech Innovation. ISBN: 9783941492714.

Purkis, S. & Klemas, V. (2011): Remote Sensing and Global Environmental Change. West Sussex, UK: Wiley-Blackwell. ISBN: 9781118687659.

Richards, J. A. (2009): Remote sensing with imaging radar. Signals and communication technology, Heidelberg: Springer. ISBN: 9783642020209.

Rodríguez, S. I., Roman, M. S., Sturhahn, S. & Terry, E. H. (2002): Sustainability Assessment and Reporting for the University of Michigan's Ann Arbor Campus: Master Thesis, University of Michigan. School of Natural Resources and Environment. https://books.google.de/books?id=xI4dgW2qzd4C.

Röling, Niels G. & Wagemakers, M. A. E (1998): Facilitating sustainable agriculture. Participatory learning and adaptive management in times of environmental uncertainty. Cambridge, U.K, New York: Cambridge University Press. DOI: 10.1046/j.1365-2664.1999.04465.x.

Rossiter, D. G. (2004): Statistical Methods for Accuracy Assessment of Classified Thematic Maps. Department of Earth Systems Analysis - University of Twente, Faculty of Geo-Information Science & Earth Observation (ITC), Enschede (NL). http://www.css.cornell.edu/faculty/dgr2/teach/R/R_ac.pdf

Sandro, M. (2010): Automatic Near Real-Time Flood Detection in High Resolution X-Band Synthetic Aperture Radar Satellite Data Using Context-Based Classification on Irregular Graphs. PhD thesis, Fakultät für Geowissenschaften, LMU München, München. https://d-nb.info/1009569163/34.

Schröter, K., Kunz, M., Elmer, F., Mühr, B. & Merz, B. (2014): What Made the June 2013 Flood in Germany an Ex-ceptional Event? A Hydro-Meteorological Evaluation. Hydrology and Earth System Sciences 11: 8125-8166. DOI: 10.5194/hessd-11-8125-2014

Senthilnath, J., Shenoy, H.V., Rajendra, R., Omkar1, S.N., Mani, V. & Diwakar, P.G. (2013): Integration of Speckle De-Noising and Image Segmentation Using Synthetic Aperture Radar Image for Flood Extent Extraction. Journal of Earth System Science 122: 559-572. DOI: 10.1007/s12040-013-0305-z

Simonović, S. P. (2009): Managing water resources. Methods and tools for a systems approach. Studies and reports in hydrology series – Earthscan, Paris, London: UNESCO.

Skakun, S., Kussul, N., Shelestov, A. & Kussul, O. (2014): Flood Hazard and Flood Risk Assessment Using a Time Series of Satellite Images: A Case Study in Namibia. Risk Analysis 34: 1521-1537. DOI: 10.1111/risa.12156

Soergel, U. (Ed.) (2010): Radar remote sensing of urban areas. Remote sensing and digital image processing, vol 15. Dordrecht: Springer Science+Business Media B.V. ISBN: 9789048137510

Solberg, S., May, J., Bogren, W., Breidenbach, J., Torp, T. & Gizachew, B. (2018): Interferometric SAR DEMs for Forest Change in Uganda 2000–2012. Remote Sensing 10 (2). DOI: 10.3390/rs10020228.

Střelcovà, Katarína (2008): Bioclimatology and natural hazards. Dordrecht, London: Springer. ISBN: 9781402088766.

Syvitski, J. P. M (2007): Principles, methods and application of particle size analysis. Cambridge: Cambridge University Press. ISBN: 9780521044615.

Tavakkoli, M. (2011): Multi-Temporal Classification of Crops Using ENVISAT ASAR Data. Ph.D. Thesis, Leibniz University of Hanover.

Tavakkoli, M., Lohmann, P. & Soergel, U. (2008): Monitoring Agricultural Activities Using Multi-Temporal ASAR ENVISAT Data. In ISPRS Congress Technical Commission VII, Peking, 2008. Vol. 37 (B 7-2): pp 735-742. http://www.isprs.org/proceedings/XXXVII/congress/7_pdf/5_WG-VII-5/02.pdf

Tevi G. & Tevi A. (2012): Remote Sensing and GIS Tech- niques for Assessment of the Soil Water Content in Order to Improve Agricultural Practice and Reduce the Negative Impact on Groundwater, Water Science & Technology Journal 66(3): 580-587. DOI: 10.2166/wst.2012.209.

Townsend, P.A. (2001): Mapping Seasonal Flooding in Forested Wetlands Using Multi-Temporal Radarsat SAR. Photogrametric Engineering & Remote Sensing 67: 857-864.

Turner, R. K. (1992): Economy and ecology: Towards sustainable development. Ecological Economics 6(2): 176–180. DOI: 10.1016/0921-8009(92)90013-I.

UN (1972): UN Documents Gathering a body of global agreements. Declaration of the United Nations Conference on the Human Environment. United Nations. Stockholm, Sweden. http://www.un-documents.net/unchedec.htm.

UN (1992): United Nations Sustainable Development, United Nations Conference on Environment & Development, 3 to 14 June 1992. AGENDA 21. United Nations. Rio de Janerio, Brazil. https://sustainabledevelopment.un.org/content/documents/Agenda21.pdf.

UN (1993): Agenda 21. Programme of action for sustainable development. Rio declaration on environment and development. New York: United Nations Department of Public Information.

UN (2002a): Johannesburg Declaration on Sustainable Development. World Summit on Sustainable Development. United Nations. Johannesburg, South Africa. http://www.un-documents.net/jburgdec.htm#fn3.

UN (2002b): Report of the World Summit on Sustainable Development. United Nations. Johannesburg, South Africa. http://www.unmillenniumproject.org/documents/131302_wssd_report_reissued.pdf.

UN (2012a): Back to Our Common Future Sustainable Development in the 21st. Summary for policymakers. United Nations. Rio de Janerio, Brazil. https://sustainabledevelopment.un.org/content/documents/UN-DESA_Back_Common_Future_En.pdf.

UN (2012b): The future we want. Resolution adopted by the General Assembly on 27 July 2012. United Nations. Rio de Janerio, Brazil. http://www.un.org/ga/search/view_doc.asp?symbol=A/RES/66/288&Lang=E.

UN (2015a): Spotlight on 2015: A New Sustainable Development Agenda and a Global Goal for Water and Sanitation. Geneve, Switzerland. United Nations (UN)-Water Technical Advisory Unit.

http://www.unwater.org/fileadmin/user_upload/unwater_new/docs/1_UN-Water_Annual_Report_2015_web.pdf.

UN (2015b): Transforming our world: the 2030 Agenda for Sustainable Development. United Nations. New York, USA. https://sustainabledevelopment.un.org/content/documents/21252030%20Agenda%20for%20Sustainable%20Development%20web.pdf.

UNEP (2011): The Bioenergy and Water Nexus, United Nations Environment Programme - UNEP.

UNESCO (2005): Full of life. UNESCO Biosphere Reserves, model regions for sustainable development. Berlin: Springer-Verlag.

UNESCO (2007): UNESCO-heute- Zeitschrift der deutschen UNESCO – Kommission UNESCO-Biosphärenreservate: Modellregionen von Weltrang, UNESCO, Germany.

UNESCO (2011):UNESCO - Biosphere Reserves in Germany, UNESCO.

Urban, B. (2003): River Elbe Ecology - Contributions to a Large Scale Environmental Project. In: Coastal Urban Environments (Ramesh, R. and Ramachandran, S., Eds), pp. 67–88. New Delhi, Kolkate, Bangalore, India: Capital Publishing Company.

Urban, B. , Krüger, F. Weniger, T. Prüter, J. Keienburg, T. Lang, F.& Graf, M.(2011): Auenböden der Elbe als Archiv für die Stoffdynamik im Einzugsgebiet. In Deutsche Bodenkundliche Gesellschaft DBG Exkursionsführer, Oldenburg/Berlin, 2011, pp. 42-59.

Urban, B., Becker, J., Mersch, I., Meyer, W. & Rottgardt, E. (2014): Berichte aus den KLIMZUG-NORD Modellgebieten, Bd. 6, Klimawandel in der Lüneburger Heide – Kulturlandschaften zukunftsfähig gestalten, Hamburg: TuTech Verlag. ISBN: 978-3941492721.

Vezzoli, C. & Manzini, E. (2008): Design for environmental sustainability. London: Springer. ISBN: 9781848001633.

Watson, R. T., Noble, I. R., Bolin, B., Ravindranath, N. H., Verardo, D. J.& Dokken, D. J. (2000): Land use, land-use change, and forestry. A special report of the IPCC. Cambridge: Cambridge University Press.

WCED (1987): Our Common Future. Geneva, Switzerland: Oxford University Press. http://www.un-documents.net/our-common-future.pdf.

WillisRe (2011). 2011 Rhein (Rhine) and Elbe Basin Floods, Germany—Report of 18th January 2011. Willis Re Analytics Event Response. http://www.willisre.com/documents/publications/Analytics/Analytics/Catastrophe_Management_Services/Event_Advisories/Willis%20Re%20Catastrophe%20Response%20Rhein%20Elbe%20Floods_v2.pdf

WHO (2005): Protecting groundwater for health: managing the quality of drinking-water sources. World Health Organization (WHO).

Wolf, R. (2013). Kurzumtriebsplantagen im Fuhrberger Feld Freisetzung und Verbrauch Klimarelevanter Spurengase und Kohlenstoffakkumulation beim Anbau nachwachsender Rohstoffe. Hamburg: Diplomica Verlag Gmbh. ISBN: 978-3842899728.

WRI (1998): World resources, 1998-99. Baltimore, Md, New York: WRI Publications; Oxford University Press.

APPENDIX A

Overview of Articles

I avouch that all information given in the AppendixA is true in each instance and overall.

Lüneburg, 25.12.2018

Dalia Mostafa Amer Farghaly

List of publications according to Guideline of Cumulative Dissertation of Faculty of Sustainability Science §1–14

Paper	Title	Author(s)	Authorship (§12)	WF	Publication type	Publication status (§9)	Conference contribution (§9b)
I	Observing the Middle Elbe Biosphere in Germany by Means of TerraSAR-X Images	DF, BU, EE	First author with predominant contribution	1	Journal article	published (2014) in International Journal of Geosciences, 2014, 5, 196-205	Using spotlight Terrasar-x images in screening the middle Elbe Biosphere Reserve in Lower Saxony. HIC 2012 - 10th International Conference on Hydroinformatics conference Proceedings, TuTech Verlag, Hamburg, reviewed paper and oral presentation, ISBN 978-3-941492-45-5
II	Towards Sustainable Land Uses within the Elbe River Biosphere Reserve in Lower Saxony, Germany by Means of TerraSAR-X Images	DF, BU, EE	First author with predominant contribution	1	Journal article	published (2016) in Journal of Geoscience and Environment Protection, 2016, 4, 97-121	Identifying the flooded arable lands within the Elbe River Lower Saxony Biosphere Reserve, Detuschland using Terrasar-x images. Paper ID 158. 8th International Congress on Climatic Change, Territorial Classification & Socio-Economic Crisis. Tiruchirappalli, Tamil Nadu, India, 23-27 April. Center for Remote Sensing & Department of Economics Bharathidasan Universtät (BDU) and Center for Interdisciplinary Studies on Environment and Development National Polytechnic Institute (IPN), Mexico D.F., Mexico, vol. 1, pp.32.
							Using Terrasar-x images to detect potentially flooded agricultural lands within the Elbe River Biosphere Reserve in Lower Saxony, Detuschland.,5th TerraSAR-X Science Team Meeting bei DLR, Oberpfaffenhofen, Detuschland,10-12 Jun. 2013.
III	Differentiating forest types using TerraSAR–X Spotlight Images based on inferential statistics and multivariate analysis	DF, BU, US, EE	First author with predominant contribution	1	Journal article	Published (2019) In Remote Sensing Applications: Society and Environment 15, p. 100238.	Differentiating forest types using Terrasar–X spotlight images based on factor analysis. The 8th International Conference for Development and Environment in the Arab World. Assiut, 22-24 Mar. 2016. Faculty of Science, Assiut University, Egypt, vol.1 pp. 69.
							Towards Sustainable forest management: Case study of using Terrasar-X spotlight images for categorizing forest types based on factor analysis. The 1st International Conference on Biological, Environmental Sciences and applications. Egypt-Luxor, 23-25 Mar. 2017. Naturals Sciences Publishing (NSP), Ref. 660, vol.1 pp. 22.
							Differentiating Forest Types using SAR Data based onFactor Analysis. 2018 International Conference on Energy, Environment, Development and Economics, Majorca - Spanien, 14-17 Jul. 2018. Oral Presentation, vol.1 pp.32.
	Total WF:			3			

* WF : Weighted Factor

Contributions of authors according to the Guideline of Cumulative Dissertation of Faculty Sustainability Science §12

Type of contributions	Paper I	Paper II	Paper III
Conception of research approach	DF, BU	DF, BU	DF, BU, US
Development of research methods	DF, BU	DF, BU	DF, BU, US
Data collection and data preparation	DF, BU, EE	DF, BU, EE	DF, BU, EE
Execution of research	DF, BU, EE	DF, BU, EE	DF, BU, EE
Analysis/Interpretation of data or preliminary results	DF, BU	DF, BU	DF, BU
Writing or substantive rewriting of the manuscript	DF, BU	DF, BU	DF, BU, US

Name of the authors:
Dalia Farghaly(DF)[1]
Brigitte Urban(BU)[1]
Emad Elba(EE)[1]
Uwe Sörgel (US)[2]

Affiliation of the authors:
1. Institute of Ecology, Subject Area Landscape Change, Leuphana University of Lüneburg, Universtätsallee 1, 21335 Lüneburg, Germany
2. Institute for Photogrammetry, University of Stuttgart, Geschwister-Scholl-Straße 24D, 70174 Stuttgart, Germany

APPENDIX B

Reprint of Articles

This dissertation is based on the following articles that are presented and referred in the framework paper.

PAPER I

TITLE:

" Observing the Middle Elbe Biosphere in Germany by Means of TerraSAR-X Images"

AUTHORS:

Dalia Farghaly, Emad Elba, Brigitte Urban

Reprinted from: Farghaly, D., Elba, E. and Urban, B. (2014): Observing the Middle Elbe Biosphere in Germany by Means of TerraSAR-X Images. International Journal of Geosciences, 5, 196-205.

http://dx.doi.org/10.4236/ijg.2014.52021.

International Journal of Geosciences, **2014, 5, 196-205**
Published Online February 2014 (http://www.scirp.org/journal/ijg)
http://dx.doi.org/10.4236/ijg.2014.52021

Observing the Middle Elbe Biosphere in Germany by Means of TerraSAR-X Images

Dalia Farghaly, Emad Elba, Brigitte Urban
Faculty of Sustainability Sciences, Institute of Ecology, Division of Landscape Change,
Leuphana University of Lüneburg, Lüneburg, Germany
Email: dalia.farghaly@stud.leuphana.de

Received January 1, 2014; revised January 31, 2014; accepted February 17, 2014

ABSTRACT

The Lower Saxonian Elbe Valley Biosphere Reserve is part of the UNESCO Biosphere Reserve "Elbe River Landscape", and used mainly for agriculture. One of tasks of the Biosphere Reserve Administration is to develop sustainable forms of land use which requires comprehensive updated land cover maps. Land use maps are hard to produce because of surveying costs and time. Nevertheless, these large areas need to be monitored. TerraSAR-X images are used to establish agricultural land use maps. In this study, two areas are selected within the Elbe Biosphere Reserve situated around the oxbows Wehninger Werder and Walmsburger Werder. Multi temporal classification methods were used to identify the different crops using maximum likelihood classifier for the years 2010 and 2011. The crop classifications were used to evaluate the effect of the number of images, the necessity of polarizations, and the consequences of some missing images within the crop calendar. These classifications were analyzed to estimate producer accuracy and Kappa index for each crop besides the overall accuracy for each agricultural land use map. The study shows that using dual polarization imagery enhances producer accuracies for many crops over the single polarization imagery, and demonstrates the importance of using frequent images during the cultivation period.

KEYWORDS

Agricultural Land Use; Elbe River; Multi Temporal Classification; TerraSAR-X; UNESCO Biosphere Reserves

1. Introduction

As a part of the UNESCO Biosphere Reserve "Flusslandschaft Elbe" (Elbe River Landscape) the floodplains of the Lower Saxonian Elbe Valley are representative of one of the largest European river landscapes as shown in **Figure 1**. Elbe River is the fourth largest river basin in Europe, after the Danube, the Visla, and the Rhine. The Elbe River flows through four countries namely Germany, the Czech Republic, Austria and Poland. 65% of the river basin lies in Germany [1]. The Elbe River Landscape Reserve has a total area of 3430 km^2 and stretches along 400 kilometers of the course of the Elbe River. As a UNESCO Biosphere Reserve it is a model region for sustainable development, which aims to achieve a balance between the interests of environmental protection and of social and economic development. It promotes environmentally-friendly agriculture, regional marketing, low-impact tourism, and an educational program for sustainable development (ESD), including research and monitoring activities [2]. Within Germany as a whole, the biosphere reserves cover almost 3% of the land area, including 15 territories designated as UNESCO biosphere reserves. They represent vital habitats, the diversity of fauna and flora, typical landscapes including mainly farm land located in the rural areas and cultivated at different levels of intensity as stated on the UNESCO website http://www.unesco.org/new/en/natural-sciences/environment/ecological-sciences/biosphere-reserves/.

The Elbe River Biosphere Reserve in Lower Saxony reaches from Schnackenburg in the south-east at Elbe-km 472.5 to Hohnstorf in the north-west at Elbe-km 569. The Elbe River kilometrage starts with zero at the Czech-Ger-

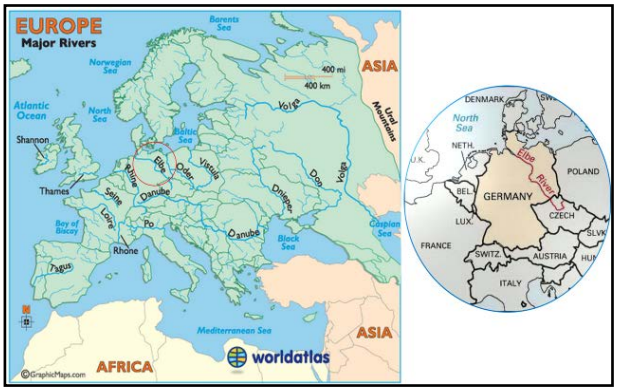

Figure 1. Major Rivers in Europe and the Elbe basin [1].

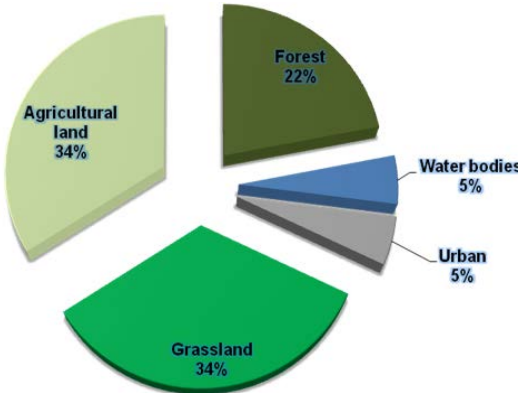

Figure 2. Distribution of land use and land cover in the Elbe River Biosphere Reserve in Lower Saxony. Source: UNESCO website http://www.unesco.org/new/en/natural-sciences/environment/ecological-sciences/biosphere-reserves.

man state border, the numbers grow in the upstream direction on the Czech side, as well as in the downstream direction on the German side [1]. The terrain of the reserve ranges from 5 m to 109 m above mean sea level. It covers a total area of about 570 square kilometers. As a historically cultural landscape the floodplains are used in various ways with a predominance of agricultural land use [3]. The variation in the current land uses is shown in Figure 2. A big division of 68% is covered with agricultural fields and grassland areas. Numerous researchers have reflected on land use effects on the environment [4-6]. Regions around rivers, mainly the biosphere areas, must be monitored to avoid environmental problems that might affect the multiple ecological, economic and social functions of those areas [7]. Pasture land situated in the recent flood plain is affected by contaminated suspended sediment loads deposited during flooding which can cause soil, crop, and fodder pollution [8]. On the other hand arable land is a possible source for groundwater and soil pollution. This floodplain has suffered from major flooding such as the 2002 flood, which caused huge damage in hazardous areas of the Elbe catchment. Thus many studies have been conducted to improve flood risk management schemes for the Elbe basin [9-11].

Planning the development of sustainable forms of land use, the Biosphere Reserve Administration "Niedersächsische Elbtalaue" requires updated, comprehensive maps. Surveying costs and time make it difficult to produce land use maps in the field [12]. As an alternative, satellite images can be used to provide the necessary information. As countries in Europe are usually covered with clouds, RADAR images are widely used to overcome weather problems. These images attest to be functional in generating land cover maps [13]. One of the most recent effective image types is TerraSAR-X images (TSX) acquired by the German Earth observation satellite, laun- ched 15 June 2007. It flies over the same location every 11 days. It uses an X-band SAR with 31 mm wavelength and 9.6 GHz frequency providing high-quality topographic information for commercial and scientific applications as stated on DLR website: http://www.dlr.de/eo/en/Portaldata/64/Resources/dokumente/TSX_brosch.pdf. Farghaly *et al.* showed the effectiveness of TSX images in distinguishing between aquatic weed types over lake Kyoga [14]. Lohmann *et al.* also demonstrated the efficiency of these images in determining the different types of crops within agricultural fields near Hanover, Lower Saxony [15].

Previous studies investigated crop production and land use maps using ENVISAT imagery. Some studies recommended the use of an appropriate range of images within a time series according to the crop-calendar, to achieve better classification results than using all of the images [16]. Many fields are cultivated by more than one type of crop during the year. Thus, such succession is difficult to model because it is controlled by phenological and ecological courses. Tavakkoli *et al.* show that using all of the images without considering the crop calendar resulted in less producer accuracy [17]. ENVISAT images have a C-band signal which passes partially through vegetation cover. This might lead to classification errors where the signals are influenced by the soil surface under the vegetation cover [18]. Thus some studies recommend using higher frequency signals such as X-band where the signals are more reflected by the vegetation cover [16]. This enables better crop classification results where the classification process identifies patterns of similar characteristics according to the corresponding observed backscattering response and their temporal progress.

This study identifies the agricultural land uses within two study areas. These areas are located within the Lower Saxonian "Elbe River Valley Meadows" Biosphere Reserve in Germany, around two oxbows the Wehninger Werder, and Walmsburger Werder (Werder = oxbow) as shown in Figure 3. Spotlight TerraSAR-X images in dual polarization (HH, VV) are used to monitor the two

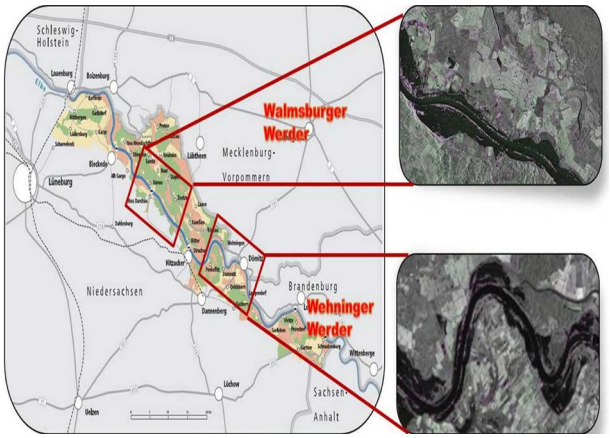

Figure 3. Location of study areas within the Lower Saxonian Elbe River Biosphere Reserve.

areas. HH means horizontal transmit and horizontal receive, while VV means vertical transmit and vertical receive. The images are used to produce several proper classifications which identify the crops cultivated in the investigated areas based on the field visits. The produced classifications are analyzed to evaluate the parameters which affect the producer accuracy of each crop in particular: polarization type, the number of manipulated images, image regularity, filter type, maintaining crop calendar, and the size of surveyed fields. The surveyed areas are large accessible fields. 50% of the surveyed area is considered as test fields. The test fields are assumed to be remote inaccessible areas.

2. Methods and Materials

2.1. Study Area

Two study areas are selected around the Wehninger Werder between Elbe-Kilometer (505 - 520), and Walmsburger Werder between Elbe-Kilometer (533 - 543) within the Lower Saxonian Elbe River Biosphere Reserve (Figure 3). Both areas are bearing several types of land use including urban and rural regions with agricultural land use dominant. The river floodplain produces high quality hay. Thus usually these meadows are mown once or twice a year, depending not only on weather conditions and flood events, but also on the Biosphere Reserve regulations to protect the fauna and flora within this particular environment [19]. The produced hay is used for feeding livestock if it is not contaminated or for Biogas production if it is contaminated [20]. 30% of this area is covered by forests, which must be maintained to ensure the sustainability of the flood plain environment. Over 65% of this area is covered by agricultural fields and grasslands which are considered the main possible sources of environmental pollution as well as they are possible sinks for flood borne contaminations. This study therefore focuses on this part of the Biosphere Reserve.

2.2. Data Collection

The used TSX images were acquired within the period from March 2010 to November 2011 as listed in Table 1. The images are Dual Polarization Spotlight Products. They are high resolution spatially enhanced images with a descending angle of 40˚ which leads to higher range and azimuth pixel spacing of 1 m. The incidence angle of 25˚ enables only 1.5 m range and azimuth pixel spacing. It was planned for this study to acquire images each 22 days, however, due to some operational reasons, some images could not be taken. Over Walmsburger Werder, there was a great gap of 66 days in 2010 during the growing period of most of the crops cultivated there, while in 2011 there were two gaps of 44 days. Over Wehninger Werder, the images had no gaps.

The accessible fields covered by these images were surveyed to determine the crops cultivated there. In year 2010, the fields were visited once in June. About 50 fields were surveyed around Walmsburger Werder. In year 2011, field visits were conducted monthly to several reachable and representative areas on similar dates to the acquisition times. Previous research had recommended surveying a greater number of fields in order to increase the validity of the obtained preliminary results [21]. Therefore, more than 150 fields were visited around Walmsburger Werder totaling 1550 hectares representative of 80% of the arable land within this area. In addition, about 300 fields were investigated around Wehninger Werder covering about 1860 hectares representing 70% of the arable land. Major crops cultivated during the period from March to October were barley, wheat, rye, rye-grass, maize, potato, sugar-beet root, rapeseed, and sunflower. Rye, wheat and barley have similar texture which causes similar back scatter values over the radar images; hence they are grouped together in the cate

Table 1. List of acquired images and calendar date of land investigations.

No	Walmsburger Werder		Wehninger Werder 2011	Ground Truth Date
	2010	2011		
1	------	26th March	------	
2	30th April	17th April	------	
3	------	------		
4	------	31st May	6th June	June
5	5th July	22nd June	28th June	
6	27th July	------	20th July	July
7	18th August	5th August	11th August	August
8	9th September	27th August	2nd September	
9	------	18th September	24th September	September
10	23rd October	10th October	16th October	October
11	14th November	1st November	7th November	

gory of cereals. Grass is harvested for animal feed or used as pasture land, and is considered as one of the crops and called grassland. In 2010, the agricultural land use classifications were generated for 6 types of crops including grassland. In 2011, classifications were conducted for 7 crops beside the grassland. The fields were divided into training fields group which were used as reference data, and a testing fields group which were used for assessing the accuracy of the produced classifications. These test fields were assumed as remote in inaccessible areas to test the possibility of considering the classification of the real remote areas. The list of the number of investigated fields for each crop and the number of the training fields, and the testing fields is presented in **Table 2**. The spatial allocation of these fields is shown in **Figure 4**.

2.3. Image Processing

TerraSAR-X images are known for speckle noise problems which affect the accuracy of classification results [18]. These speckle noises are due to coherent superposition of multiple backscatter sources. Therefore, speckle reduction must be applied to the images in order to remove the speckle noise. The TSX images must be filtered in order to remove or decrease these noises to permit better discrimination of scene targets [22]. Lee filter is an adaptive filter which is based on the assumption that the mean and variance of the pixel of interest are

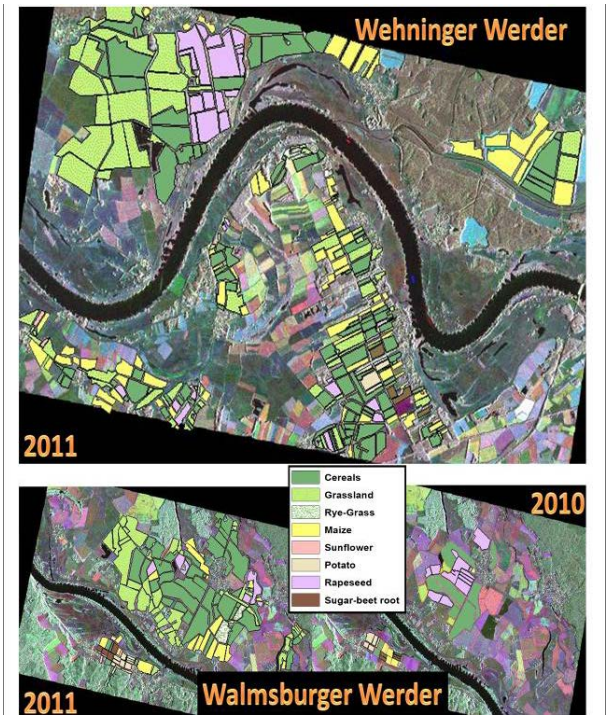

Figure 4. Distribution of different crops over the inspected fields around Walmsburger and Wehninger Werder.

Table 2. List of crop types and number of used fields in testing the classification results.

Crop Type	Cultivation period	Survey 2010			Survey 2011					
		Walmsburger Werder			Walmsburger Werder			Wehninger Werder		
		Training	Test	**Total**	Training	Test	**Total**	Training	Test	**Total**
Cereals	Mar.-Aug	4	6	**10**	17	30	**47**	46	60	**106**
Rye-grass	Mar.-Aug.	0	0	**0**	1	1	**2**	1	1	**2**
Grassland	Mar.-Nov.	1	2	**3**	21	33	**54**	29	43	**72**
Maize	May-Nov.	4	6	**10**	9	10	**19**	36	43	**79**
Sunflower	Mar.-Nov.	0	0	**0**	4	6	**10**	1	1	**2**
Potato	Mar.-Sep.	3	3	**6**	5	11	**16**	2	3	**5**
Rapeseed	Mar-Aug.	5	7	**12**	3	4	**7**	9	21	**30**
Sugar-beet	Mar.-Oct.	3	3	**6**	2	2	**4**	2	2	**4**
Total		20	27	**47**	62	97	**159**	126	174	**300**

equal to the local mean and variance of all pixels within the moving window. This preserves image sharpness and details while suppressing noise [23,24]. Many images of the same location are taken at different frequent dates. Thus, multi-temporal speckle filtering is applied to exploit the space-varying temporal correlation of speckle between the images, which reduces the system inherent multiplicative noise. The De-Grandi filter is an optimum weighting filter which was introduced to balance differences in reflectivity between images at different times. This enhances the image sharpness and enables identifying more details [25].

For both study areas, the images with both their acquisitions were coregistered to correct for relative translational shift and rotational and scale differences through performing spatial registration and potentially resampling. This was done using SARSCAPE module of the ENVI program after importing them as TerraSAR-X standard formats. The coregistered images were geocoded to provide a radiometric calibration and a cartographic reference system. The images were filtered in order to remove or decrease the speckle noise using Lee and Degrandi filter as mentioned before. The lee filter was applied using ERDAS imagine software through the Speckle Suppression option under Radar Interpreter menu. The coefficient of variation for the subset of the geocoded images was calculated for each image. The Lee filter was selected from the list of available filters and the coefficient of variation value was inserted. The window size was set to 7 pixels. The filtered images were stacked together to have one image consisting of 14 layers presenting 7 dates in both VV and HH polarization for Walmsburger Werder in 2010, and 18 layers presenting 9 dates in 2011, in addition to 16 layers presenting 8 dates for Wehninger

Werder in 2011. The effect of using Lee filter on the image sharpness is shown in **Figure 4**. The De-Grandi Filter was applied using SARSCAPE Module under ENVI program on the coregistered images. The resulted filtered images were stacked together to provide 3 images as stated before for Walmsburger Werder in 2010 and 2011, as well as for Wehninger Werder in 2011. The effect of this filter on the image sharpness is shown in **Figure 5**. The De-Grandi image looks non-pixilated, more homogenous and similar to the optical ones other than the Lee filter images.

2.4. Image Classification

Due to the limitation of the possible polarizations (HH, VV) of the TerraSAR-X sensor data, using only unique date images for establishing the required agricul- tural classification is unlikely to achieve accurate results. Therefore, multi temporal approaches were used to increase the classification accuracy through enabling mapping of temporal changes due to plant growth. The classifications were generated by stacking the different available imagery into three images representing the different acquired dates with the available polarization covering the crop period for both study areas. Maximum likelihood classifier was used to identify the cultivated crops using ERDAS Imagine. The classifications were produced based on several attempts using all available acquired dates, besides attempts representing partial periods, in addition to attempts using single polarization. Three crop calendar classifications were produced using the Model Maker of ERDAS imagine to combine the crops together according to their cultivation period for both study areas in 2010 and 2011.

2.5. Accuracy Assessment of the Classifications

The produced classifications were analyzed using the spatial module under ARCGIS to estimate the distribution of the classification with respect to the crop distribution within the test fields. The distribution results were exported into dBase format and thus transformed into excel files to calculate accuracy assessment parameters including the user accuracy for each crop, the producer accuracy for each crop, the Kappa index for the whole classification, and the total accuracy for the entire classification [26]. The results of the produced classifications are presented and explained below.

3. Results and Discussions

For each filter, 30 classifications were generated for the pilot area around the Walmsburger Werder in 2010, as well as 38 classifications in 2011, in addition to 32 classifications around the Wehninger Werder in 2011. The produced classifications were assessed and the external producer accuracy for each crop over the testing area and the total accuracy were estimated. **Tables 3** and **4** present the accuracy assessment results for fields around the Walmsburger Werder in 2010 and 2011 respectively,

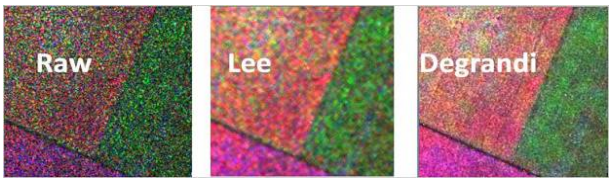

Figure 5. Effect of using Lee and De Grandi filters on removing the speckle noises.

Table 3. External producer accuracy for each crop and the total accuracy at Walmsburger Werder using De Grandi and Lee filter images in year 2010.

No of Layers	Period	External Producer Accuracy %																	
		De Grandi Filter image									Lee Filter image								
		Cereals	Grassland	Maize	Potato	Sugar-beet	Sunflower	Rapeseed	Rye-grass	**Total**	Cereals	Grassland	Maize	Potato	Sugar-beet	Sunflower	Rapeseed	Rye-grass	**Total**
6	30 Apr-27 jul	67	79	36	96	60		81		**73**	61	85	38	90	51		82		**71**
	5 Jul-18 Aug	55	78	51	97	59		77		**67**	48	79	41	88	54		74		**62**
8	30 Apr-18 Aug	63	77	53	98	62		84		**74**	60	87	47	94	55		82		**71**
	5 Jul-9 Sep	66	69	57	87	59		81		**73**	58	84	43	76	56		74		**65**
10	30 Apr-9 Sep	73	70	59	92	60		88		**79**	65	90	48	92	57		82		**73**
	5 Jul-23 Oct	78	73	59	90	73		88		**82**	69	91	48	81	57		75		**71**
12	30 Apr-23 Oct	82	72	62	98	73		93		**86**	71	92	52	94	58		83		**77**
	5 Jul-14 Nov	78	71	60	91	74		92		**83**	69	92	50	82	57		78		**73**
14	30 Apr-14 Nov	83	71	64	98	76		96		**88**	72	93	52	95	58		85		**78**
	CAL	74	78	62	94	76		89		**81**	70	94	52	94	60		79		**75**

Table 4. External producer accuracy for each crop and the total accuracy at Walmsburger Werder using De Grandi and Lee filter images in year 2011.

No of Layers	Period	External Producer Accuracy %																	
		De Grandi Filter image									Lee Filter image								
		Cereals	Grassland	Maize	Potato	Sugar-beet	Sunflower	Rapeseed	Rye-grass	**Total**	Cereals	Grassland	Maize	Potato	Sugar-beet	Sunflower	Rapeseed	Rye-grass	**Total**
8	17 Apr-05 Aug	87	84	80	78	97	61	94	96	**86**	73	74	73	67	88	46	91	92	**75**
	31 May-27 Aug	87	82	83	77	85	51	73	96	**85**	77	78	72	60	78	22	67	94	**76**
10	26 Mar-05 Aug	91	87	87	89	95	78	88	96	**90**	80	81	74	70	91	63	90	94	**80**
	17 Apr-27 Aug	91	86	87	91	97	73	87	96	**89**	80	81	75	71	90	55	90	94	**80**
	31 May-18 Sep	91	83	88	92	35	45	74	97	**87**	82	81	76	81	61	24	67	96	**80**
12	26 Mar-27 Aug	91	87	87	89	95	78	88	96	**90**	80	81	74	70	91	63	90	94	**80**
	17 Apr-18 Sep	93	87	91	95	43	67	86	96	**91**	84	83	79	87	78	54	89	95	**84**
	31 May-10 Oct	95	84	86	89	37	50	78	97	**89**	87	83	76	78	59	36	70	96	**83**
14	26 Mar-18 Sep	93	88	91	91	42	72	88	96	**91**	84	83	79	84	78	62	89	95	**83**
	17 Apr-10 Oct	95	87	89	94	40	69	86	96	**91**	89	85	80	84	71	60	90	95	**87**
	31 May-01 Nov	94	84	89	92	38	57	84	93	**90**	85	83	78	81	44	41	74	94	**83**
16	26 Mar-10 Oct	95	89	89	91	40	74	88	96	**92**	87	81	72	78	72	56	86	94	**83**
	17 Apr-01 Nov	95	87	91	93	39	70	89	93	**91**	88	85	81	85	55	63	91	94	**86**
18	26 Mar-01 Nov	95	88	91	91	39	75	90	93	**92**	88	85	80	83	53	69	91	94	**86**
8	26 Mar-10 Oct_HH	92	87	84	88	39	73	88	97	**89**	80	80	73	69	68	61	84	95	**79**
	26 Mar-10 Oct_VV	94	85	86	91	42	73	85	96	**90**	87	81	72	78	72	56	86	94	**83**
9	26 Mar-01 Nov_HH	90	87	86	88	39	75	91	93	**88**	77	82	74	71	56	64	86	94	**78**
	26 Mar-01 Nov_VV	94	85	88	92	39	76	87	93	**90**	85	81	73	78	51	60	87	93	**82**
	CAL	97	89	90	94	40	73	93	95	**93**	90	80	81	89	77	61	92	93	**86**

while **Table 5** presents the results for the agricultural fields around the Wehninger Werder in 2011. The classification according to crop calendar was called CAL.

According to **Tables 3-5**, using De Grandi filter leads to about 10% better classification results than using the Lee filtered images except for grasslands in 2010 where Lee filter has better producer accuracy by about 15% as shown in **Figure 6**. The best result is attained for potato fields cultivated around the Wehninger Werder, where its external producer accuracy is 100%. On the other hand, the worst result is gained for maize fields around Walmsburger in 2010 with only 36%. Moreover, the sugar-beet root cultivated around Walmsburger Werder in 2011 has only 40% external producer accuracy. The achieved producer accuracy result shows that using more layers improved the classification total accuracy for both the Walmsburger and Wehninger Werder. However, it is not applicable at the crop level, as rye-grass fields around Wehninger Werder attain less producer accuracy when more images are used, although using only VV polarization leads to higher classification accuracy. Better results were achieved for the other crops using both polarizations for both study areas and even for the rye-grass fields around Walmsburger Werder. On the other hand, sugar-beet root covering the fields from March till October around Walmsburger Werder has less producer accuracy when more layers are used contradicting the crop calendar. In 2011, the classification result around Walmsburger Werder is enhanced by over 10% for the total producer accuracy with respect to 2010, as well as about 20% in case of cereal fields, and over 30% for maize as shown in **Figure 7**.

Generally, the classifications produced according to the crop calendar have higher total producer accuracy than using all images with the exception of sugar-beet root as stated above. For the arable land around Walmsburger

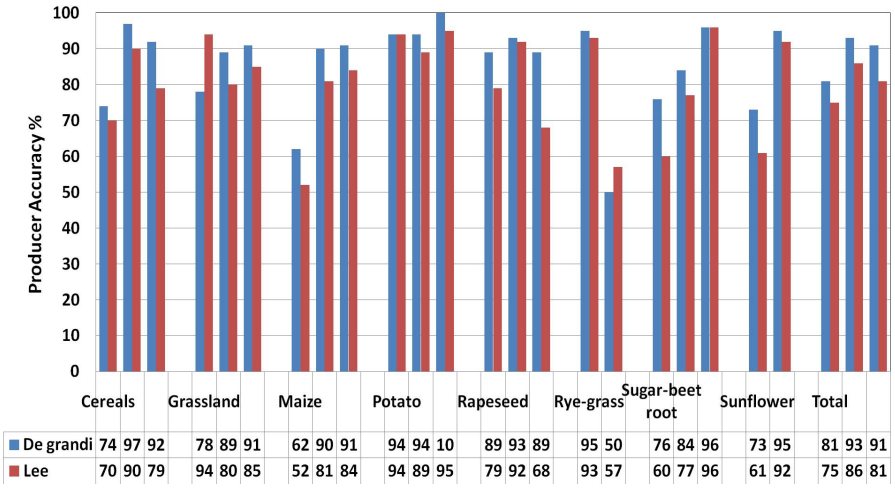

Figure 6. Summary of the producer accuracy for the different crops and the total accuracy using both Lee and De Grandi filtered imagery according to the crop calendar.

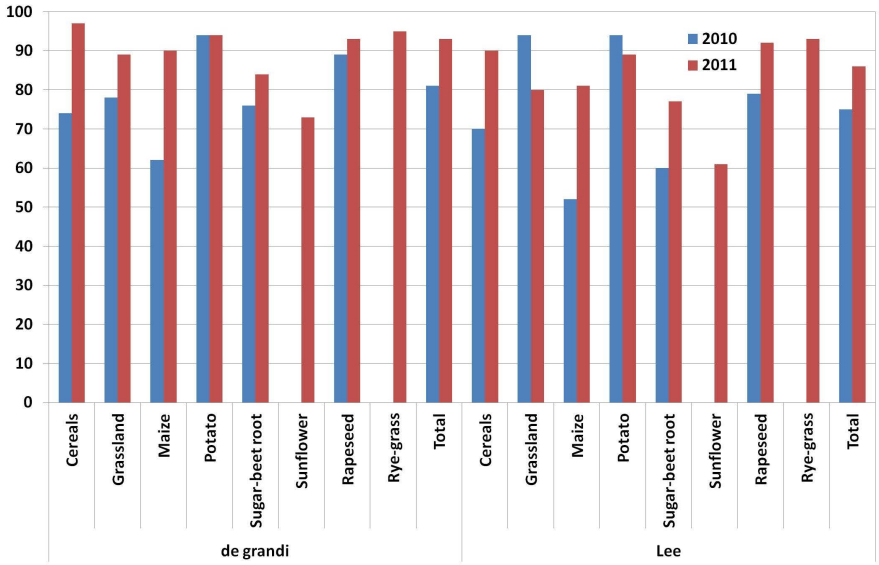

Figure 7. Summary of the producer accuracy for the different crops and the total accuracy using both Lee and De Grandi filtered imagery according to the crop calendar around Walmsburger Werder in year 2010 and 2011.

Werder, using images for the period from March onwards usually leads to higher producer accuracies than using images from April or May except for maize, as it is sown only late April or at the beginning of May. Thus, availability of frequent images covering most of the crop calendar period results in increasing the classification accuracies. This indicates that the classification results for the Wehninger Werder can be enhanced by an image series taken before June.

In year 2010, the use of images from April improves the producer accuracy for cereals, rapeseeds, and potato fields. Yet, using the images starting from July improves the classification results for maize and sugar-beet root fields. Missing an image in July for the fields cultivated around the Walmsburger Werder in 2011 and thus having a gap of 44 days instead of 22 days, caused slightly lower producer accuracies compared to the Wehninger Werder where a complete series of images from June until November had been available. Moreover, the increase of the gap to about 66 days decreased the classification producer accuracy by about 10% in case of year 2010, particularly because these 66 days fell into the growing season for most of the plants. The external producer accuracies over the test fields were high. Hence, the classification for the remote non accessible area can be trusted also.

4. Concluding Remarks

Image filtering was essential for enhancing crop classification results. The multi temporal filter De Grandi enhanced the producer accuracy by about 10% compared to

Table 5. External producer accuracy for each crop and the total accuracy at Wehninger Werder using De Grandi and Lee filter images.

No of Layers	Period	External Producer Accuracy %																	
		De Grandi Filter image									Lee Filter image								
		Cereals	Grassland	Maize	Potato	Sugar-beet	Sunflower	Rapeseed	Rye-grass	**Total**	Cereals	Grassland	Maize	Potato	Sugar-beet	Sunflower	Rapeseed	Rye-grass	**Total**
6	06Jun-20July	68	81	75	80	79	44	66	57	**73**	53	69	66	68	84	41	45	52	**59**
	28Jun-11Aug	55	80	69	45	82	73	57	58	**66**	79	85	84	95	96	92	68	57	**81**
8	06Jun-_11Aug	92	91	91	100	96	95	89	50	**91**	57	82	67	71	87	59	50	53	**66**
	28Jun-02Sep	64	83	78	88	81	82	57	61	**72**	49	81	62	71	91	66	43	53	**61**
10	06Jun-_02Sep	77	88	86	97	91	68	72	62	**82**	61	84	74	84	91	67	51	56	**70**
	28Jun-24Sep	68	85	78	98	89	81	60	47	**74**	55	84	70	85	96	65	46	54	**66**
12	06Jun-24Sep	81	90	87	99	94	71	75	47	**84**	66	87	79	91	96	66	53	55	**74**
	28Jun-17Oct	83	89	85	98	90	85	82	43	**85**	68	90	74	83	96	70	63	56	**76**
14	06Jun-17Oct	91	92	90	99	94	77	90	44	**91**	78	91	81	90	96	72	71	58	**82**
	28Jun-07Nov	84	92	89	99	96	97	87	47	**88**	69	91	78	87	97	91	73	80	**79**
16	06Jun-07Nov	93	93	92	100	98	95	92	48	**93**	79	92	82	94	97	91	79	80	**84**
7	06Jun-17Oct_HH	74	87	81	96	89	55	74	13	**79**	61	86	73	76	94	56	55	30	**70**
	06Jun-17Oct_VV	89	89	81	98	92	85	86	86	**87**	74	89	71	87	95	62	60	70	**77**
8	06Jun-07Nov_HH	77	90	84	98	94	87	82	28	**83**	62	87	74	85	96	85	64	64	**73**
	06Jun-07Nov_VV	90	91	85	99	96	96	91	87	**90**	75	90	72	91	97	88	72	81	**79**
	CAL	92	91	91	100	96	95	89	50	**91**	79	85	84	95	96	92	68	57	**81**

the Lee filter. Using large ground truth data of over 150 fields in 2011 enabled better classification accuracy than using just 50 fields as in 2010. Using sequence images covering the growing season usually improved the classification results. Moreover, missing images within the cultivation period decreased the attained classification producer accuracy. Furthermore, using dual polarization images enabled higher classification producer accuracy than single polarization sets.

As mentioned previously, the produced classifications according to the crop calendar achieved more significant results than using all images for most of the crops except for rye-grass around the Wehninger Werder and sugar-beet root around the Walmsburger Werder. Greatest producer accuracy was achieved for the rye-grass fields around the Wehninger Werder if VV polarization was used exclusively. The sugar-beet root fields around Walmsburger Werder achieved the highest producer accuracy using the image series ranging from March until the end of August. Hence, by combining the set used for producing the classification according to the crop calendar with the best classifications for sugar-beet root and rye-grass, classification accuracy will be enhanced.

Finally, it is recommended to use frequent images in dual polarization covering the whole cultivation period. The crops must be classified according to their cultivation period and then modeled together to simulate reality. This study was conducted on accessible fields. Over 50% of these fields were used as testing fields for evaluating the external producer accuracy for the generated classifications. The classification result showed high external producer accuracy. Thus this method can be applied to other remote areas. It is recommended to usually monitor the whole Biosphere Reserve using TerraSAR-X images to prevent any environmental problems due to misuse of these protected areas..

Acknowledgements

We are greatly indepted to the administration of the Biosphere Reserve “Niedersächsische Elbtalaue” (Lower Saxonian Elbe Valley) and the German Aerospace Centre (Deutsches Zentrum für Luft-und Raumfahrt, DLR) for providing the satellite images for this study. We highly

acknowledge the support of this research by a PhD graduate scholarship of LEUPHANA University Lueneburg awarded to Farghaly.

REFERENCES

[1] U. Brämick, F. Fladung and P. Doering-Arjes, "Aalmanagementplan—Flussgebietsgemeinschaft Elbe," Institut für Binnenfischerei, 2008. http://www.portal-fischerei.de/fileadmin/redaktion/dokumente/fischerei/Bund/Bestandsmanagement/FlussgebietsgemeinschaftElbe.pdf

[2] G. Puhlmann and S. Reinhardt, "Partnerships between River Biosphere Reserves," UNESCO Publications, 2007, pp. 75-77.

[3] W. Härdtle, B. Redecker, T. Assmann and H. Meyer, "Vegetation Responses to Environmental Conditions in Floodplain Grasslands: Prerequisites for Preserving Plant Species Diversity," *Basic and Applied Ecology*, Vol. 7, No. 3, 2006, pp. 280-288. http://dx.doi.org/10.1016/j.baae.2005.09.003

[4] R. N. Lubowski, S. Bucholtz, R. Claassen, M. J. Roberts, J. C. Cooper, A. Gueorguieva and R. Johansson, "Environmental Effects of Agricultural Land-Use Change," United States Department of Agriculture (USDA), Economic Research Service, Economic Research Report No. 25, 2006. http://ageconsearch.umn.edu/bitstream/33591/1/er060025.pdf

[5] F. Krüger and A. Gröngröft, "The Difficult Assessment of Heavy Metal Contamination of Soils and Plants in Elbe River Floodplains," *Acta Hydrochimica et Hydrobiologic*, Vol. 31, No. 4-5, 2003, pp. 436-443.

[6] B. Urban, "River Elbe Ecology—Contributions to a Large Scale Environmental Project," In: R. Ramesh and S. Ramachandran, Eds., *Coastal Urban Environments*, Capital Publishing Company, New Delhi, 2003, pp. 67-88.

[7] G. Tevi and A. Tevi, "Remote Sensing and GIS Techniques for Assessment of the Soil Water Content in Order to Improve Agricultural Practice and Reduce the Negative Impact on Groundwater," *Water Science & Technology Journal*, Vol. 66, No. 3, 2012, pp. 580-587. http://dx.doi.org/10.2166/wst.2012.209

[8] B. Urban, F. Krüger, T. Weniger, J. Prüter, T. Keienburg, F. Lang and M. Graf, "Auenböden der Elbe als Archiv für die Stoffdynamik im Einzugsgebiet," Proceedings *Deutsche Bodenkundliche Gesellschaft DBG Exkursionsführer*, Oldenburg/Berlin, 2011, pp. 42-59.

[9] C. Sehnert, S. Huang and K. Lindenschmidt, "Quantifying Structural Uncertainty due to Discretisation Resolution and Dimensionality in a Hydrodynamic Polder Model," *Journal of Hydroinformatics*, Vol. 11, No. 1, pp. 19-30.

[10] A. E. Mynett and Z. Vojinovic, "Hydroinformatics in Multi-Colours-Part Red: Urban Flood and Disaster Management," *Journal of Hydroinformatics*, Vol. 11, No. 3-4, 2009, pp. 166-179.

[11] B. Koppe, B. Llacay and G. Peffer, "RAMWASS Decision Support System (DSS) for the Risk Assessment of Water-Sediment-Soil Systems—Application of a DSS Prototype to a Test Site in the Lower Part of the Elbe River Valley, Germany," *Proceedings of the European Conference on Flood Risk Management Research into Practice* (*FLOODrisk*), CRC Press, London, 2008.

[12] E. M. Makhanya, S. E. Piper and M. Townsend, "Mapping Rural Land Use in Selected Subsistence Farming Areas of South Africa Using Remote Sensing Products," *Proceedings IntArchPhRS*. Band XXIX, Part B 7, Washington, D.C., 1992, pp. 675-682.

[13] S. J. Purkis and V. V. Klemas, "Remote Sensing and Global Environmental Change," Wiley-Blackwell, Chichester, West Sussex, 2011.

[14] D. Farghaly, B. Urban, P. Lohmann and E. Elba, "Differentiation and Extend of Aquatic Weeds over Lake Kyoga, Uganda by Multiple Remote Sensing Technology," *Proceedings 4th TerraSAR-X Science Team Meeting*, DLR-Oberpfaffenhofen, 2011. http://sss.terrasar-x.dlr.de/papers_sci_meet_4/oral/LAN0499_Farghaly.pdf

[15] P. Lohmann, U. Soergel, M. Tavakkoli and D. Farghaly, "Multi-Temporal Classification for Crop Discrimination Using TerraSAR-X Spotlight Images," *Proceedings IntArchPhRS* (38), Part 1-4-7/WS, Hannover, 6 S., CD, 2009. http://www.isprs.org/proceedings/XXXVIII/1_4_7-W5/paper/Lohmann-129.pdf

[16] M. Tavakkoli, "Multi-Temporal Classification of Crops Using ENVISAT ASAR Data," Ph.D. Dissertation, Leibniz University of Hannover, 2011.

[17] M. Tavakkoli, P. Lohmann and U. Soergel, "Monitoring Agricultural Activities Using Multi-Temporal ASAR ENVISAT Data," *Proceedings IntArchPhRS*, Band XXXVII, Teil B 7-2, Peking, 2008, pp. 735-742

[18] J. A. Richards, "Remote Sensing with Imaging Radar," Springer, Australia, 2009. http://dx.doi.org/10.1007/978-3-642-02020-9

[19] Landwirtschaftskammer Niedersachsen, "Endbericht—Machbarkeitsuntersuchung zur Monovergärung von Grassilagen schadstoffkontaminierter Standorte aus Deichvorland der Elbe," 2011. http://www.lwk-niedersachsen.de/index.cfm/portal/6/nav/203/article/14596.html

[20] I. Leyer, "Auengrünland der Mittelelbe-Niederung," Vegetationskundliche und-ökologische Untersuchungen in der rezenten Aue, der Altaue und am Auenrand der Elbe, J. Cramer, Borntraeger, Berlin, 2002.

[21] P. Lohmann, U. Soergel and D. Farghaly, "Classification of Agricultural Sites Using Time-Series of High Resolution Dual-Polarisation TerraSAR-X Spotlight Images," *Proceedings 29th EARSeL Symposium—Imaging Europe*, Chania, 2009. http://www.ipi.uni-hannover.de/uploads/tx_tkpublikationen/2009_lohmann_Paper_Earsel_TSX.pdf

[22] M. Mansourpour, M. A. Rajabi and J. A. R. Blais, "Effects and Performance of Speckle Noise Reduction Filters on Active Radar and SAR Images," *Proceedings IntArchPhRS*, Band XXXVI 1/ W41, Ankara, 2006. http://www.isprs.org/proceedings/XXXVI/1-W41/makale

ler/Rajabi_Specle_Noise.pdf

[23] L. Gagnon, "Wavelet Filtering of Speckle Noise—Some Numerical Results," *Proceedings* 12*th Conference on Vision Interface* (VI'99) Trois-Rivières, Québec, 1999, pp. 336-343.

[24] J. Lee, T. L. Ainsworth and K. Chen, "Speckle Filtering of Dual-Polarization and Polarimetric Sar Data Based on Improved Sigma Filter," *Proceedings IGARSS*, 2008.

[25] G. F. De Grandi, M. Leysen, J. S. Lee and D. Schuler, "Radar Reflectivity Estimation Using Multiplicative SAR Scenes of the Same Target: Technique and Applications," *Proceedings IGARSS*, 1997.

[26] D. G. Rossiter, "Statistical Methods for Accuracy Assessment of Classified Thematic Maps," 2004. http://www.itc.nl/~rossiter/teach/R/R_ac.pdf

PAPER II

TITLE:

'Towards Sustainable Land Uses within the Elbe River Biosphere Reserve in Lower Saxony, Germany by Means of TerraSAR-X Images'

AUTHORS:

Dalia Farghaly, Emad Elba, Brigitte Urban

Reprinted from: Farghaly, D., Elba, E. Urban, B. (2016): Towards Sustainable Land Uses within the Elbe River Biosphere Reserve in Lower Saxony, Germany by Means of TerraSAR-X Images. Journal of Geoscience and Environment Protection, 04,97-121. doi: 10.4236/gep.2016.43009.

Journal of Geoscience and Environment Protection, 2016, 4, 97-121
Published Online March 2016 in SciRes. http://www.scirp.org/journal/gep
http://dx.doi.org/10.4236/gep.2016.43009

Towards Sustainable Land Uses within the Elbe River Biosphere Reserve in Lower Saxony, Germany by Means of TerraSAR-X Images

Dalia Farghaly, Emad Elba, Brigitte Urban

Faculty of Sustainability Sciences, Institute of Ecology, Subject Area Landscape Change, LEUPHANA University of Lüneburg, Lüneburg, Germany
Email: dalia.farghaly@stud.leuphana.de

Received 29 January 2016; accepted 28 March 2016; published 31 March 2016

Abstract

Floods are one of the major hazards worldwide. They are the source of huge risks in rural and urban areas, resulting in severe impacts on the civil society, industry and the economy. The Elbe River has suffered from many severe floods during recent decades. In this study, the zones flooded during 2011 were analyzed using TerraSAR-X images and a digital elevation model for the area in order to identify possible ways to mitigate flood hazards in the future, regarding sustainable land-use. Two study areas are investigated, around the Walmsburg oxbow and the Wehningen oxbow. These are located between Elbe-Kilometer (505-520) and (533-543), respectively, within the Lower Saxonian Elbe River Biosphere Reserve. Those areas are characterized by several types of land use, with agricultural land use being predominant. The study investigated the possibility of using a Decision-Tree object-based classifier for determining the major land uses and the extent of the inundation areas. The inundation areas identify for 2011 submerged some agricultural fields that must be added to existing flood risk maps, and future cultivation activities there prevented to avoid the possible economic losses. Furthermore, part of the residential area is located within the high flood zone, and must be included in risk maps to avoid the possible human and economic losses, to achieve sustainable land use for the areas studied.

Keywords

Elbe River, Floods, Land Use, SAR, TerraSAR-X, Decision-Tree, Object-Based Classification, Risk Maps

How to cite this paper: Farghaly, D., Elba, E. and Urban, B. (2016) Towards Sustainable Land Uses within the Elbe River Biosphere Reserve in Lower Saxony, Germany by Means of TerraSAR-X Images. *Journal of Geoscience and Environment Protection*, **4**, 97-121. http://dx.doi.org/10.4236/gep.2016.43009

1. Introduction

The Elbe River is the fourth largest river basin in Europe, after the Danube, the Vistula, and the Rhine [1]. The Elbe runs through Austria, the Czech Republic, Poland, and Germany. The river is about 1094 km long, with about 727 km, or 66% of its length, being in Germany. The river basin area covers about 148,000 km^2. 65% of the catchment lies in Germany, with an area of about 97,000 km^2 [2]-[4]. The Elbe has several gauges to measure water levels along the river, as shown in **Figure 1** [5]. The Czech-German state border marks the zero point for the Elbe kilometrage, with the numbers increasing in the upstream direction on the Czech side, and increasing in the downstream direction on the German side [1] [6].

The Elbe floodplain was designated as a Biosphere Reserve (Flusslandschaft Elbe) by UNESCO in 1997. It consists of four reserves, namely the Biosphärenreservat Mittelelbe in Sachsen-Anhalt, the Biosphärenreservat Flusslandschaft Elbe-Brandenburg, the Biosphärenreservat Flusslandschaft Elbe—Mecklenburg-Vorpommern, and the Biosphärenreservat Niedersächsische Elbtalaue [7] [8]. The Elbe River Biosphere Reserve in Lower Saxony reaches from Schnackenburg in the southeast, at Elbe-km 472.5, to Hohnstorf in the northwest, at Elbe-km 569, and has an area of about 568 km^2. The elevation of the terrain ranges from 5 m to 109 m above mean sea level. The floodplains are used in various ways, with a predominance of agricultural land use. Equal portions of 34% are covered by agricultural fields and grassland areas, while a portion of 22% is covered by forest. The rest is divided equally between water bodies and residential areas [9]-[11]. The Elbe floodplain suffered from large-scale century flooding in 2002, which caused huge damage in hazardous areas of the Elbe catchment. Consequently, many studies have been conducted to improve flood-risk management plans for the Elbe basin [12] [13].

In Germany, 21 people were killed, 100 people were injured, and 200,000 people were evacuated from the 300 km^2 inundation extent area along 800 km of the river, resulting in economic losses of 11.6 billion, caused by the large-scale century flooding in 2002 [14]-[17]. Since 2002, Germany has conducted several measures to improve flood-risk management and reduce the flood hazards [18] [19]. Therefore, although the two extreme century floods in 2011 and 2013 were actually higher than that in 2002, they did not cause as much damage as the one in 2002 [14]. In recent years, flood protection structures throughout Germany have been extensively upgraded. Flooding occurred in 2011 and resulted in damage in the catchments of the Rhine, the Danube, the Weser,

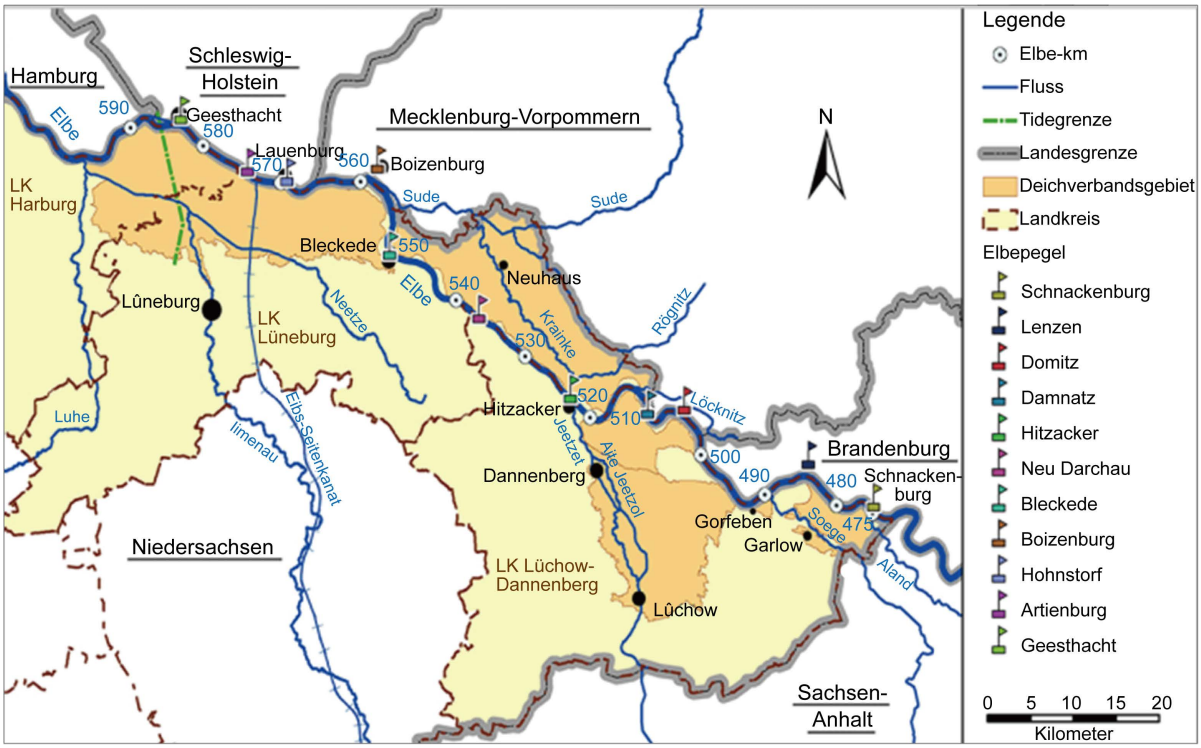

Figure 1. Gauge locations along the Elbe [5].

and the Elbe. However, in spite of the extent of the flooding, disastrous damage did not occur. The total damage was estimated to be more than 100 million Euro in Germany, an amount that was much smaller than the 11.6 milliard Euro in 2002, for example [12] [20]. Likewise, in some areas, damage was minimal or almost completely avoided during the floods in 2013. Nevertheless, the 2013 floods also caused severe problems in other areas: eight people were killed, and 52,000 were evacuated across parts of the 200 km^2 drowned area, leading to a loss of approximately 12 milliard Euro [21]-[23].

Comparing of the areas affected in 2013 with existing flood hazard and risk maps, one can see that these flood maps are usually reliable [24]. However, some investigations in flooded areas showed that some people affected by the flood of 2013 had already forgotten about the damage that occurred in the 2002 floods and, faced with the recurrent flooding in 2013, were unable to deal with the disaster since many believed they could only have infrequent exposure to century floods [14]. Awareness of flood risks played a major role in how serious the damage caused by the 2013 flood was in any given area. Thus, it is essential that people are aware of flooding as an intrinsic part of their environment, an awareness that can be achieved through flood hazard and risk maps that give them an idea about flood prevention and protection plans [24] [25]. These maps should be made more widely accessible and used more actively. To ensure efficient use of flood maps and risk awareness programs, they must be integrated into the planning processes for risk mitigation policies and new construction projects. There was no real legislative limitation on building new construction in areas designated as hazardous by flood maps. After the 2002 flood, legislative limitations were declared limiting new settlements in flood-prone areas; however, they were undermined to a very considerable scale by several exceptions. The extreme flood of 2013 and the consequent damages demonstrate that new flood risk management plans are required [14].

Flood risk is the combination of the probability of a flood event and of the possible deleterious consequences to human health, the environment and economic activity associated with the flood event. Flood risk management includes the comprehensive and continuous assessment and evaluation of flood hazard and flood risks, to mitigate the floods and/or the impact of floods. The flood risk management programs integrate five measures namely, prevention, protection, awareness, emergency response, and recovery. Prevention measures seek to prevent damage caused by floods by avoiding construction of houses and industries in present and future flood-prone areas, by adapting future developments to the risk of flooding, by promoting proper land-use, and by adapting to changing risk factors such as climate change. Protection measures seek to take both structural and non-structural measures to mitigate the impact of floods in a specific location by construction of flood dikes, and early warning systems. Awareness measures seek to inform the population about flood risks, settlement expansion in safe places using suitable forms of construction, and what to do in the event of a flood. Emergency response measures seek to develop emergency response plans in the case of a flood. Recovery measures seek to return to normal conditions as soon as possible and mitigate both the social and economic impacts on the affected population [26]-[29]. For effective and efficient flood risk management, comprehensive information about the existing hazards and risks throughout the river basin, including flood type, the probability of a particular flood event (low, medium, high), the flood extent, water depth, flow velocity and possible damages, is required [26] [30] [31]. Therefore, flood maps are useful tools that provide information about hazards, vulnerabilities, and risks of a given area.

Flood maps include flood hazard maps, which identify the extent of flooded areas at different flood probabilities. They also include flood risk maps, which indicate the possible harmful consequences associated with floods of different probabilities, especially when correlated with land use maps. Furthermore, detection maps can show the inundation extents of former floods [30]-[32]. These flood maps should be included into spatial and emergency planning beside the information from Geographic Information Systems (GIS) to achieve reduction and mitigation of possible damage [28] [33]. Historical flood detection maps, land use maps, and other sources of historical information about former flood areas are essential in identifying flood hazards and to create risk maps that can serve as a basis for crucial flood protection, land zoning, and development restrictions in flood hazard areas. In short, there is a need for up-to-date flood detection and land use maps [28] [34]-[37]. Furthermore, flood-detection mapping is required in many applications such as disaster management, risk damage assessment, and rehabilitation processes. Flood-mapping monitoring techniques use pre- and post-satellite imagery [38]-[40]. Floods often happen in combination with heavy rains and dense cloud cover which affect optical satellite images. Synthetic Aperture Radar (SAR) imagery is not affected by these weather conditions because it does not rely on sunlight, and thus can also be used at night. Hence, SAR imagery is especially practical in flood detection mapping. Therefore, there are many studies about using this type of imagery as a flood detection tool [41] [42].

Generally, flood mapping is obtained using image classification, where each individual pixel is classified based on all existing information using the grey values and spatial information of an image [26] [30]-[32]. The satellite imagery can be classified on a pixel-based or object-based basis. Pixel-based image processing classifies single pixels according to their spectral reflectance. Object-based image processing has two steps: segmentation and classification. Segmentation is the process of dividing an image into a network of homogeneous image objects by grouping together neighboring pixels with similar feature values such as brightness, texture, color, etc. The segments ideally correspond to real-world objects and contain additional information relevant to classification, such as shape, texture and relationships to neighboring objects. Image texture provides information about the spatial arrangement of color or intensities in an image or selected region of an image. The classification of image objects (contextual classification) is carried out after segmentation. The contextual classification is based not only on spectral statistics, but also on the additional information including shape, texture and network relationship, and this enables the segmented image objects to be related to land cover classes. Contextual classification offers some advantages over traditional classification, because segmentation reduces the total number of elements that need to be handled during classification, thus significantly reducing the work needed to perform classification. Moreover, classification segmenting with homogeneous regions reduces salt-and-pepper noise in the classification results [35] [43]-[45].

Several studies have investigated the effect of the surface roughness on the radar backscattering. Surface roughness is the main factor affecting radar backscattering and determines the angular distribution of surface scattering, as shown in **Figure 2** [46]. The greater the roughness of a surface, the more the incident radiation will be backscattered to the radar; thus, the rougher a surface, the lighter it will appear in radar imagery. Smooth surface boundaries, such as water areas, act as mirrors and scatter the energy away from the sensor. In this case, the angle of reflection, θ_e, is equal to the angle of incidence, leading to a very low signal return, in turn producing relatively dark pixels in radar data. With an increasing roughness, the fraction of backscatter to the sensor grows larger. Very rough surfaces scattered the energy equally in all directions, including back to the sensor, and thus return a significant part of the transmitted energy back to the sensor [43] [45] [47].

Several studies have also investigated the effect of the wavelength of SAR sensors on mapping water and the vegetation canopy. The longer the system's wavelength, the greater the ability of the signal to penetrate the vegetation canopy, as shown in **Figure 3** [43] [46]. L-band SAR sensors, with wavelengths of 19 to 77 cm, are effective for mapping flooding in forest environments. By contrast, C-band sensors, with wavelengths of 4.8 to 7.7 cm, and X-band sensors, with wavelengths of 2.8 to 5.2 cm, cannot penetrate the vegetation canopy, because

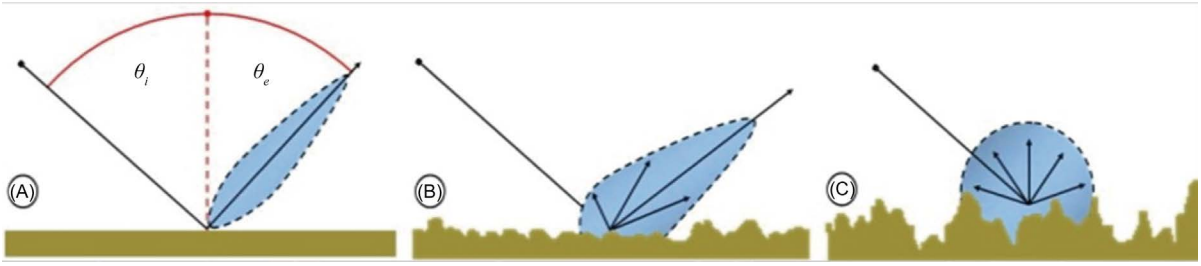

Figure 2. Radar reflection of (A) smooth, (B) moderately roughened and (C) strongly roughened surfaces [43] [46].

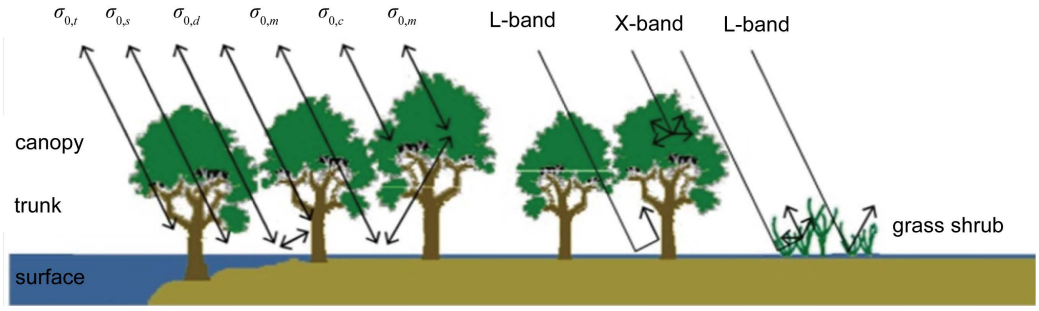

Figure 3. Conceptual illustration of the major sources of backscatter from vegetation and effect of flooded vegetation on X- and L-band SAR [43] [46].

these wavelengths produce more surface scattering from the top layer of the forest canopy. Therefore, neither C-band nor X-band SAR sensors are effective for mapping flooding in forest environments [45] [48] [49].

The effectiveness of different SAR and optical images in water delineation and flood detection applications has been evaluated in the literature using several classification methods. Numerous studies used optical images in identifying the extent of water areas. Reference [50] used Landsat TM imagery in extracting contour lines that mapped the bed of the High Aswan Dam Reservoir and allowed the lake's current morphology to be determined. Reference [42] created the Modified Normalized Difference Water Index (MNDWI) using Shuttle Radar Topographic Mission (SRTM) DEM and ASTER and LANDSAT satellite images to identify moist surfaces or saturated areas to separate flooded and non-flooded areas and to generate a flood hazard map. Reference [51] used Landsat TM imagery to map Lake Kyoga from 1972 till 2004, and Aster imagery in 2008 and 2009, to study the history of problematic aquatic plants in the lake. Supervised classification was performed for each image to identify the lake boundary.

Numerous studies have investigated the effectiveness of SAR imagery in identifying flooded areas. Several investigations applied Thresholding—methods to SAR imagery in order to locate flooded areas. Reference [32] used Threshold-based image segmentation and texture analysis methods in processing Multi-temporal NOAA AVHAR and RADARSAT images to achieve real-time and all-weather monitoring of floods. Reference [44] studied the possibility of optimizing the threshold ranges for the classification of flood water in SAR images for quick flood inundation mapping and response during flood disasters. For different polarizations, the mean backscattering signature profiles of various water bodies were analyzed to discriminate flood water from other water bodies. The study showed that using HH polarization imagery enables better delineation of the land-water surface.

Reference [52] developed an algorithm to map flooded areas from COSMO-SkyMed X-band SAR imagery based on fuzzy logic that can integrate theoretical knowledge about the radar return from inundated areas, described by means of three electromagnetic scattering models, with simple hydraulic considerations and contextual information using also auxiliary data, such as a land cover map and a digital elevation model. Reference [35] tested three different speckle noise removal filters including Lee, Frost, and Gamma MAP filters. The Gamma MAP filtered image had the best results and was segmented using Gray Level Co-occurrence Matrix (GLCM) and Mean Shift Segmentation (MSS). It was found that MSS is efficient for flood mapping.

Although many procedures have been studied in the literature, the present research focuses on Decision-Tree methodology, which has not been comprehensively evaluated. The present research employs remote sensing tools in identifying the detection maps and land use/land cover LULC maps using TerraSAR-X (TSX) imagery for two study areas within the Elbe Biosphere reserve in Lower Saxony "Niedersächsische Elbtalaue". Both the LULC and flood-detection maps are generated using a Decision-Tree object-based classifier. These maps can be used in updating the flood hazards and risk maps of this area, and to enable sustainable use of the land resources in the study area.

2. Methods and Materials

2.1. Study Area

Two pilot areas are selected, around the Wehningen Oxbow, lying between Elbe-Kilometers (505-520), and the Walmsburg Oxbow, between Elbe-Kilometers (533-543), within the Lower Saxonian Elbe River Biosphere Reserve (**Figure 4**). 30% of this area is covered by forests, which must be maintained to ensure the sustainability of the flood plain environment. Over 65% of this area is covered by agricultural fields and grasslands.

2.2. Data Collection

The water levels measured by Wasser- und Schifffahrtsverwaltung des Bundes (WSV), and provided by Bundesanstalt für Gewässerkunde (BfG), at the Neu Darchau gauge (Walmsburg Oxbow) and at the Damnatz gauge (Wehningen Oxbow) were collected for the periods from January 2010 until December 2012 and during June 2013. The readings of both gauges were converted to real water levels above mean sea level. The TerraSAR-X images (TSX) used were acquired during the period from March 2010 to January 2012 provided by the German Aerospace Centre (DLR). These images are acquired by the German Earth observation satellite. Its orbit passes over the same location every 11 days. It uses an X-band SAR, with 31 mm wavelength and 9.6 GHz, frequency

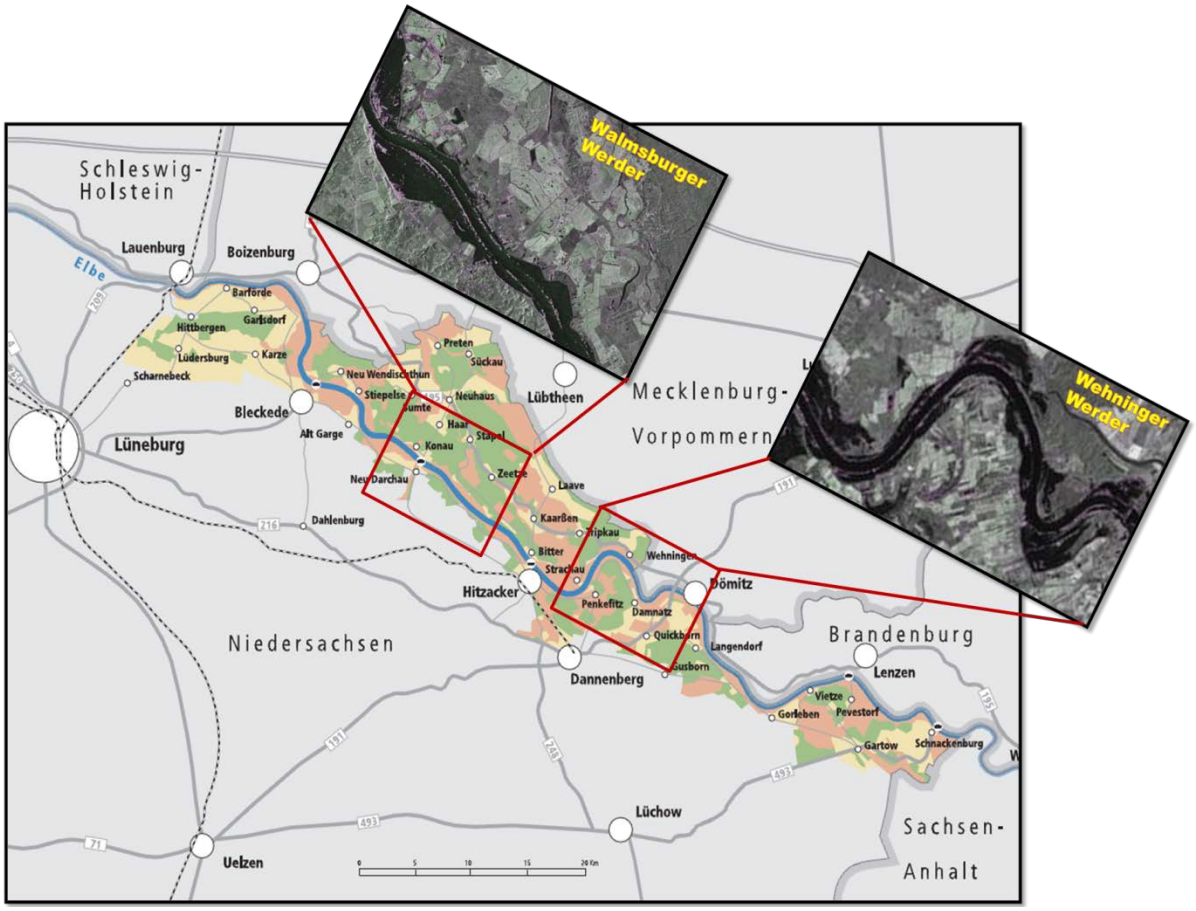

Figure 4. Location of study areas within the Lower Saxonian Elbe River Biosphere Reserve.

providing high-quality topographic information [53]. Orders were submitted to obtain images covering the flood peaks but, due to some technical problems, images of the peak water levels were not available. The TSX images were Dual Polarization Spotlight products, generated by the DLR as Multi-look Ground-range Detected (MGD) products with Spatially Enhanced (SE) processing. MGD has reduced speckle and approximately square resolution cells on the ground. The dual polarization TSX imagery collects data at HH for horizontal transmit and horizontal receive and VV—for vertical transmit and vertical receive. The image coordinates are oriented along the flight direction and the ground range. Geometric projection is in the azimuth-ground range without terrain correction [53]. The images are of high resolution, with a descending angle of 40˚ which leads to a higher range and an azimuth pixel spacing of 1 m. **Figure 5** and **Figure 6** show the recorded water levels and the acquired images according to date.

At Walmsburg Oxbow, the highest water level of 13.58 m above sea level (asl) was measured on 11 June 2013. During the high flood in January 2011, the highest water level of 13.16 m asl was measured on 23 January, while, the maximum accessible water level among the TSX images of 12.35 m asl was acquired on 19 January 2011 for that particular flood. The lowest water level of 6.98 m asl was measured on 2 September 2012 while the least accessible water level among the TSX images of 7.24 m asl was acquired on 22 June 2011. All the acquired images were taken in the same descending orbit direction. Therefore, the image acquired on 22 June 2011 was used for determining the pre-flood status, and the image acquired on 19 January 2011 was used for investigating the post-flood status.

At Wehningen Oxbow, the highest water level of 17.02 m asl was measured on 11 June 2013. During the high flood in January 2011, the highest water level of 16.57 m asl was measured on 23 January, while the maximum accessible water level among the TSX images of 16.17 m asl was acquired on 25 January 2011. The lowest water level of 10.59 m asl was measured on 22 July 2010, while the least accessible water level among the TSX

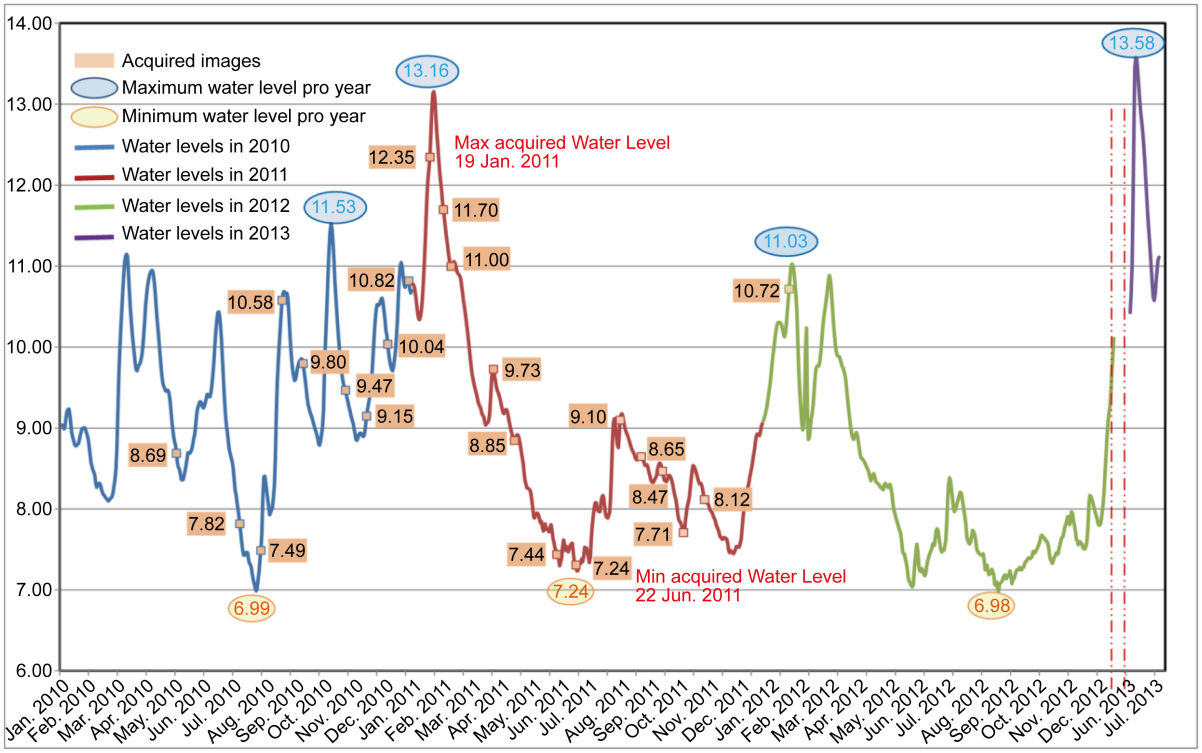

Figure 5. The water levels measured at Neu Darchau gauge around Walmsburg Oxbow from January 2010 to December 2012 in m above sea level.

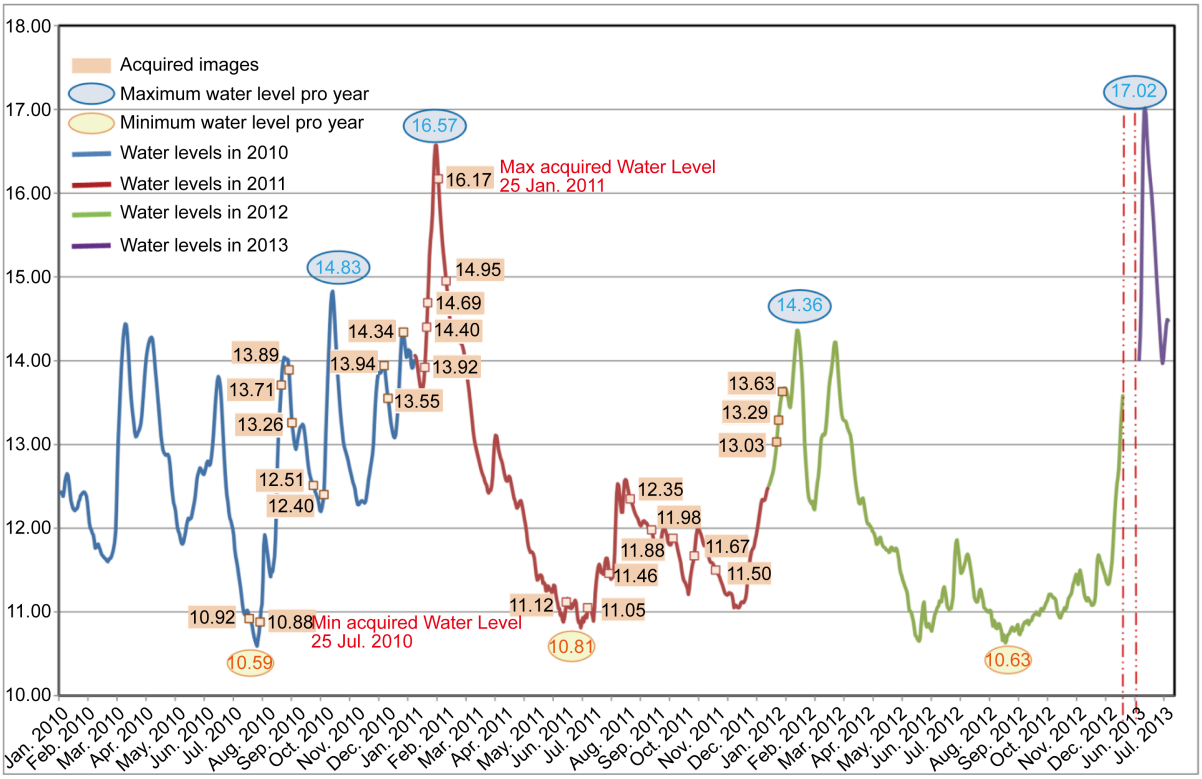

Figure 6. The water levels measured at Damnatz gauge around Wehningen Oxbow from January 2010 to December 2012 in m above sea level.

images of 10.88 m asl was acquired on 25 July 2010. Some of the acquired images were taken in descending orbit direction while others were acquired in the ascending orbit direction. The image acquired on 25 July 2010 was taken in the ascending orbit direction whereas the image acquired on 25 January 2011was taken in the descending orbit direction. It is better to process pre- and post-images with same orbit direction. Hence, another image with low water level was chosen to study the pre-flood status. On 28 June 2011, the image was acquired in the descending orbit direction, and the measured water level was 11.05 m asl. Therefore, the image acquired on 28 June 2011 was used for determining the pre-flood status, and the image acquired on 25 January 2011 was used for investigating the post-flood status.

For both oxbows, the pre-flood images were used to define land use, while the post-flood images were used in mapping the flooded areas. The land-use/land cover LULC maps and the detection maps were used in evaluating the hazards resulting from the January 2011 flood and to identify the risk zones, as shown in **Figure 7**. These images must first be processed, and then classified, to generate the LULC maps and detection maps for both areas; subsequently, the risk zones can be defined.

2.3. Image Processing

For both study areas, the images with both their acquisitions were coregistered so that relative translational shift and rotational and scale differences could be corrected through performing spatial registration and, potentially, resampling. This was done using the SARSCAPE module of the ENVI program after importing the images as TerraSAR-X standard formats. The coregistered images were geocoded to provide a radiometric calibration and a cartographic reference system. The resultant geocoded images for both the HH and VV polarizations were stacked together to provide two images for pre-flood and post-flood status at both Walmsburg Oxbow and Wehningen Oxbow. Image rectification and georeference transformation were applied to the four stacked images using ERDAS Imagine 9.3 software. The images were loaded into ERDAS Imagine for data preparation and reprojection. The SAR images were geometrically transformed to the Universal Transverse Mercator (UTM) projection with spheroid WGS 84 and zone 32 North, and resampled into one meter pixel size using the projective transform model under the Geocorrect image Tool. The four images were filtered with the Lee filter in order to remove or decrease speckle noise. The Lee-filter was applied using the ERDAS Imagine software through the Speckle Suppression option under the Radar Interpreter menu. The coefficient of variation for the subset of the geocoded images was calculated for each image. The Lee filter was selected from the list of available filters and the value for the coefficient of variation was inserted. The window size was set to seven pixels.

2.4. Image Classification

The object-based classification method investigated for mapping the land-use/land-cover LULC maps for both study areas, as shown in **Figure 8**. The object-based classification method was processed by the rule-based classifier in the ENVI EX program. The LULC maps initially produced were enhanced using the neighborhood

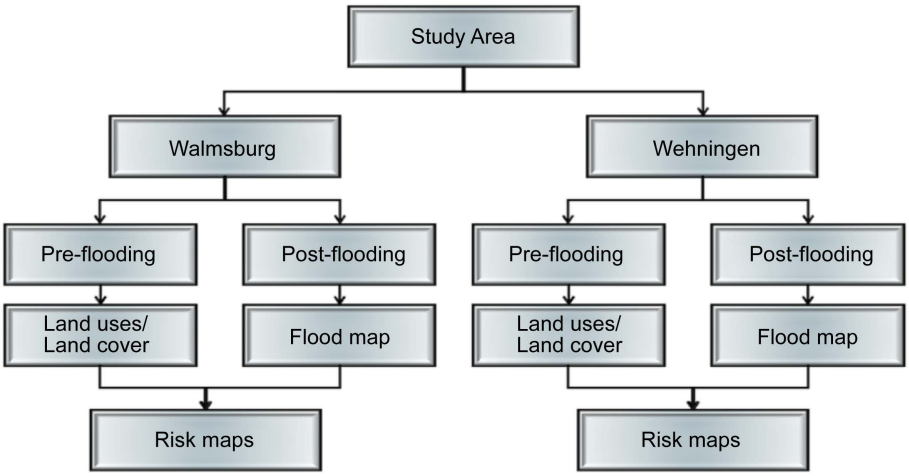

Figure 7. Methodology for identifying the risk zones based on January 2011 flood.

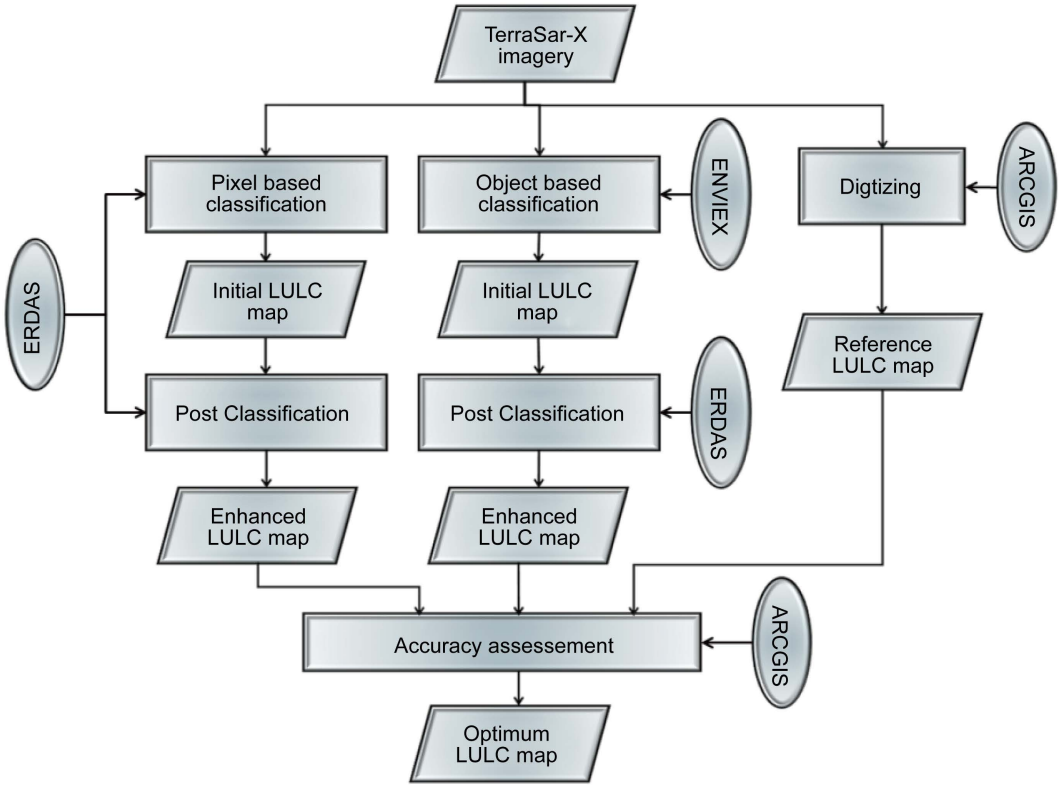

Figure 8. The methodology flow chart for producing LULC maps using pre-flood imagery.

filter. It is difficult to obtain up-to-date reference maps for LULC. The available maps were old and did not accurately represent the current land cover. Therefore, reference LULC maps were digitized from the TSX imagery using the ARCGIS program to assess the classification accuracy, as shown in **Figure 9**. The resulting enhanced LULC maps were analyzed using the spatial module in ARCGIS through calculating cross-tabulated areas between the digitized and the resultant LULC classifications. The resulting tables were processed in Microsoft Excel to estimate the error matrix (or confusion matrix), which is a method for determining the accuracy of classified classes with respect to the reference data [43]. The results of the object-based classification were compared in order to determine the optimum method for mapping the LULC classification.

As discussed in the introduction, the roughness of a surface affects the backscatter from it. The greater the roughness, the more scattering back to the radar there is, and the lighter the surface appears in radar imagery, leading to variation in the image texture [45]. Image texture measures the relationships between pixels and their neighbors and plays an important role in interpreting SAR imagery, especially high spatial resolution images [43]. SAR imagery has a single band which is based on intensity of grey level formed from radar backscatter, and thus texture is the main source of information used to study land cover and land use in pixel-based analysis [45]. To derive further information beyond the spectral information of SAR imagery, object-oriented image analysis can be used to extract information regarding shape, size and relationship of image objects [43]. Therefore, object-based analysis was used in this study.

Envi EX has a tool that utilizes object-based processing named Feature Extraction. Feature Extraction is a tool for extracting information from high-resolution panchromatic or multispectral imagery based on spatial, spectral, and texture characteristics. It uses an object-based approach to classify imagery. It is a combined process of segmenting an image into regions of pixels, computing attributes for each region to create objects, and classifying the objects (with rule-based or supervised classification) based on those attributes, to extract features. The workflow consists of two main steps: Find Objects and Extract Features. The Find Objects task is subdivided into four steps: Segment, Merge, Refine, and Compute Attributes. During the segmentation process, pixels with similar feature values (brightness, texture, color, shape) are grouped into small objects. During the region-merging process, small adjacent segments are aggregated into larger, textured areas based on a combination of

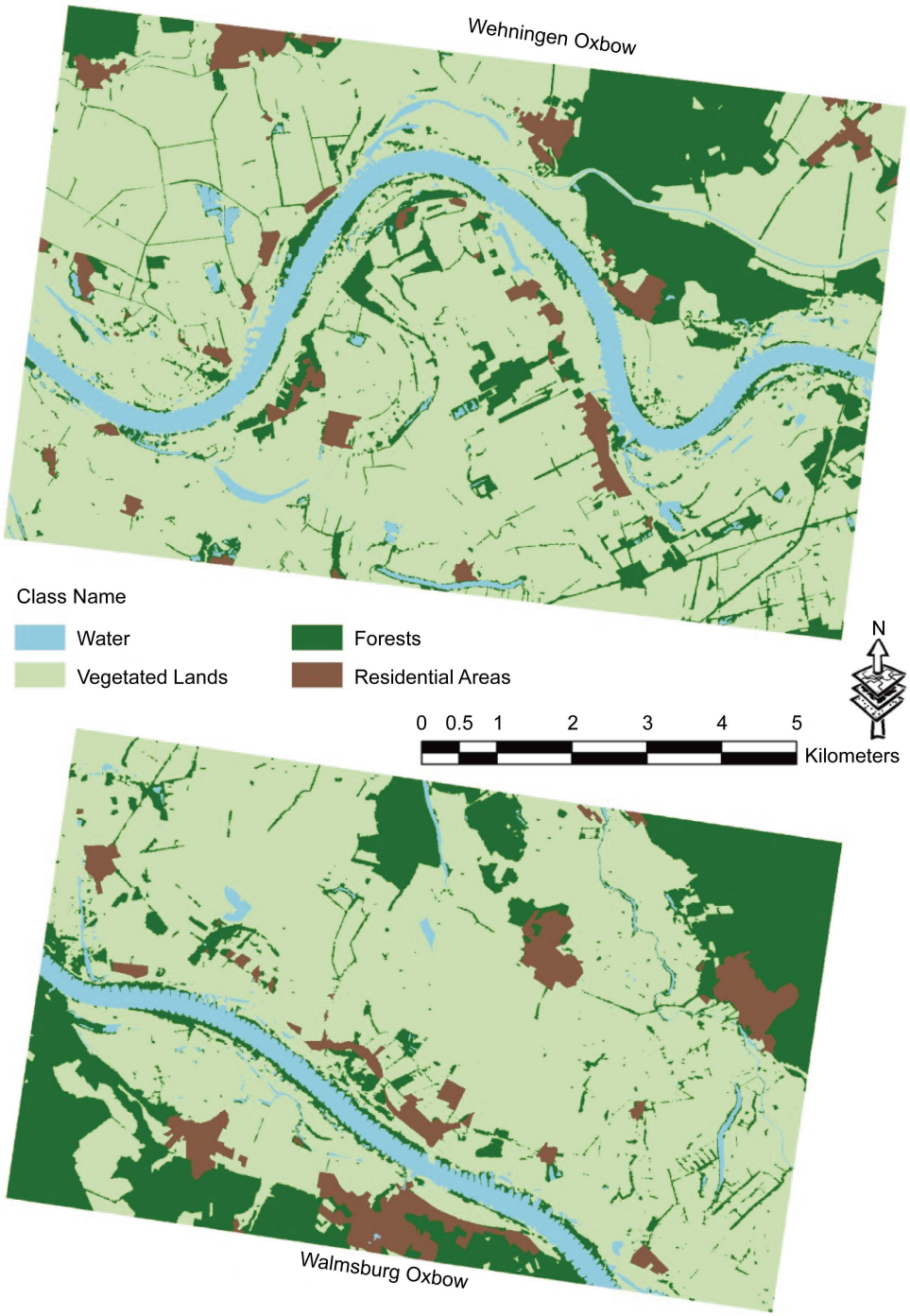

Figure 9. Reference maps for LULC classifications at Wehningen Oxbow and Walmsburg Oxbow.

spectral and spatial information. During the Compute-Attributes process, spatial, spectral, and texture attributes are computed for each object. After completing this task, the Extract Features task can be performed; this consists of supervised or rule-based classification. In the supervised classification process, the training data (samples of known identity) are used to assign objects of unknown identity to one or more known features. The training data can be defined manually or through importing ground truth data in the form of point and polygon shape files. The supervised classifier uses either the K-Nearest-Neighbor method or the Support Vector Machine method. In the rule-based classification process, features are defined by building one or multiple rules based on

object attributes. This requires human knowledge and reasoning about the extracted features. Finally, the classification results can be exported to shape files and/or raster images [54].

The Decision-Tree method builds classification in the form of a tree structure. The Decision Tree classifier performs multistage classifications by using a series of binary decisions to place pixels or objects into classes. Each decision divides the pixels in a set of images into two classes based on an expression. Each new class can be divided into two more classes based on another expression. As many decision nodes as needed can be utilized. The results of the decisions are classes. The Decision-Tree classification method can be applied to pixel-based classification in the same way as traditional classification algorithms would be applied. It can also be used to generate rules for knowledge-based and object-based classification with different types of attributes [43]. The main features of the LULC map are water, forest, vegetated lands and residential areas. Each feature has different roughness and texture characteristics.

In this research, a Decision-Tree classification algorithm was applied using the rule-based classifier, as shown in **Figure 10**. The pre-flood images in both study areas were used to identify the land uses. The radar signals returned from water bodies, such as rivers and lakes, have low backscatter. These areas, therefore, are mostly dark on the TSX imagery. The backscatter from forests and residential areas is mainly volume scattering. The backscatter from vegetation-covered areas, such as grasslands, croplands and bare soil fields, depends on the crop types and their distribution on the fields. The scattering from roads is affected by the trees on either side, so they show up as bright lines on radar imagery. In contrast, roads not lined with trees are less visible and may be mistaken for water. Generally, the land cover types in both study areas are complex or mixed, so that different coverages may show similar physical scattering mechanisms. Therefore, the water class and land class were defined in a first step. Then, the land class was isolated and classified as either flat terrain, such as vegetated lands, or uneven terrain, including forests and residential areas. Lastly, the uneven terrain class was detached and further classified as either forest class or residential class. Land classified as vegetated was also subdivided as either cropland or grass; this classification was imported here from previously performed and reported work [55].

The Decision-Tree approach requires comprehensive knowledge of data about the features of the terrain and, furthermore, physical understanding of these. Since each class corresponds to a specific scattering property, decision boundaries were determined based on knowledge acquired experimentally by the analysis of the scattering characteristics of each class. The feature extraction workflow computed spectral, textural, and spatial attributes for the merged objects. In order to locate decision boundaries for separation of the various classes, the histograms of the computed attributes were analyzed to identify peaks, valleys, shoulders, and curvatures. The concepts of natural breaks and clustering were used to define the decision boundaries. Natural breaks and clustering are both methods of manual data classification through dividing data into classes based on natural groups in the data distribution. Natural breaks occur in the histogram at the low points of valley, while cluster divisions occur at the midpoints between peaks or at the shoulders of the histogram [56]. The histograms created for spectral, texture, and spatial characteristics of the TSX imagery were analyzed at the peaks, valleys and shoulders. The effective points which separate classes were employed as decision boundaries, as shown in **Figure 11**.

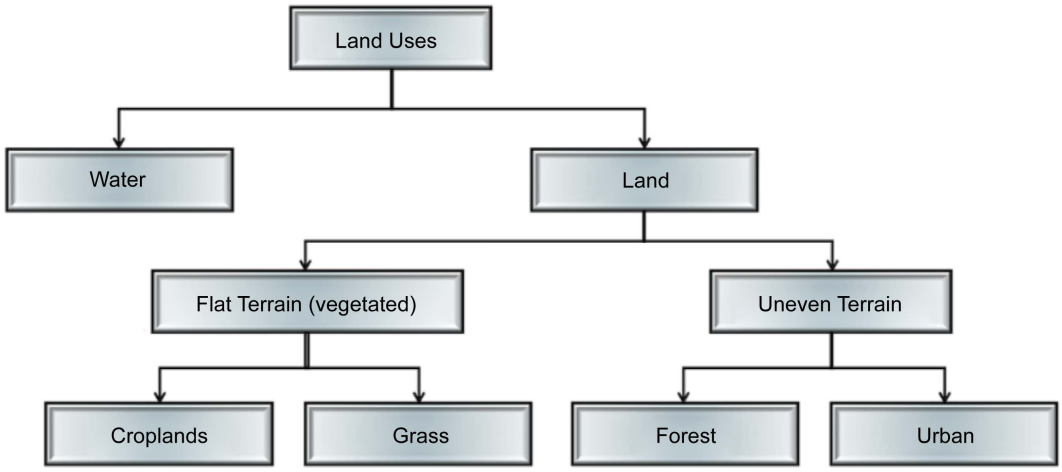

Figure 10. A Decision-Tree classification algorithm for mapping LULC using the pre-flood imagery.

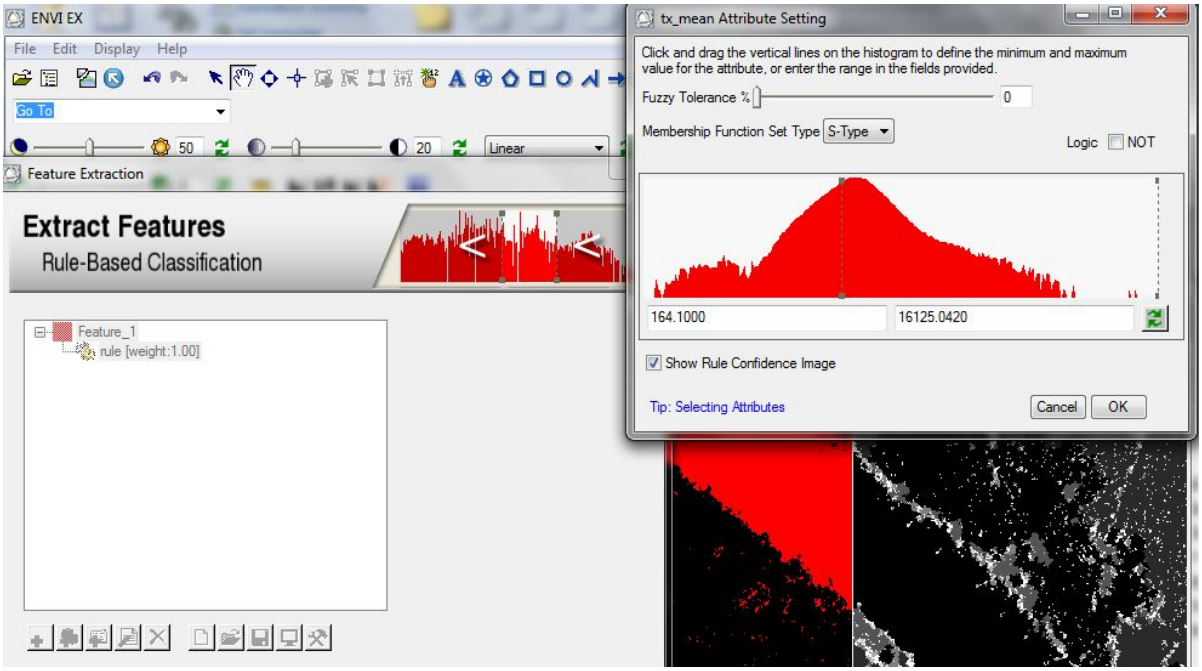

Figure 11. Identifying decision boundaries according to the valley, peak and shoulder of the attributes histogram in the feature extraction workflow under ENVI EX.

For mapping the flood extent areas for both study locations, the optimum classification methods with respect to the LULC classification results were applied. The flood extent maps initially produced were corrected using the digital elevation model (DEM) for this area and the resulting LULC maps. The DEM was used to remove the regions misclassified as water within the area around the river that had a land level higher than the water level measured at the gauges. The LULC maps were used to remove the forest and residential areas which were misclassified as water due to the limitations of x-band imagery in mapping the water areas beneath forest and urban coverage [43] [57]. It is difficult to obtain a reference map for extent of a given flood event due to accessibility problems during the flood. Therefore, a reference flood map was digitized from the TSX imagery using the ARCGIS program to assess the classification accuracy. The resulting corrected flood maps were analyzed using the spatial module under ARCGIS to calculate cross-tabulated areas between this digitized reference map and the resulting classifications and subsequently to estimate the confusion matrix for the water class. The flood extent areas generated in 2011 were compared to the flood extent areas for June 2013 created by [58]. Finally, the LULC maps were used in determining if the inundated land was vegetated or residential, and hence in defining the risk zones in January 2011 and June 2013. The results of the classifications produced are presented and explained below.

3. Results and Discussion

3.1. LULC Classification

For both study areas, the raw and Lee-filtered images were processed to identify the land use classes using the object-based approach. The land uses were delineated manually to evaluate the accuracy of the resulting classification. The reference digitized LULC maps for both study areas have four main classes, as previously stated. The images at Walmsburg Oxbow has 5% water extent, 66% vegetated lands, 23% forests and 6% residential areas. The images at Wehningen Oxbow has 8% water extent, 71% vegetated lands, 17% forests and 4% residential areas. In order to generate the rule-based classifications, the workflow for feature extraction in ENVI EX was applied six times for each study area, using HH−, VV−, and HH/VV− polarization of the raw and Lee-filtered images. Three different combinations of class pairs were chosen for feature separation to represent the three branches of the Decision-Tree. These combinations are 1) water and land, 2) vegetated lands and uneven lands, and 3) residential areas and forests.

For branch (1), 64 classifications were generated to map the water and land classes. From the spectral-attributes, the band-average was used; the mean and variance were used from the texture-attributes; and solidity, convexity, compact and elongation were used from the spatial-attributes. In addition, some rule sets were used to combine certain attributes together to enhance the classification results. Rule set 11 combined the band-average and mean-texture; rule set 12 included texture-mean and solidity-attributes; rule set 13 added the roundness to texture-mean and solidity-attributes; rule set 4 incorporated elongation with texture-mean-attributes, solidity and roundness-attributes. The producer accuracy and the total accuracy are shown in **Table 1**. For branch (2), the

Table 1. Summary of producer accuracy (%) for water class and land class (Vegetated Land, Forest, Resedential Areas) applying the object-based procedure.

			Producer Accuracy %								
Polarization	Rules	Filter Type	Wehningen Oxbow			Walmsburg Oxbow			Average		
			Water	Land	Total	Water	Land	Total	Water	Land	Total
HH	Average Band > 45	Raw	86	99	98	92	99	99	89	99	99
		Lee	83	94	93	87	99	99	85	97	96
	Average Band > 55	Raw	92	97	97	94	98	98	93	97	97
		Lee	88	92	92	91	99	98	89	95	95
VV	Average Band > 45	Raw	87	99	98	91	99	99	89	99	99
		Lee	84	94	93	87	99	99	85	97	96
	Average Band > 55	Raw	92	95	95	94	98	98	93	97	96
		Lee	89	90	90	90	97	97	90	93	93
HH/VV	Average Band	Raw	92	97	97	94	98	97	93	97	97
		Lee	90	89	89	92	97	97	91	93	93
	Rule Set 11	Raw	92	98	97	94	98	97	93	98	97
		Lee	88	92	92	92	97	97	90	95	95
	Texture Mean > 55	Raw	92	98	97	94	98	98	93	98	98
		Lee	88	93	92	90	99	98	89	96	95
	Texture Variance	Raw	87	99	98	84	99	99	86	99	98
		Lee	77	94	93	68	99	98	72	97	96
	Texture Mean > 45	Raw	84	99	99	94	98	98	89	99	98
		Lee	83	94	93	90	99	98	86	97	96
	Solidity	Raw	65	99	97	74	99	98	69	99	98
		Lee	38	95	90	68	99	98	53	97	94
	Convexity	Raw	64	49	50	99	62	64	82	56	57
		Lee	68	88	86	68	84	83	68	86	85
	Compact	Raw	64	99	97	72	99	97	68	99	97
		Lee	74	87	86	68	99	98	71	93	92
	Elongation	Raw	76	26	29	73	99	99	74	63	64
		Lee	77	95	94	69	99	98	73	98	96
	Rule Set 12	Raw	85	99	98	92	99	99	88	99	99
		Lee	83	94	93	87	99	99	85	97	96
	Rule Set 13	Raw	87	98	97	92	99	99	90	98	98
		Lee	84	94	93	87	99	99	85	97	96
	Rule Set 14	Raw	82	94	93	86	99	98	84	97	96
		Lee	82	94	93	82	99	99	82	97	96

land class mask was used to isolate the land areas from each image. The masked images were used in generating different classifications for the vegetated land and uneven land classes. 52 classifications were generated to map the vegetated lands and uneven lands. From the spectral-attributes, the band-average was used; the mean, variance and entropy were used from the texture-attributes; and area, solidity, convexity, compact, elongation and roundness were used from the spatial-attributes. In addition, one rule set was used to combine the band-average and mean-texture. The producer accuracy and the total accuracy are summarized in **Table 2**. For branch (3), the uneven land class mask was used to isolate the uneven lands from each image. The masked images were used in generating different classifications for the residential area and forest classes. 44 classifications were generated to

Table 2. Summary of the producer accuracy (%) for Vegetated Land and Uneven Land classes (Forest, Residential Areas) applying the object-based procedure.

			Producer Accuracy %								
Polarization	Rules	Filter Type	Wehningen Oxbow			Walmsburg Oxbow			Average		
			Vegetated Land	Uneven Land	Total	Vegetated Land	Uneven Land	Total	Vegetated Land	Uneven Land	Total
HH	Average Band	Raw	80	59	75	87	63	80	83	61	77
		Lee	87	67	83	90	48	79	90	58	81
VV	Average Band	Raw	86	40	76	85	52	75	86	46	75
		Lee	88	64	82	88	46	75	88	55	79
HH/VV	Average Band	Raw	80	62	76	80	64	75	80	63	75
		Lee	87	68	83	85	72	81	86	70	82
	Rule Set 21	Raw	80	54	74	80	64	75	80	59	75
		Lee	87	56	79	86	51	75	86	53	77
	Texture Mean	Raw	80	58	75	82	76	73	81	67	74
		Lee	88	61	82	83	67	79	86	64	80
	Texture Variance	Raw	80	74	77	76	71	74	78	72	75
		Lee	92	76	88	86	74	84	89	75	86
	Solidity	Raw	81	56	75	87	50	75	84	53	75
		Lee	75	58	70	80	44	69	77	51	70
	Convexity	Raw	80	43	71	84	48	73	82	45	72
		Lee	86	63	80	81	56	74	84	60	77
	Compact	Raw	80	52	74	87	35	71	84	43	72
		Lee	86	61	80	74	55	68	80	58	74
	Elongation	Raw	87	68	82	85	66	80	86	67	81
		Lee	86	57	79	88	51	77	87	54	78
	Area	Raw	85	47	76	80	35	66	82	41	71
		Lee	88	68	84	86	65	80	87	66	82
	Round	Raw	79	53	73	77	64	73	78	58	73
		Lee	92	38	79	86	50	75	89	44	77
	Texture Entropy	Raw	87	59	76	77	62	72	82	60	74
		Lee	91	77	87	87	81	84	89	79	86

map the forests and residential areas. From the spectral attributes, the band average was used, the mean, variance and entropy were used from the texture-attributes; and solidity, convexity, rectangle fit and roundness were used from the spatial-attributes. In addition, one rule set was used to combine the band-average and texture-mean attributes. The producer accuracy and the total accuracy are summarized in **Table 3**.

As shown in **Tables 1-3**, using dual-polarization HH/VV led to higher total producer accuracy than the total producer accuracies employing either HH− or VV− polarization only. In contrast to the vegetated/uneven land classification results, using raw images facilitated higher producer accuracies than the Lee-filtered images in the results of both land/water and forests/residential classifications. The most useful features for separating the water class from the land class were texture-mean and band-average. Other attributes are not efficient in separating water from land. Applying either rule set 11 or texture-mean attributes enabled slightly better producer accuracy for the land class than employing the average band attributes. The best producer accuracy for the water class was 94% using the raw images with either single or dual polarization based on the average-band-attribute and texture-mean-attribute rules at Walmsburg Oxbow, while the lowest producer accuracy, of only 38%, was achieved at Wahgingen Oxbow when using Lee-filter images based on the convexity-attribute rule. The best total producer accuracy was 99%, using the raw images with single or dual polarization based on many rules at Walmsburg

Table 3. Summary of producer accuracy (%) for the Forest and Residential Area classes applying the object-based procedure.

			Producer Accuracy %								
Polarization	Rules	Filter Type	Wehningen Oxbow			Walmsburg Oxbow			Average		
			Forests	Residential Areas	Total	Forests	Residential Araes	Total	Forests	Residential Araes	Total
HH	Average Band	Raw	86	63	82	79	60	76	83	62	79
		Lee	85	45	78	78	34	68	82	40	73
VV	Average Band	Raw	85	76	82	81	73	77	83	75	80
		Lee	83	53	78	76	45	69	80	49	74
HH/VV	Average Band	Raw	84	76	83	81	74	80	83	75	82
		Lee	83	53	77	79	48	72	81	51	75
	Rule Set 31	Raw	85	76	83	82	75	80	84	76	82
		Lee	83	52	77	79	50	75	81	51	76
	Texture Mean	Raw	83	78	82	80	75	79	82	77	81
		Lee	75	60	72	76	59	70	76	60	71
	Texture Variance	Raw	61	52	59	11	71	27	36	62	43
		Lee	64	59	62	66	43	69	65	51	66
	Texture Entropy	Raw	71	69	71	68	56	66	70	63	69
		Lee	68	38	62	86	26	73	77	32	68
	Solidity	Raw	70	65	69	86	39	76	78	52	73
		Lee	85	23	77	77	27	67	81	25	72
	Convexity	Raw	40	73	46	53	54	53	47	64	50
		Lee	44	63	48	58	49	56	51	56	52
	Rectangle-fit	Raw	89	50	82	80	48	76	85	49	79
		Lee	75	38	68	79	24	67	77	31	68
	Round	Raw	46	74	53	78	35	69	62	60	61
		Lee	62	40	58	84	18	70	73	29	64

Oxbow, while the lowest total producer accuracy of only 50% was achieved, again at Wehningen Oxbow, using the Lee-filter images based on the convexity-attribute rule.

The objects misclassified into the water class corresponded to the shadow of the forest areas. The shadow areas have less texture-mean than the water areas of the Elbe River. Therefore, rule set 12 was applied with a lower texture-mean value to isolate the main river, as shown in **Figure 12**. **Figure 12(A)** shows the TSX imagery at Wehningen Oxbow. **Figure 12(B)** shows the land class in yellow, based on a texture means greater than 55. Several areas of the forest shadow which were misclassified as water are circled. **Figure 12(C)** shows the land class in green based on a texture mean greater than 45. Several water areas which were misclassified as land are circled. **Figure 12(D)** shows the land class, in red, based on rule set 13. Several water areas which were correctly re-classified as water are circled. Using the solidity-attribute in rule set 12 improved the water class by 1%. Moreover, the roundness-attribute improved the water class by 2% in rule set 13. On the other hand, employing more attributes, such as elongation and length, failed to enhance the water class results and led to lower producer accuracies.

The most useful features for separating vegetated lands class from the uneven lands class were, first, texture-entropy, followed by texture-variance and band-average, respectively. Elongation and area spatial-attributes succeeded to a certain degree in differentiating the two classes. Other attributes were only negligibly successful in separating them. Applying rule set 21, led to less total producer accuracy than employing the band-average-attributes. The elongation-attribute rule enabled better classification results for raw imagery while the texture-entropy-rule enabled higher classification accuracy for Lee-filtered images. The greatest producer accuracy for vegetated lands class was 92%, using the Lee-filtered dual-polarized images at Wehningen Oxbow based on the texture-variance-rule, while the lowest producer accuracy, of only 74%, was achieved at Walmsburg Oxbow

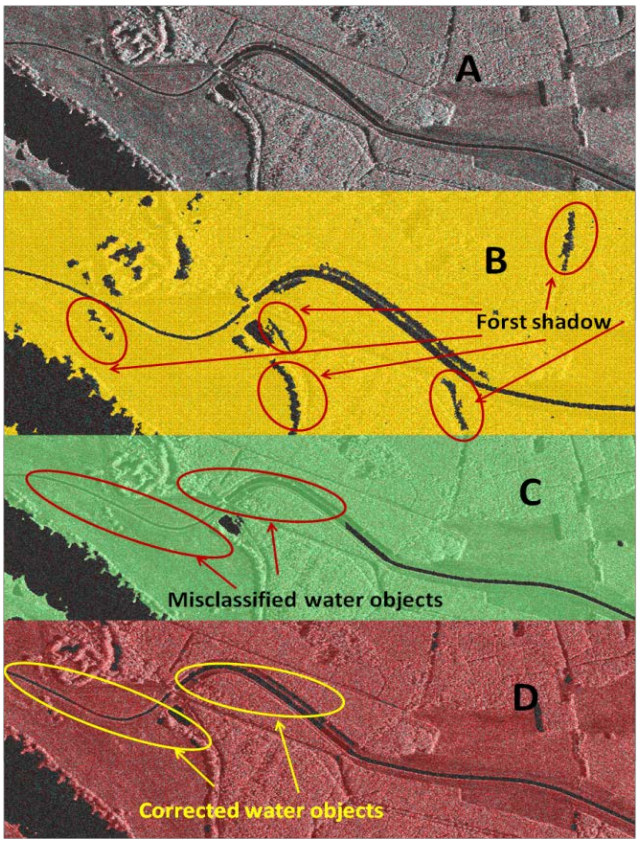

Figure 12. (A) The dual polarization TSX imagery at Wahgingen Oxbow; (B) Land class produced based on texture mean greater than 55 and the forest shadows which are misclassified as water; (C) Land class produced based on texture mean greater than 45 and several water areas which are misclassified as land; (D) Land class produced based on rule set 13 and several water areas which are corrected and classified as water.

using the Lee-filtered images based on the compact-attribute rule. The maximum producer accuracy for the uneven land class was 81%, using the Lee-filtered dual-polarized images at Walmsburg Oxbow based on the texture-entropy-rule, while the lowest producer accuracy of only 35% was achieved at same study area, again when using the raw images based on the compact-attribute-rule. The best total producer accuracy was 88%, using Lee-filtered images at Wagingen Oxbow based also on texture-variance-rule, while the lowest total producer accuracy, of only 66%, was achieved once more at Walmsburg Oxbow using raw images based on the area-attribute-rule. The objects misclassified as vegetated lands in the uneven land class mostly correspond to existing vegetated areas within the residential areas (e.g. parks or gardens), as shown in **Figure 13**. **Figure 13(A)** shows the TSX imagery at Wehningen Oxbow. **Figure 13(B)** shows the uneven land class produced at the same position based on texture-entropy overlaid on the TSX image in red. **Figure 13(C)** shows the reference map at the same position for the uneven land class, in red, and vegetated lands class, in green. Here, for the uneven land class, it is difficult to separate vegetated areas from buildings within the residential areas. In general, the vegetated areas comprise 15% to 30% of the residential areas in the cities and the villages. Therefore the producer accuracy of the uneven land class was limited to about 80%. Nonetheless, the classification has higher accuracy with more details than the reference map.

The effective features for separating the forest class from the residential area class were texture-mean, band-average, and their combination in rule set 31. Other attributes were not able to differentiate the two classes. Applying rule set 31 led to slightly better total producer accuracy than employing the band-average-attribute or texture-mean attribute individually. This rule set produced the highest classification accuracy for both raw and Lee-filtered images. The greatest producer accuracy for the forest class was 89%, using the dual-polarized raw images at Wehningen Oxbow based on the rectangle-fit rule, while the lowest producer accuracy, of only 11%, was achieved at Walmsburg Oxbow using raw images based on the texture-variance-attribute rule. The best producer accuracy for the residential area class was 78%, using the dual-polarized raw images at Wehningen

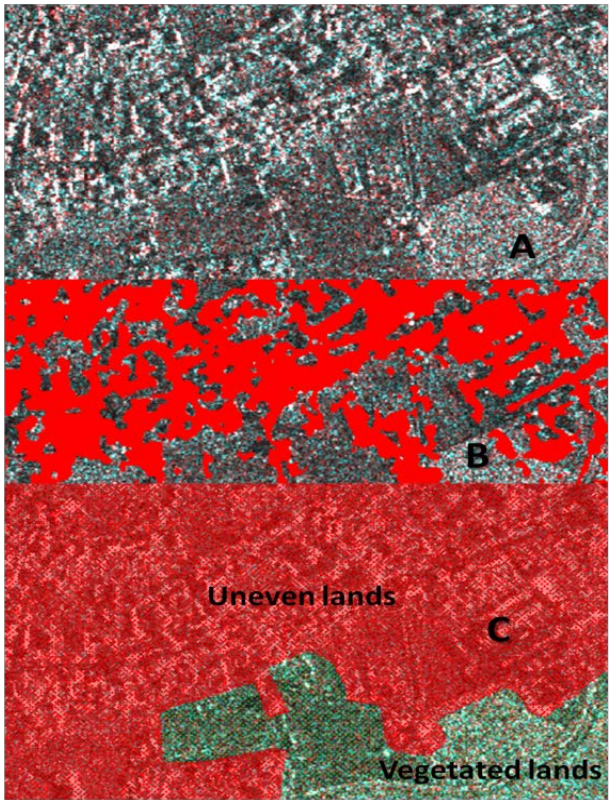

Figure 13. (A) The dual polarization TSX imagery at Wehningen Oxbow; (B) Uneven land class produced at the same position based on texture entropy overlaid on the TSX image in red; (C) The reference map at the same position for the uneven land class (in red) and the vegetated land class (green).

Oxbow based on the texture-mean-attribute rule, while the lowest producer accuracy of only 23% was achieved at the same study area using the Lee-filtered images based on the solidity-attribute rule. The highest total producer accuracy was 83%, using the raw images at Wehningen Oxbow based on the average-band-attributes rule, while the lowest total producer accuracy, of only 27%, was achieved at Walmsburg Oxbow using the raw imagery based on the text-variance-attribute rule. The objects misclassified as forests in the residential area class correspond to vegetated areas within the residential areas, as shown in **Figure 13**. Therefore, the producer accuracy of the residential area class was limited to about 78%. Based on the classification results from the three branches, the ultimate Decision-Tree for identifying the major land uses using the raw imagery is shown in **Figure 14**.

3.2. Flood Detection Maps

Based on the LULC classifications results for identifying water areas, using the average band attribute and/or the texture-mean attribute in the rule-based classifier enabled identification of about 90% of the water cover. Therefore, post-flood images in January 2011 were processed to be used as the pre-flood ones, and classified using the rule-based classifier with the average-band attribute and the texture-mean-attribute. The initial flood extent areas were corrected using the DEM and the LULC maps. The confusion matrices for both areas before and after post-classification are shown in summary in **Table 4**.

In **Table 4**, the NH enhancement method refers to the producer accuracies obtained by applying the neighborhood filter, and the residential method refers to the producer accuracies resulting from correcting for areas misclassified as water within the residential area; the forest method refers to the producer accuracies resulting from correcting areas misclassified as water within the forests, while the LULC method means those producer accuracies obtained by correcting areas misclassified as water within the forest and residential areas. In addition, the DEM method gives the producer accuracies after correcting the areas misclassified as water at altitude higher than the gauge water level for this area around the river. The LULC & DEM method provides the producer accuracies when corrected according to both DEM and LULC. As **Table 4** reveals, the results of the rule-based classifier using the texture-mean attribute presented slightly higher total producer accuracies than the rule-based classifier with the average-band attribute. Using the Lee-filtered images led to lower producer accuracies for the water class. Correcting areas misclassified as water within the residential areas enhanced the total producer accuracy by about 0.1%, while correcting areas misclassified as water within the forest resulted in an increase in the land producer accuracy of about 1.5% and, consequently, in the total producer accuracy of about 1%. On the other hand, the DEM method did not improve the classification results, and consequently the combined LULC & DEM method only had results similar to the LULC enhancement method alone.

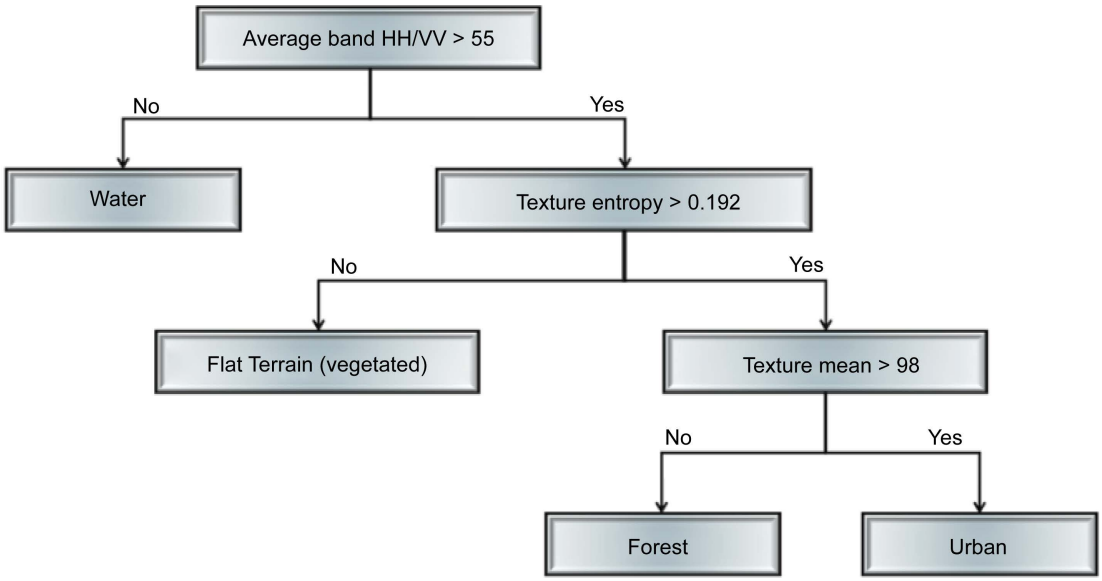

Figure 14. Suggested Decision-Tree classification algorithm for mapping LULC using pre-flood raw imagery.

Table 4. Summary of producer accuracy (%) for water and land classes applying the object-based procedure for post-flood imagery.

Rule	Enhancement Means	Filter Type	Producer Accuracy %								
			Wehningen Oxbow			Walmsburg Oxbow			Average		
			Land	Water	Total	Land	Water	Total	Land	Water	Total
Average Band	NH	Raw	97.9	96.4	97.5	97.3	98.0	97.4	97.6	97.2	97.5
		Lee	98.1	94.0	97.0	98.2	97.8	98.2	98.2	95.9	97.6
	Residential	Raw	98.0	96.4	97.6	97.6	97.9	97.7	97.8	97.2	97.6
		Lee	98.2	94.0	97.1	98.6	97.8	98.4	98.4	95.9	97.8
	Forest	Raw	99.1	96.4	98.4	98.7	97.9	98.6	98.9	97.2	98.5
		Lee	99.1	94.0	97.8	99.4	97.8	99.1	99.2	95.9	98.5
	DEM	Raw	97.9	96.4	97.5	97.4	97.8	97.5	97.7	97.1	97.5
		Lee	98.2	94.0	97.1	98.3	97.7	98.2	98.2	95.8	97.6
	LULC	Raw	99.2	96.4	98.5	99.0	97.9	98.8	99.1	97.2	98.6
		Lee	99.3	94.0	97.9	99.7	97.8	99.4	99.5	95.9	98.6
	LULC & DEM	Raw	99.2	96.4	98.5	99.0	97.9	98.8	99.1	97.2	98.6
		Lee	99.3	94.0	97.9	99.7	97.8	99.4	99.5	95.9	98.6
Texture Mean	NH	Raw	97.9	97.0	97.7	97.5	97.9	97.5	97.7	97.4	97.6
		Lee	98.0	94.5	97.1	97.9	98.5	98.0	98.0	96.5	97.6
	Residential	Raw	98.0	97.0	97.7	97.7	97.8	97.7	97.8	97.4	97.7
		Lee	98.2	94.5	97.2	98.3	98.5	98.3	98.2	96.5	97.8
	Forest	Raw	99.1	97.0	98.6	98.8	97.8	98.6	99.0	97.4	98.6
		Lee	99.1	94.5	97.9	99.2	98.5	99.1	99.1	96.5	98.5
	DEM	Raw	97.9	96.9	97.7	97.6	97.7	97.6	97.7	97.3	97.6
		Lee	98.1	94.5	97.1	98.1	98.4	98.1	98.1	96.4	97.6
	LULC	Raw	99.2	97.0	98.6	99.0	97.8	98.8	99.1	97.4	98.7
		Lee	99.2	94.5	98.0	99.6	98.5	99.4	99.4	96.5	98.7
	LULC & DEM	Raw	99.2	97.0	98.6	99.0	97.8	98.8	99.1	97.4	98.7
		Lee	99.2	94.5	98.0	99.6	98.5	99.4	99.4	96.5	98.7

3.3. Hazard Areas during the Floods of 2011 and 2013

The flood detection maps produced for January 2011 were compared to the flood extent areas in June 2013 as represented by DLR (2013), and to the high flood zone maps. The flood extent areas were approximately identical for 2011 and 2013 floods, as shown in **Figure 15** and **Figure 16**. Therefore, the flooded areas as shown in the maps produced for 2011 were used in defining the hazard areas for the winter flood in January 2011 and the summer flood in June 2013. The reference LULC maps, and the agricultural land use maps during the summer of 2011, produced by Farghaly *et al*. (2014), were overlaid onto the flooded areas identified for January 2011 in order to determine the hazard areas, as also shown in **Figure 15** and **Figure 16**.

Figure 15 was used to study the area around Walmsburg Oxbow. The residential areas did not experience any hazards. On the other hand, four large cultivated fields were fully or partially submerged in 2011. These fields may be expected to be entirely submerged in future high floods since they are located within the high flood zone.

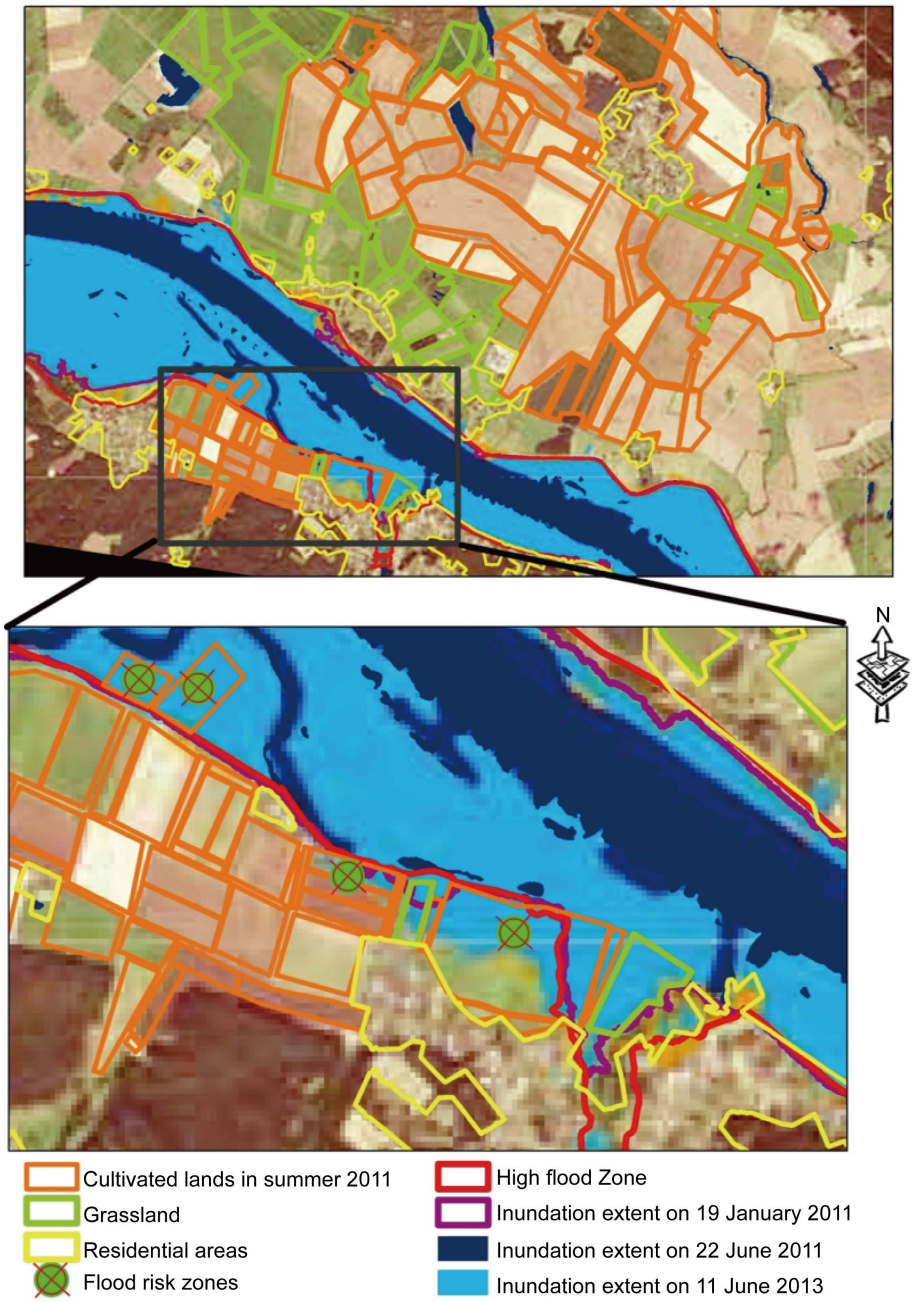

Figure 15. The flood extent of the flood in 2013 created by DLR overlaid with the flood extent in June and January 2011, the residential areas and agricultural land use in Summer 2011 at Walmsburg Oxbow.

In spite of the fact that these fields were flooded in January 2011, they were cultivated with maize and potatoes in summer 2011. During the flood of summer 2013, these cultivated areas were again inundated and caused economic losses to the owners of the land. To achieve sustainable land use in this area, these fields must be included in the flood hazard maps and regulations established to prevent cultivation in these areas, permitting the fields to be used only as grassland, in order to avoid economic losses.

In **Figure 16**, the cultivated area around Wehningen Oxbow, in contrast to the Walmsburg Oxbow, was not submerged and did not endure any hazards. On the other hand, part of the residential area in the Strachauer Rad, in the city of Dannenberg, Lower Saxony, is located within the high flood zone. However, this area was not

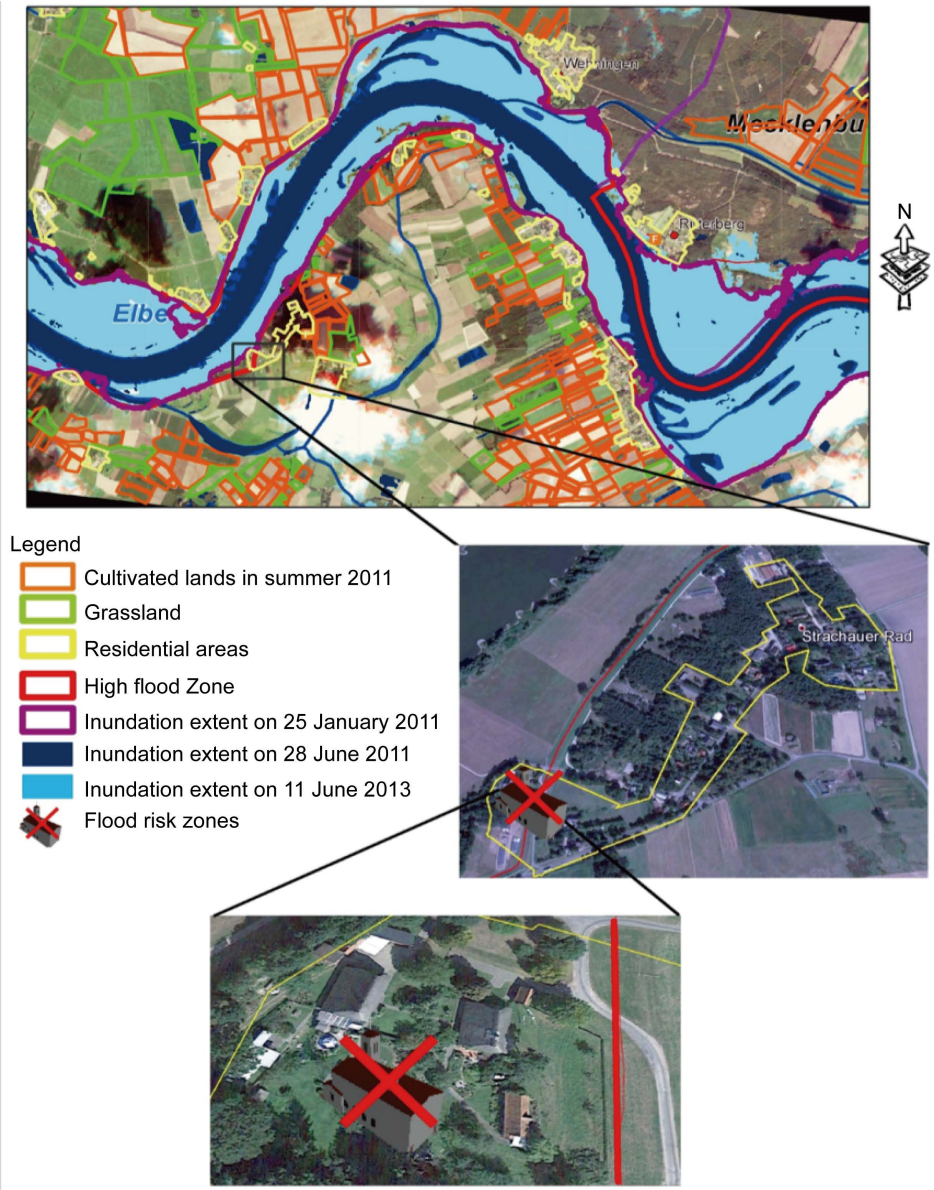

Figure 16. The flood extent due to the floods in 2013 produced by DLR overlaid with the flood extent in June 2011 and January 2011, the residential areas and the agricultural land use in summer 2011 at Wehningen Oxbow.

submerged during the most recent high floods, in 2011 and 2013. Nevertheless, this part of the city should be added to the hazard and risk maps to avoid the possible human and economic losses that may occur due to higher floods. This flood mapping will support sustainable land use in this area.

4. Concluding Remarks

In order to achieve sustainable land use on the Middle Elbe River floodplain, up-to-date land use maps during the pre-flood period are essential to determine the hazards that may arise during the post-flood period. In particular, the locations of residential areas must be verified against the maps to ensure that they are safely removed from the high flood zone. Therefore, the residential areas that lie within the extent of flood zone must be included on the risk maps to support the regulatory prevention of (further) building within these risk zones. Moreover, the arable land which has suffered partially or fully from flood events must also be added to the ha-

zard maps to decrease potential economic losses and to achieve sustainable land use.

The merging of similar pixels into objects diminishes the problem of speckle noise in the TSX imagery and, thus, enables high producer accuracies from the raw images without filtering. The raw images lead to similar or even better results than the Lee-filtered images. Therefore, it is recommended to use the object-based classifier with the raw images to save time and effort. Especially during flood events, flood extent maps are immediately required to identify hazard areas to help reduce human and economic losses. Further, the use of dual-polarized images enhances the classification results and leads to higher producer accuracies than the mono-polarized images. Therefore, it is recommended to use dual-polarization images to attain more accurate LULC maps.

The resulting Decision-Tree procedure, using the rule-based classifier in ENVI EX, resulted in considerably better total producer accuracies, such that about 95% of the water area was accurately defined, as well as about 90% of vegetated lands being correctly determined, and around 80% of the forest and the residential area classes recognized. The 20% misclassified areas within the forest and residential areas were due to the existence of vegetated areas and trees within the residential areas around the buildings.

The use of texture and spatial attributes with the spectral attributes enhanced the classification results. Applying rules based on the band-average, as a spectral attribute, and the texture-mean facilitated correct identification of about 95% of the flood extent for post-flood imagery. Furthermore, the use of the texture-entropy attribute enabled recognition of about 90% of the vegetated lands. The texture-mean attribute enabled efficient distinguishing of residential areas and forest classes.

To conclude, the results show that similar rule sets can be used for the Decision-Tree procedure on two remote study areas in the Elbe River flood plains to achieve higher classification producer accuracies. Thus, the suggested Decision-Tree should be applicable to other remote areas. Therefore, it is recommended to continuously monitor the entire Biosphere Reserve using TSX imagery to deal with construction and/or cultivation within the flood zone. Construction and cultivation in flood plains should be carefully planned according to the flood risk maps to ensure sustainable land use within the Elbe Biosphere.

Acknowledgements

We are greatly indebted to the administration of the Biosphere Reserve “Niedersächsische Elbtalaue” (Lower Saxonian Elbe Valley Biosphere Reserve) and to the German Aerospace Centre (Deutsches Zentrum für Luft- und Raumfahrt, DLR) for providing the satellite images used in this study. We acknowledge the important support of this research provided by a PhD graduate scholarship awarded by LEUPHANA University Lüneburg to Dalia Farghaly.

References

[1] Brämick, U., Fladung, F. and Doering-Arjes, P. (2008) Aalmanagementplan-Flussgebietsgemeinschaft Elbe, Institut für Binnenfischerei e.V. Potsdam-Sacrow, Potsdam.

[2] Hauf, Y. (2005) The River Basin District Elbe and the Coordinating Areas, MONERIS (Modelling Nutrient Emissions in River Systems). River Basin Community Elbe, Potsdam Institute for Climate Impact Research, Potsdam.

[3] IKSE (2005) Informationsblatt der IKSE Nr. 1 Gastbeiträge und Weitere Informationen Wasserrahmenrichtlinie im Einzugsgebiet der Elbe. Internationale Kommission zum Schutz der Elbe (IKSE), Magdeburg.

[4] Kunkel, R. and Wendland, F. (1998) Der Landschaftswasserhaushalt im Flußeinzugsgebiet der Elbe Verfahren, Datengrundlagen und Bilanzgrößen. Schriften des Forschungszentrums Jülich Reihe Umwelt, 12, Forschungszentrum, Zentralbibliothek, Jülich.

[5] NLWKN (2014) Gauges Location along Elbe River, Niedersächsischer Landesbetrieb für Wasserwirtschaft, Küsten- und Naturschutz (NLWKN), Hochwassermeldedienste.

[6] Jutta, G. and Inga, M. (2011) Die Elbe Von der Quelle bis zur Mündung. The Elbe, Komet Verlag, Köln.

[7] UNESCO (2011) UNESCO—Biosphere Reserves in Germany.

[8] Prüter, J., Keienburg, T. and Schreck, C. (2014) Klimafogenanpassung im Biosphärenreservat Niedersächsiche Elbtalaue—Modellregion für nachhaltige Entwicklung Berichte aus den Klimzug-Nord Modellgebieten—Band 5, neue Ausg, TuTech Innovation, Hamburg.

[9] Härdtle, W., Redecker, B., Assmann, T. and Meyer, H. (2006) Vegetation Responses to Environmental Conditions in Floodplain Grasslands: Prerequisites for Preserving Plant Species Diversity. *Basic and Applied Ecology*, **7**, 280-288. http://dx.doi.org/10.1016/j.baae.2005.09.003

[10] Urban, B. (2003) River Elbe Ecology—Contributions to a Large Scale Environmental Project. In: Ramesh, R. and Ramachandran, S., Eds., *Coastal Urban Environments*, Capital Publishing Company, New Delhi, Kolkate, Bangalore, 67-88.

[11] Ludewig, K., Korell, L., Loeffler, F., Scholz, M., Mosner, E. and Jensen, K. (2014) Vegetation Patterns of Floodplain Meadows along the Climatic Gradient at the Middle Elbe River. *Flora*, **209**, 446-455. http://dx.doi.org/10.1016/j.flora.2014.04.006

[12] Kienzler, S., Pech, I., Kreibich, H., Müller, M. and Thieken, A.H. (2014) After the Extreme Flood in 2002: Changes in Preparedness, Response and Recovery of Flood-Affected Residents in Germany between 2005 and 2011. *Natural Hazards and Earth System Sciences*, **2**, 6397-6451. http://dx.doi.org/10.5194/nhessd-2-6397-2014

[13] Mudersbuch, M., Bender, J., Kelln, V. and Jensen, J. (Eds.) (2013) Analysis Flood Frequencies at the Elbe River—Do Recent Extreme Events Affect Design Levels? *Proceedings of the International Conference on Water Resources and Environment Research* (*ICWRER*), Koblenz, 3-7 June 2013, 346-362.

[14] Gremli, R., Keller, B., Sepp, T. and Szönyi, M. (2014) European Floods: Using Lessons Learned to Reduce Risks. Zurich Insurance Group Ltd, Zurich.

[15] Bessel, T., Möhrle, S., Dittrich, A., Schröter, K., Mühr, B., Elmer, F., Kunz-Plapp, F., Trieselmann, W. and Kunz, M. (2013) June 2013 Flood in Central Europe—Focus Germany Report 2—Update 1: Impact and Management. Center for Disaster Management and Risk Reduction Technology—CEDIM Forensic Disaster Analysis Group (FDA), Karlsruhe.

[16] Schröter, K., Kunz, M., Elmer, F., Mühr, B. and Merz, B. (2014) What Made the June 2013 Flood in Germany an Exceptional Event? A Hydro-Meteorological Evaluation. *Hydrology and Earth System Sciences*, **11**, 8125-8166. http://dx.doi.org/10.5194/hessd-11-8125-2014

[17] Geller, W. (2004) Schadstoffbelastung nach dem Elbe-Hochwasser 2002 Endbericht des Ad-hoc-Projekts "Schadstoffuntersuchungen nach dem Hochwasser vom August 2002—Ermittlung der Gefährdungspotentiale an Elbe und Mulde" BMBF-Förderkennzeichen PTJ 0330492, UFZ; Kompetenzzentrum Digitaldr, Leipzig, Nürnberg.

[18] Kundzewicz, Z.W., Pińskwar, I. and Brakenridge, G.R. (2013) Large Floods in Europe, 1985-2009. *Hydrological Sciences Journal*, **58**, 1-7. http://dx.doi.org/10.1080/02626667.2012.745082

[19] Begg, C., Luther, J., Kuhlicke, C. and Steinführer, A. (2011) Participation in Central European Flood Risk Management: Social Capacity Building in Practice. Centre for Environmental Research—UFZ, Leipzig.

[20] Balthasar, B. and Edwards, T. (2011) 2011 Rhein (Rhine) and Elbe Basin Floods, Germany—Report of 18th January 2011, Willis Re Analytics Event Response, London.

[21] LHW (2014) Bericht über das Hochwasser im Juni 2013 in Sachsen-Anhalt Entstehung, Ablauf, Management und statistische Einordnung, Landesbetrieb für Hockwasserschutz und Wasserwirtscaft (LHW) Sachsen-Anhalt, AG Oberflächenwasser der FGG Elbe, Magdeburg.

[22] Dallmann, G. (2013) Hydrologische Zusammenfassung zum Hochwasser an Elbe und Weser im Juni 2013. Niedersächsisches Ministerium für Umwelt, Energie und Klimaschutz, Hannover.

[23] Kerner, M. (2014) Risk Nexus. Central European Floods 2013: A Retrospective Flood Resilience Review 05.14. Zurich Insurance Company Ltd, Zurich.

[24] Ouma, Y. and Tateishi, R. (2014) Urban Flood Vulnerability and Risk Mapping Using Integrated Multi-Parametric AHP and GIS: Methodological Overview and Case Study Assessment. *Water*, **6**, 1515-1545. http://dx.doi.org/10.3390/w6061515

[25] Pradhan, B. (2009) Flood Susceptible Mapping and Risk Area Delineation Using Logistic Regression, GIS and Remote Sensing. *Journal of Spatial Hydrology*, **9**, 1-18.

[26] APFM (2013) Flood Mapping. Integrated Flood Management Tools Series No. 20. Associated Programme on Flood Management (APFM), World Meteorological Organization (WMO) and the Global Water Partnership (GWP). Jason DeCaires Taylor, ProLitteris, Zurich.

[27] UNECE (2009) Transboundary Flood Risk Management: Experiences from the UNECE Region. Convention on the Protection and Use of Transboundary Watercourses and International Lakes, United Nations Economic Commission for Europe (UNECE). UNO, New York, Geneva.

[28] Moel, H., Alphen, J. and Aerts, J.C.J.H. (2009) Flood Maps in Europe—Methods, Availability and Use. *Natural Hazards and Earth System Sciences*, **9**, 289-301. http://dx.doi.org/10.5194/nhess-9-289-2009

[29] FLOODsite (2008) Integrated Flood Risk Analysis and Management Methodologies Pilot Study "Elbe River Basin" Executive Summary. Report No.: T21-08-02, Leibniz Institute of Ecological and Regional Development (IOER), Dresden.

[30] EXCIMAPAP (2007) Handbook on Good Practices for Flood Mapping in Europe, European Exchange Circle on Flood Mapping (EXCIMAPAP).

[31] FEMA (2009) Guide to Flood Maps Using the Flood Map to Improve Your Understanding of Risk. The Federal Emergency Management Agency (FEMA), Arlington.

[32] Chenghu, Z., Luo, J., Zang, C., Li, B. and Wang, S. (2000) Flood Monitoring Using Multi-Temporal AVHRR and RADARSAT Imagery. *Photogrametric Engineering & Remote Sensing*, **66**, 633-638.

[33] Leenaers, H. and Okx, J.P. (2007) The Use of Digital Elevation Models for Flood Hazard Mapping. *Earth Surface Processes and Landforms*, **14**, 631-640. http://dx.doi.org/10.1002/esp.3290140617

[34] Schnebele, E. and Cervone, G. (2013) Improving Remote Sensing Flood Assessment Using Volunteered Geographical Data. *Natural Hazards and Earth System Sciences*, **13**, 669-677. http://dx.doi.org/10.5194/nhess-13-669-2013

[35] Senthilnath, J., Shenoy, H.V., Rajendra, R., Omkar1, S.N., Mani, V. and Diwakar, P.G. (2013) Integration of Speckle De-Noising and Image Segmentation Using Synthetic Aperture Radar Image for Flood Extent Extraction. *Journal of Earth System Science*, **122**, 559-572. http://dx.doi.org/10.1007/s12040-013-0305-z

[36] Skakun, S., Kussul, N., Shelestov, A. and Kussul, O. (2014) Flood Hazard and Flood Risk Assessment Using a Time Series of Satellite Images: A Case Study in Namibia. *Risk Analysis*, **34**, 1521-1537. http://dx.doi.org/10.1111/risa.12156

[37] Zwenzner, H. and Voigt, S. (2009) Improved Estimation of Flood Parameters by Combining Space Based SAR Data with Very High Resolution Digital Elevation Data. *Hydrology and Earth System Sciences*, **13**, 567-576. http://dx.doi.org/10.5194/hess-13-567-2009

[38] Bhatt, C.M., Rao, G.S., Begum, A., Manjusree, P., Sharma, S.V.S.P., Prasanna, L. and Bhanumurthy, V. (2013) Satellite Images for Extraction of Flood Disaster Footprints and Assessing the Disaster Impact: Brahmaputra Floods of June-July 2012, Assam, India. *Current Science*, **104**, 1692-1700.

[39] Smith, L.C. (1997) Satellite Remote Sensing of River Inundation Area, Stage, and Discharge: A Review. *Hydrological Processes*, **11**, 1427-1439. http://dx.doi.org/10.1002/(SICI)1099-1085(199708)11:10<1427::AID-HYP473>3.0.CO;2-S

[40] Townsend, P.A. (2001) Mapping Seasonal Flooding in Forested Wetlands Using Multi-Temporal Radarsat SAR. *Photogrametric Engineering & Remote Sensing*, **67**, 857-864.

[41] Giustarini, L., Hostache, R., Matgen, P., Schumann, G.-P., Bates, P.D. and Mason, D.C. (2013) A Change Detection Approach to Flood Mapping in Urban Areas Using TerraSAR-X. *IEEE Transactions on Geoscience and Remote Sensing*, **51**, 2417-2430. http://dx.doi.org/10.1109/TGRS.2012.2210901

[42] Ho, L.T.K., Umitsu, M. and Yamaguchi, Y. (2010) Flood Hazard Mapping by Satellite Images and SRTM DEM in the Vu Gia—Thu Bon Alluvial Plain, Central Vietnam. *International Archives of the Photogrammetry, Remote Sensing and Spatial Information Science*, **38**, 275-280.

[43] Lillesand, T.M., Kiefer, R.W. and Chipman, J.W. (2008) Remote Sensing and Image Interpretation. 6th Edition, John Wiley & Sons, Hoboken.

[44] Manjusree, P., Prasanna K.L., Bhatt, C.M., Rao, G.S. and Bhanumurthy, V. (2012) Optimization of Threshold Ranges for Rapid Flood Inundation Mapping by Evaluating Backscatter Profiles of High Incidence Angle SAR Images. *International Journal of Disaster Risk Science*, **3**, 113-122. http://dx.doi.org/10.1007/s13753-012-0011-5

[45] Richards, J.A. (2009) Remote Sensing with Imaging Radar. Signals and Communication Technology. Springer-Verlag, Berlin. http://dx.doi.org/10.1007/978-3-642-02020-9

[46] Sandro, M. (2010) Automatic Near Real-Time Flood Detection in High Resolution X-Band Synthetic Aperture Radar Satellite Data Using Context-Based Classification on Irregular Graphs. Dissertation, Fakultät für Geowissenschaften, LMU München, München.

[47] Ulaby, F.T., Moore, R.K. and Fung, A.K. (1982) Microwave Remote Sensing: Active and Passive. Theory. Vol. II—Radar Remote Sensing and Surface Scattering and Emission. Addison-Wesley Publishing Company, Boston.

[48] Zalite, K., Voormansik, K., Olesk, A., Noorma, M. and Reinart, A. (2014) Effects of Inundated Vegetation on X-Band HH-VV Backscatter and Phase Difference. *IEEE Journal of Selected Topics in Applied Earth Observations and Remote Sensing*, **7**, 1402-1406. http://dx.doi.org/10.1109/JSTARS.2013.2279552

[49] Ramsey, E., Rangoonwala, A. and Bannister, T. (2013) Coastal Flood Inundation Monitoring with Satellite C-Band and L-Band Synthetic Aperture Radar Data. *Journal of the American Water Resources Association*, **49**, 1239-1260. http://dx.doi.org/10.1111/jawr.12082

[50] Elba, E., Farghaly, D. and Urban, B. (2014) Modeling High Aswan Dam Reservoir Morphology Using Remote Sensing to Reduce Evaporation. *International Journal of Geosciences*, **5**, 156-169. http://dx.doi.org/10.4236/ijg.2014.52017

[51] Farghaly, D., Urban, B., Lohmann, P. and Elba, E. (Eds.) (2011) Differentiation and Extend of Aquatic Weeds over Lake Kyoga, Uganda by Multiple Remote Sensing Technology. DLR.

[52] Pulvirenti, L., Pierdicca, N., Chini, M. and Guerriero, L. (2011) An Algorithm for Operational Flood Mapping from Synthetic Aperture Radar (SAR) Data Using Fuzzy Logic. *Natural Hazards and Earth System Sciences*, **11**, 529-540.

http://dx.doi.org/10.5194/nhess-11-529-2011

[53] DLR (2007) TerraSAR-X Das Deutsche Radar-Auge im All. The German Radar Eye in Space. Deutschen Zentrum für Luft und Raumfahrt (DLR), Göttingen.

[54] ENVI (2008) ENVI Feature Extraction Module User's Guide: Feature Extraction Module Version 4.6. http://www.exelisvis.com/portals/0/pdfs/envi/feature_extraction_module.pdf

[55] Farghaly, D., Elba, E. and Urban, B. (2014) Observing the Middle Elbe Biosphere in Germany by Means of Terra-SAR-X Images. *International Journal of Geosciences*, **5**, 196-205. http://dx.doi.org/10.4236/ijg.2014.52021

[56] Burt, J.E., Barber, G.M. and Rigby, D.L. (2009) Elementary Statistics for Geographers. 3rd Edition, Guilford Press, New York, London.

[57] Lang, M., Townsend, P. and Kasischke, E. (2008) Influence of Incidence Angle on Detecting Flooded Forests Using C-HH Synthetic Aperture Radar Data. *Remote Sensing of Environment*, **112**, 3898-3907. http://dx.doi.org/10.1016/j.rse.2008.06.013

[58] DLR (2013) Germany Floods 2013—Monitoring. Center for Satellite Based Crisis Information (ZKI)—DLR, Elbe Dannenberg, Internet.

PAPER III

TITLE:

"Differentiating forest types using TerraSAR–X Spotlight Images based on inferential statistics and multivariate analysis"

AUTHORS:

Dalia Farghaly, Brigitte Urban, Uwe Sörgel, Emad Elba

Reprinted from: Farghaly, D., Urban, B., Sörgel, U., Elba, E. (2016): Differentiating forest types using TerraSAR–X Spotlight Images based on inferential statistics and multivariate analysis. Journal of Remote Sensing Applications: Society and Environment, DOI: 10.1016/j.rsase.2019.100238.

Remote Sensing Applications: Society and Environment 15 (2019) 100238

Contents lists available at ScienceDirect

Remote Sensing Applications: Society and Environment

journal homepage: www.elsevier.com/locate/rsase

Differentiating forest types using TerraSAR–X spotlight images based on inferential statistics and multivariate analysis

Dalia Farghaly[a,*], Brigitte Urban[a], Uwe Sörgel[b], Emad Elba[a]

[a] Faculty of Sustainability Sciences, Institute of Ecology, Division of Landscape Change, LEUPHANA University of Lueneburg, Lueneburg, Germany
[b] Institute for Photogrammetry, Stuttgart University, Germany

ARTICLE INFO

Keywords:
Factor analysis
Z-Test
TerraSAR-X
Forest
Coniferous forests
Deciduous forests
SAR
Groundwater

ABSTRACT

This study investigated the potential of applying statistical analysis tests, for example, two sample Z-test and the Factor Analysis (FA) tool, on the TerraSAR-X backscattering coefficient, for distinguishing between different types of forests and detecting changes in distribution and extent of them. Two sample Z-test is an inferential statistical test that determines whether there is a statistically significant difference between the means in the data from two independent groups. FA is a multivariate analysis that can examine the structure or relationship between variables. Twelve pilot plots for forests of 17 ha were surveyed in a water protection catchment near Hanover, Germany. The forest types were deciduous, coniferous, and mixed. In order to sustain groundwater quality, deciduous trees were planted over a period of several years to gradually replace the coniferous trees in the catchment area. Regular forest observations were required to ensure that the percentages of deciduous and mixed forests in this catchment area were increasing relative to coniferous forests. Fourteen dual-co-polarized TerraSAR-X (HH/VV) images were used to monitor the forests in the period from March 2008 to January 2009. The values of the backscattering coefficient (σ_0) for the test plots were statistically analyzed using the two sample Z-test and the Factor Analysis tools.

The study showed that Factor analysis tools succeeded in differentiating between the coniferous forest and both the deciduous forest and the mixed forest, but failed to discriminate between the deciduous and the mixed forest. Only one factor was extracted for each sample plot of the coniferous forest with approximately equal loadings during the whole acquisition period from March 2008 to January 2009. However, two factors were extracted for each deciduous or mixed forest sample plot, where one factor had high loadings during the leaf-on period from May to October, and the other one had high loadings during the leaf-off period from November to April. Furthermore, the research revealed that the two sample Z-test differentiated the deciduous and mixed forests from the coniferous forest, and discriminated between deciduous forest and mixed forest. Statistically significant differences were observed between the mean backscatter values of the HH-polarized acquisitions for the deciduous forest and the mixed forest during the leaf-off period from November to April, but no statistically significant difference was found during the leaf-on period from May to October. Moreover, plot samples for the deciduous forest had slightly higher mean backscattering coefficients than those for the mixed forest during the leaf-off period.

Applying the Factor Analysis and the two sample Z-test on the backscattering coefficient of multi-temporal TerraSAR-X data facilitates distinction of forest types, tracks changes in forest patterns, and estimates the extent of environmental disasters in forest regions. This accomplishes sustainable forest management, which can play an important role not only in preserving groundwater quality but also in achieving climate change adaptation goals.

1. Introduction

The Fuhrberger Feld groundwater catchment area is situated approximately 30 km north of the city of Hanover in northwestern Germany, the capital of state of Lower Saxony (Fig. 1). This catchment area serves as an aquifer supplying about 90% of the municipal water for the 650.000 inhabitants living in Hanover region (Wolf, 2013). With an area of approximately 300 km^2, the Fuhrberger Feld is the largest

* Corresponding author.
E-mail address: dalia.farghaly@stud.leuphana.de (D. Farghaly).

https://doi.org/10.1016/j.rsase.2019.100238
Received 12 January 2019; Received in revised form 12 May 2019; Accepted 20 May 2019
Available online 26 May 2019

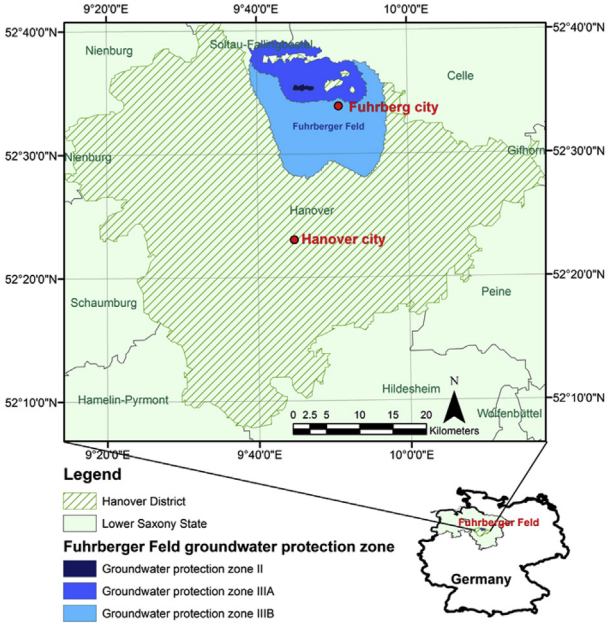

Fig. 1. Location of Fuhrberger Feld catchment area and the groundwater protection zones in Lower Saxony, Germany- Shape files source for Lower Saxony ATKIS (Amtliches Topographisch-Kartographisches Informationssystem).

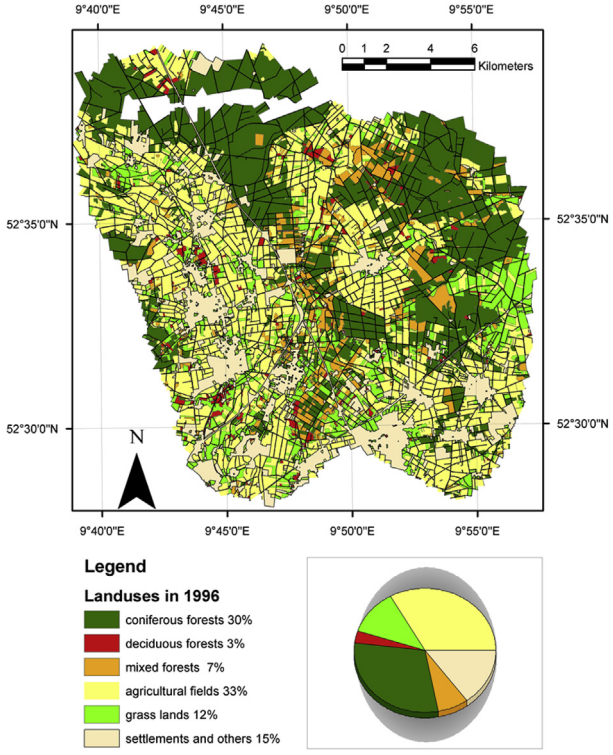

Fig. 2. Land uses in the Fuhrberger Feld groundwater protection zone in 1996 - Shape files source for Lower Saxony ATKIS (Amtliche Topographisch-Kartographische Informationssystem).

protected drinking water catchment area in northern Germany from which 50 Million cubic metres are extracted annually (BGR, 2009; Enercity, 2015). According to national guidelines that define groundwater protection zones, Fuhrberger Feld consists of 3 protection zones: Zone I, 'Well Field Protection Zone,' which is designed to protect individual wells and their immediate environment against any contamination and interference with a buffer zone with a fixed diameter of 10 m; Zone II, 'Narrow Protection Zone,' which is meant to provide protection against contamination by pathogenic bacteria and viruses within a 50-day travel time, is largely forested, and can be used for limited development, for example road construction or agriculture; Zone III, 'Wide Protection Zone,' which is designed to protect wells against long-range impairments, especially against contamination by non-degradable or less readily degradable chemical or radioactive substances and which covers the entire subsurface catchment area. If the catchment area is very large, i.e., if it has a boundary more than 2 km from the well, it may be subdivided into Zone III A and Zone III B with different levels of land use restrictions, as seen in Fig. 1 (BGR, 2009; WHO, 2005).

In this groundwater catchment area, the land uses are classified into approximately 45% agricultural fields and grassland, 40% forests, 7% settlements, and 8% other uses. Of the forested areas 75% are covered in coniferous forest, 5% in deciduous forest, and the remaining 20% is mixed forest, as shown in Fig. 2 (BGR, 2009; Enercity, 2015). Since agriculture is the dominant use in this area, groundwater protection is a major priority. Therefore, several measures have been taken to avoid the negative impacts of agricultural land use on groundwater quality. These include (i) voluntary agreements with farmers to minimize use of fertilizer, (ii) initiatives to increase the percentage of deciduous forests in the catchment area, and (iii) setting aside arable land to reduce nitrate leaching from soils (Enercity, 2015; UNEP, 2011). Since 1996, Lower Saxony has worked on projects for forest conversion in general and the reconstruction of coniferous forests into mixed deciduous forests in particular to achieve, using the name of the related projects, Tree by Tree sustainability. This approach not only positively affects the climate, but also the groundwater balance. This is due to the fact that conifers are characterized by having high evaporation rates through the entire year, have rough bark that reduces water runoff, and have a high grass cover. As a result, seepage is also limited. In contrast, deciduous trees, especially when they have no leaves, contribute to the replenishment of groundwater. Their smooth bark optimizes water drainage, they have a lower grass cover, and as a consequence, seepage is optimized. A one hectare site rebuilt with mixed forest produces annually 800,000 L more groundwater and drinking water than pure coniferous forest monocultures. (Enercity, 2015; Becker, 2013; Becker et al., 2014; Kim et al., 2010; Urban et al., 2014). In the Fuhrberger Feld water reserve alone, 650,000 deciduous trees have been planted annually since 1996 to gradually replace the coniferous trees. By 2015, 3500 ha had been converted from coniferous into mixed deciduous forest and 14 million deciduous trees had been planted in this protection zone (Enercity, 2015).

To ensure that the percentages of the area covered by deciduous and the mixed forests in this catchment area are increasing, it is essential to monitor the forests. Forest mapping and monitoring surveys are often based on costly and time-consuming field work since forest areas are large and remote. These processes require satellite remote sensing data that facilitates the mapping of large forest areas (McRoberts et al., 2010). Optical sensors with passive remote sensing systems are usually implemented to monitor forests with a distinct emphasis on infrared channels. The effectiveness of these systems is limited by weather factors such as clouds or poor solar illumination (Dobson et al., 1995). In general, Germany is characterized by heavy rainfall and dense cloud cover; the average annual precipitation is over 780 mm with a total annual sunshine of 1528 h (DWD, 2015). For this reason, optical satellite images can rarely be used. Active remote sensing systems, for instance synthetic aperture radar (SAR), are only slightly influenced by weather conditions (Oliver and Quegan, 2004). That is why SAR imagery is considered essential when it comes to mapping forests in Germany. Several studies have been conducted using these active systems as a forest mapping tool (Iizuka and Tateishi, 2014; Joshi et al., 2015; Kuplich and Curran, 1999; Ortiz, 2011). A very recent and effective source of information are TerraSAR–X images (TSX), which are from the German Earth observation satellite that was launched on 15 June

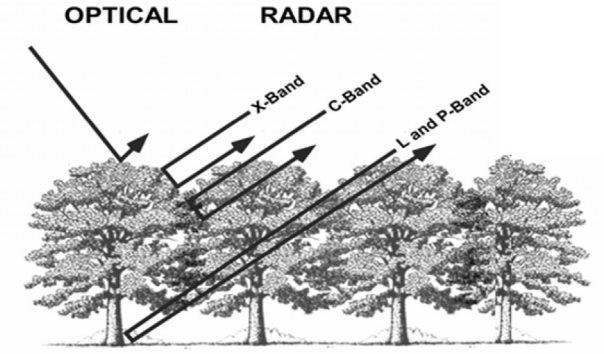

Fig. 3. Diagram indicating the conceptual differences in the depth to which various sensors will penetrate the forest canopy and demonstrating the ability of L- and P-band radar to penetrate leaves and twigs and only to be reflected by larger structures (Richards, 2009).

2007. Its orbit passes over the same location every 11 days. It uses an X-band SAR, with a 31 mm wavelength and 9.6 GHz frequency, providing high-quality topographic information for commercial and scientific applications (DLR, 2007).

The wavelength of green light is about 500 nm, whereas the wavelength of the illumination from microwave sensors ranged from 1 mm to 1 m, about two thousand to two million times the one for the green light. Consequently, the physical interaction of microwave illumination with forests is very different from that in the optical range. As shown in Fig. 3, the microwave portion of the spectrum is directly sensitive to the structure of the forest itself (Purkis and Klemas, 2011; Richards, 2009): the shorter wavelength bands (X and C) are sensitive to small twigs and leaves; therefore, it can provide information at the uppermost canopy level. In contrast, long wavelength bands (L and P) are sensitive to boles and branches; as a result, they can provide information on the woody structure and underlying ground surface (Purkis and Klemas, 2011; Richards, 2009).

Dobson et al. (1995) utilized ERS-1 (C-band) and JERS-1 (L-band) imagery for land cover classification in Michigan, USA. They distinguished between coniferous and deciduous forests with classification accuracies of 64% (ERS-1), 66% (JERS-1), and 94% when the two were combined. Ortiz et al. (2012) examined High Resolution Spot Light TerraSAR-X images to map forest dominated by deciduous and coniferous trees. The SAR images were preprocessed with a Shuttle Radar Topography Mission (SRTM) DEM (resolution approximately 90 m), an airborne laser scanning (ALS) digital terrain model (DTM) (5 m resolution), and an ALS digital surface model (DSM) (5 m resolution). They found that the orthorectification of the SAR images using the high resolution ALS DEMs reduced the number of errors in pixel location and improved the classification accuracy of forest types, with kappa coefficients ranging from 0.41 to 0.49. In addition, the radar backscatter of plots dominated by coniferous trees was found to have lower scattering coefficients than plots dominated by deciduous trees.

Multivariate statistical techniques such as Factor Analysis (FA) offer a more integrated approach to multi-element analysis, in which the interrelationships of all the elements in a data set are modeled concurrently. FA is a statistical method for determining the regularity and order of phenomena and as such can be applied to identifying the underlying structure in data. In other words, it explains multivariate relationships (correlations) between observations (indicators) by a smaller number of not directly observable variables (factors), while these factors are responsible for the correlations between the observable variables. It is also used for data reduction; in this case it describes variability between observed variables in terms of fewer unobserved variables (factors) and attribute space is reduced from a large number of observed variables to a smaller number of factors. It is widely implemented in disciplines in which large quantities of data are analyzed, such as the social, behavioral, and physical sciences, including geology and geochemistry (Gorsuch, 1983; Mulaik, 2009; Venables and Ripley, 2002). This method is a standard function of the statistical software package SPSS, which was operated in this study.

Factor Analysis can be employed for exploratory or confirmatory purposes. In the case of Exploratory Factor Analysis (EFA), data is reduced to a smaller set of summary variables and to identify the underlining theoretical structure of phenomena. EFA can be used to determine the underlying factor structure of a set of measured variables without imposing any predetermined structure on the outcome. The intermediate results of this analysis are common factors that are presented in the interrelationships among the observed variables. EFA can be carried out by using one of two modes: (1) R-mode Factor Analysis, which can reveal combinations of variables that explain the variation among objects, i.e., observations are analyzed regarding objects by clustering the observations on the objects; and (2) Q-mode Factor Analysis, which is used to identify combinations of objects that may explain the variation among the variables, i.e., objects are analyzed regarding observations by clustering the objects on the observations. R-mode is the major Factor Analysis mode, because Q-mode has been replaced by cluster analysis (Klovan, 1975). The main three goals of EFA are 1) to help in determining the number of latent constructs underlying a set of variables, 2) to provide a means of explaining variation among variables using a few new variables created during the analytical process (factors), and 3) to identify the meaning of factors or the latent constructs. Confirmatory factor analysis (CFA) is used to test how well the measured variables represent the number of constructs. With the help of CFA, it is possible to confirm or reject the findings of an EFA. It seeks to verify whether the number of factors and the loadings of measured (indicator) variables on them conform to the expected results on the basis of a pre-established theory (Gorsuch, 1983; Mulaik, 2009; Klovan, 1975; Syvitski, 2007).

Kondratyev and Pokrovsky (1979) sought to answer the question whether spectral intervals for multichannel surveys can contribute to solving complex problems of oceanology, hydrology, geology, forestry, and agriculture. A Factor Analysis algorithm was suggested to determine the optimal parameters of remote observations, taking into account the many requirements concerning information in complex studies of the environment and earth resources. Recommendations with regard to the parameters of spectral instruments necessary for studying these resources were given. Today, Factor Analysis has become an important statistical instrument in modern science, for example environmental studies. Kaplunovsky (2005) studied the properties of Factor Analysis as a robust method for investigations in environmental studies of air, water, and land ecological systems.

Liu et al. (2012) presented a new approach to factor rotation for functional remote sensing data. The study investigated the rotation of the functional principal components toward a predefined space of periodic functions designed to reduce the total variation into components that are nearly-periodic and nearly-aperiodic with a predefined period. The study aimed to find interpret Table sources of variability in gridded time series of vegetation index measurements obtained from remote sensing.

Riitters et al. (1995) calculated fifty-five metrics of landscape patterns and structures for 85 maps of land use and land cover and used a multivariate Factor Analysis to identify the common dimensions of these patterns and structures, which were measured by a reduced set of 26 metrics. The first six factors explained about 87% of the variation in the 26 landscape metrics and were interpreted as composite measures of average patch compaction, overall image texture, average patch shape, patch perimeter-area scaling, number of attribute classes, and large-patch density-area scaling. The study suggested that these factors can be represented in a simpler way by six univariate metrics: average perimeter-area ratio, contagion, standardized patch shape, patch area scaling, number of attribute classes, and large-patch density-area scaling.

Lohmann et al. (2010) investigated the multi-temporal classifications of TerraSAR–X image pairs (HH and VV) covering a time period from March to November. The study used Factor Analysis to reduce the data required from satellite images for each surveyed area to determine the bands that must be considered to identify areas similar to the training areas, an approach that improves the results of the classification process. The study showed that even when not using all images of a given season, but only those that are indicated by the crop-calendar or those that show high loadings in the Factor Analysis, a classification accuracy of more than 90% can be achieved.

The two sample Z-test is an inferential statistical test that determines whether there is a statistically significant difference between the means of two independent groups. Generally, an independent sample T-test and a two sample Z-test can be used to compare means, however the independent sample T-test is not applicable for large sample sizes greater than 30. Usually the number of pixels in a SAR imagery is more than 30, thus only the two sample Z-test can be applied to such large sample size imagery datasets. The Z-test can be applied on two normally distributed and independent samples (Fisher, 1987; King and Mody, 2011; Markowski and Markowski, 1990). The Z-test was rarely used in analyzing the backscatter of SAR imagery, however it was applied on evaluating several classification results. For example, Kumar et al., 2017 used Kernel-based support vector machines, maximum likelihood and normalised difference vegetation index classification schemes to evaluate their crop classification effectiveness. The classifications results were statistically analyzed and compared using Z-test and χ2-test.

Previous studies on Fuhrberger Feld have focused on agricultural land uses and crop classification without monitoring the forest pattern (Lohmann et al., 2010; Bargiel and Herrmann, 2011; Haarena and Bathkeb, 2008; Tavakkoli Sabour et al., 2008). Since forest pattern plays an important role in the ground water recharge and quality, it is required for continuous monitoring of the forest distribution there. Previous studies using satellite images were only able to clearly distinguish between different types of forests by integrating additional data such as DEMs (Ortiz et al., 2012; Solberg et al., 2018). They also did not explore the potential of statistical analysis tools such as two sample Z-test (TZT) and Factor Analysis (EFA) as a means of analyzing the vast amount of information acquired by satellite imagery. This study evaluates the potential of EFA and TZT in analyzing the backscattering coefficient (σ_0) of sample forest regions in Multi-temporal TerraSAR-X imagery as an unconventional but accurate and cost-effective monitoring tool in distinguishing between different types of forest. This kind of tool could, for example, help decision makers and other stakeholders to monitor and estimate the percentage of mixed forest and thus manage the ground water protection area in a sustainable manner.

Sections 2 provides an overview of the study area and the SAR data, and describes the methods. The results are summarized in Section 3 and discussed in Sections 4. Finally, some conclusions and suggestions are given in Section 5.

2. Materials and methods

2.1. Study area

Ten thousands hectares of forests are situated in the Fuhrberg catchment area (BMEL, 2015; Häusler and Scherer-Lorenzen, 2001). Twelve areas of 17 ha, which represent approximately 0.2% of the forested land in the catchment area, were surveyed for the purpose of this study (Fig. 4). These plots represent the three forests types in the area: coniferous, deciduous, and mixed forest. There were four plots for each forest types chosen for analysis.

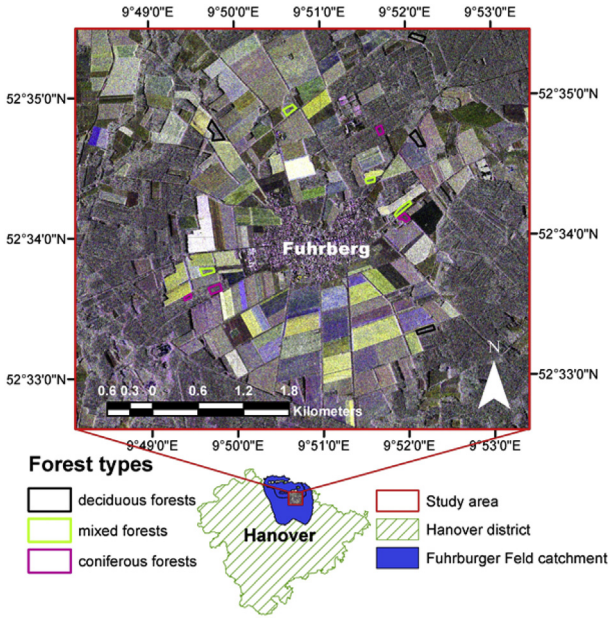

Fig. 4. Location of study area and overlaid RGB color composite of TerraSAR-X images taken on 18 May 2008, 09 June 2008 and 01 July 2008 showing the investigated plots in the Fuhrberger Feld catchment area around the city of Fuhrberg: Shape files source of Hanover district boundary and Fuhrberger Feld catchment boundary- ATKIS (Amtliche Topographisch-Kartographische Informationssystem)

2.2. Data collection

In this study, dual-co-polarized TerraSAR-X (HH/VV) images were used to monitor the forests in the Fuhrberg catchment area. These Spotlight TerraSAR-X (TSX) images were acquired between March 2008 and January 2009 by the German Aerospace Centre (DLR), and processed as Multi-look Ground-range Detected (MGD) products with Spatially Enhanced (SE) processing. MGD has reduced speckle and approximately square resolution cells on the ground. The image coordinates are oriented along the flight direction and the ground range. Geometric projection is in azimuth-ground range without terrain correction (DLR, 2007). They are high resolution images with an ascending angle of 34.75°, and have high range and azimuth pixel spacing of 1 m. Table 1 lists the images and the date when they were acquired.

2.3. Image processing

Twenty-eight images were used in total, 14 images in HH polarization and 14 in VV polarization. These images were coregistered to correct for relative translational shift and rotational and scale differences by performing spatial registration and potential resampling. This was done using the SARSCAPE module of the ENVI program after importing them in TerraSAR-X standard format. The resulting images were then geocoded to provide a radiometric calibration and a cartographic reference system. In the next step, the images for HH and VV polarization acquired on the same date were stacked together to create 14 images for the study area with 2 bands. Image rectification and georeference transformation were then applied to the stacked images using ERDAS Imagine software. The images were loaded into ERDAS Imagine for data preparation and reprojection. The TSX images were geometrically transformed to Universal Transverse Mercator (UTM) projection with spheroid WGS 84 and Zone 32 North and resampled into 1 m pixel size using the projective transform model from Geometric Correction tool. The images were filtered to remove or decrease the speckle using the Lee filter. This filter is available as one of the options for speckle suppression offered under the Radar Interpreter menu in ERDAS

Table 1
List of different bands in the stacked image and acquisition dates, polarization type, and the life cycle of tree leaves.

Acquisition Date	Variable	Polarization	Leaf cycle	Acquisition Date	Variable	Polarization	Leaf cycle
13.03.2008	B1	HH	Leaf-off	05.09.2008	B15	HH	Leaf - on
	B2	VV			B16	VV	
04.04.2008	B3	HH		27.09.2008	B17	HH	
	B4	VV			B18	VV	
18.05.2008	B5	HH	Leaf - on	19.10.2008	B19	HH	
	B6	VV			B20	VV	
09.06.2008	B7	HH		10.11.2008	B21	HH	Leaf-off
	B8	VV			B22	VV	
01.07.2008	B9	HH		12.12.2008	B23	HH	
	B10	VV			B24	VV	
23.07.2008	B11	HH		04.01.2009	B25	HH	
	B12	VV			B26	VV	
14.08.2008	B13	HH		26.01.2009	B27	HH	
	B14	VV			B28	VV	

imagine. A coefficient of variation for the subset of the geocoded images was calculated for each image, and was implemented for processing with the Lee filter. The window size was set to seven pixels.

2.4. Multi-temporal classification

From May to October, the leaves are usually present on the trees so it is called the leaf-on period. From November until February, the leaves have fallen from most of the trees and is called the leaf-off period. Due to the limitation of the possible polarizations (HH, VV) of the TerraSAR-X sensor data, using only unique date images for establishing forest classification is unlikely to achieve accurate results. Therefore, multi-temporal approaches were used to increase the classification accuracy through enabling mapping of temporal changes resulting from leaf-off/leaf-on periods. The classifications were generated by stacking the different available lee-filtered images into one image representing the different acquired dates with the available polarization covering the whole period from March 2008 to January 2009. Table 1 shows a list of different bands in the stacked image and acquisition dates, polarization type, and the life cycle of tree leaves for this study area.

Maximum likelihood classifier (MLK) was used to identify the forest types using ERDAS Imagine. The classifications produced were based on several attempts using all available acquired dates, as well as attempts representing leaf-on period and leaf-off period, in addition to attempts using particular polarization. The classifications were produced to assess the accuracy in distinguishing between three forest types namely; coniferous, deciduous and mixed. In additions, the classifications were generated to distinguish between deciduous and mixed forest versus coniferous forest. The 12 surveyed forest plots were used as reference data, and half of them were used as training samples in producing the supervised classifications. The classifications produced were analyzed using the spatial module under ARCGIS to estimate the distribution of the classification with respect to the forest type for the 12 test plots. The distribution results were exported into dBase format and then transformed into excel files to calculate accuracy assessment parameters including, the producer accuracy for each forest, and the total accuracy for the entire classification.

2.5. Statistical analysis

The Lee-filtered imagery and the non-filtered imagery were then resampled into 5 m pixel size due to limitations resulting from the large size of the file. Finally, the subsets of the 12 plots examined in this study were created in ERDAS imagine to analyze the backscattering coefficient (σ_0) for each pixel in decibels (dB). The $\sigma_0$values of the 12 subsets of forests were transferred to ASCII files using the tools available under ERDAS imagine. Similarly, the forest areas in the TerraSAR-x imagery around fuhrberger feld were investigated based on the shape files from Lower Saxony ATKIS (Amtliche Topographisch-Kartographische Informationssystem). The total area of these forests is approximately 1000 ha, stand for 10% of the total forest area in the Fuhrberger Feld catchment. The forest area is divided into 10% deciduous forest, 30% mixed forest and 60% coniferous forest. For the Lee-filtered imagery and the non-filtered one, 12 ASCII files representing the 12 plots and three ASCII files representing the different forest types in the imagery were then used as input for SPSS. The sizes of the forest plots are listed in Table 2.

Twenty-eight variables were analyzed with the SPSS stand, as listed in Table 3, for the backscatter coefficient (σ_0) of 14 acquisition dates in both HH and VV polarization. Boxplots were employed to visualize the data distribution. Each boxplot shows five statistical parameters (minimum, first quartile, median, third quartile, and maximum. This presentation is useful when different variables represent a single characteristic measured at different times (King and Mody, 2011).

To determine the appropriateness of the data and to measure the homogeneity of variables, the Kaiser-Meyer-Olkin (KMO) test measures were applied to Lee-filtered data. The results of these tests show the extent to which the indicators of a construct are related to one another. These results were checked to examine whether the data is appropriate for subsequent Factor Analysis (Finch, 2011; Trendafilov, 1994; Thompson, 2004). Four main stages were applied in the analysis. First, initial solutions were produced to determine the inter-correlation matrix among all of the variables. An inter-correlation matrix is a k × k (where k equals the number of variables) array of the correlation coefficients of the variables with one another. Second, an appropriate number of components (factors) was extracted from the correlation matrix based on the initial solutions for factors with eigenvalues greater than or equal to 1.0. In some cases, one or more variables may load about the same on more than one factor, and for this reason, it is difficult to clearly identify factors. Therefore and thirdly, factors were rotated in order to clarify the relationship between the variables and

Table 2
List of the size and area of the forest plots in m^2.

No.	Forest Type	No. of pixels	Area (m2)	Total Area	Percentage%
1	Coniferous	553	13825	57700	34
2	Coniferous	426	10650		
3	Coniferous	705	17625		
4	Coniferous	624	15600		
5	Mixed	505	12625	55550	33
6	Mixed	540	13500		
7	Mixed	542	13550		
8	Mixed	635	15875		
9	Deciduous	499	12475	57175	34
10	Deciduous	623	15575		
11	Deciduous	681	17025		
12	Deciduous	484	12100		

Table 3
External producer accuracy in percentage for each forest and the overall total accuracy for two-type and three-type classification.

polarization	Period	Two-type Classification accuracy (%)			Three- type Classification accuracy (%)			
		deciduous and mixed	coniferous	total	deciduous	coniferous	Mixed	total
hh	Whole	77	79	78	48	77	44	53
	leaf on	63	79	66	28	75	45	44
	leaf off	75	79	76	49	77	30	49
vv	Whole	78	82	79	51	80	42	54
	Leaf-on	67	81	70	34	78	45	47
	Leaf-off	77	82	78	52	81	31	51
hh/vv	Whole	82	84	82	59	81	50	61
	Leaf-on	68	80	71	33	70	38	43
	Leaf-off	78	82	79	51	80	39	54

the factors. While various methods can be applied for factor rotation, the Orthogonal Varimax method is the most commonly used one, which produces factor structures that are uncorrelated (Trendafilov, 1994; Thompson, 2004).

Finally, results were derived by analyzing the factor load of each variable to identify the different factors. The EFA was carried out for each polarization individually. For each polarization, the EFA was performed on every forest plot individually and for each forest type in the pilot area. For the study area around Fuhrberger Feld, the EFA was executed for each polarization on each forest type separately. In addition, the three forest types were merged together in one SPSS file with 84 variables (three forest types*14 acquisition dates*two polarizations), and EFA was applied for each polarization.

To find out a statistical procedure which can be used to distinguish between different types of forest, the Two sample Z-test was used to test whether the mean backscatter coefficient of the deciduous forest is statistically significant different from the mean backscatter coefficient of coniferous forest and from that of mixed forest. A new SPSS file was generated for the four variables acquisition dates, polarization type, forest type, and the backscatter coefficient. This file was used to check if the values of the backscatter coefficient were normally distributed and to calculate the number of records (n_i), the mean ($\overline{x_i}$) and the standard division (σ_i) of each examined group. The Z-score (Z) was calculated according to equation (1).

$$Z = \frac{(\overline{x_1} - \overline{x_2})}{\sqrt{\frac{\sigma_1^2}{n_1} + \frac{\sigma_2^2}{n_2}}} \quad (1)$$

where: $\overline{x_1}$ *and* $\overline{x_2}$ are sample averages of group1 and group2.$\sigma_1$and σ_2 are the standard deviations of both populations and n

and n_2 are the number of samples in each group (King and Mody, 2011).

A two tailed Probability Value (P-Value) was estimated from Z-score tables for two tailed hypothesis. Finally the P-value was evaluated at a confidence level of 95%. If the P-Value was less than 0.05, then there was a significant difference between the two groups. If the P-Value was larger than 0.05, then there was likely no significant difference between the two groups.

These tests were applied on the whole period from March 2008 to January 2009 for each polarization individually. The tests were carried out to compare the mean backscatter coefficient of each forest on every acquisition date and during the two leaf-cycles individually. These statistical analysis tests were carried out for the 12 sample plots, and for the entire forest canopy in the study area around Fuhrberger Feld.

3. Results

3.1. Results of multi temporal classification

For the lee-filtered imagery, 18 supervised MLK classifications were generated for the pilot area around Fuhrberger Feld. Two-type classification was undertaken nine times to distinguish coniferous forest from deciduous and mixed forest, to test the use of each polarization individually and simultaneously during leaf-on, leaf-off and the whole acquisition period. Similarly, three-type classification was undertaken nine times to discriminate between coniferous forest, deciduous forest and mixed forest. The resulting classifications were assessed and the external producer accuracy for forest type and the overall total accuracy were estimated for each classification. Table 3 presents the accuracy assessment results for the two-types and the three-type forest classifications.

For the two-type classification, the produced accuracy ranged from 63% to 82% for the class of deciduous and mixed forest, and from 79% to 84% for the class of coniferous forest, while the total producer accuracy ranged from 66 % to 82%. The highest classification accuracy was achieved using both co-polarizations acquired during the whole period, while the lowest classification accuracy was achieved during the leaf-on period from the HH-polarized data.

The accuracy of the three-type classification was less than the two-type classification. The produced accuracy ranged from 28% to 59% for the deciduous forest class, from 30% to 50% for the mixed forest class, and from 70% to 80% for the coniferous forest class. The results of total producer accuracy ranged from 43% to a maximum 61%. The highest classification accuracy for all classes was produced using both co-polarizations during the whole time series. In contrast, the lowest classification accuracy was achieved from HH-polarized data during the leaf-on period for the deciduous class, and during the leaf-off period for the mixed forest class, while the lowest one for the coniferous class was produced using both co-polarizations during leaf-off period. The lowest total producer accuracy was achieved from both co-polarizations during the Leaf-on period.

3.2. Results of statistical analysis

For the study area, the non-filtered imagery and images processed with the Lee filter were interpreted. The boxplots of the backscatter coefficient (σ_0) in (dB)on sample plots dominated by coniferous, deciduous, or mixed forest in the non-filtered imagery and the one pre-processed with the Lee filter were created to represent the minimum, first quartile, median, third quartile, and maximum σ_0. These boxplots were used for a comparison of the multi-temporal behavior of the backscattered coefficient in a year during the leaf-off and leaf-on periods obtained from VV and HH acquisitions. Fig. 5 shows the boxplots for the non-filtered imagery, whereas Fig. 6 shows the boxplots for the imagery processed with the Lee filter over the different forest plots.

As shown in Fig. 5, the boxplots for the non-filtered TSX data indicated an invariable trend in median backscattering coefficient and were characterized by a large variance over the course of entire year. The σ_0 median was -10.5 ± 1.0 dB. Similar trends with regard to the multi-temporal behavior of σ_0 were observed during both the leaf-on and the leaf-off periods. The distribution of backscattering was rather symmetric. Different forest plots had similar responses, which could be

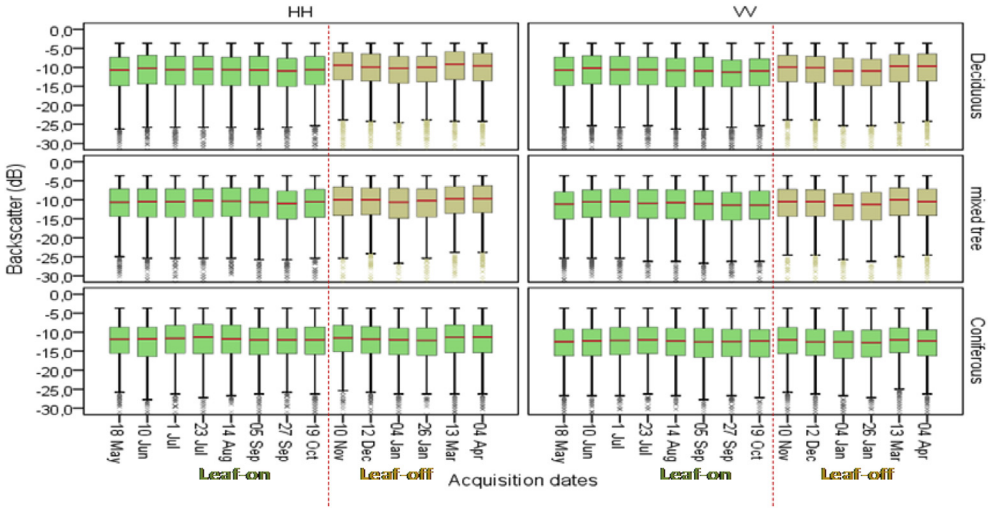

Fig. 5. Boxplots representing the multi-temporal behavior of backscattering coefficient values obtained from dual-co-polarized non-filtered TSX images for the different types of forest in the sample plots.

explained by the saturation of the X band signal by volumetric scattering due to high plant biomass. The lowest seasonal backscattering coefficient was observed for different forest plots, with 95% of the intervals ranging from −15.5 dB to −14 dB in the 25% percentile, while the highest seasonal values ranged from −8 dB to −6.5 dB in the 75% percentile. VV polarized data showed patterns and a multi-temporal behavior over the year similar to that for HH, except in terms of magnitude.

As shown in Fig. 6, the boxplots for the Lee-filtered TSX data indicate that the median backscattering coefficient did not change over the course of the year and that there is less variance over the course of the year than in the case of the non-filtered one. The median backscattering coefficient was −10 ± 1.0 dB. Similar trends in the multi-temporal behavior of $\sigma_0$were also observed during both the leaf-on and the leaf-off periods, as was a symmetric distribution of the backscattering. The responses captured by the Lee-filtered imagery were similar to those captured by the non-filtered one. The lowest seasonal backscattering coefficient was observed at different forest plots, with 95% of the intervals ranging from −12.5 dB to −11 dB in the 25% percentile range. In contrast, the highest seasonal coefficient ranged from −9.5 dB to −8.0 dB in the 75% percentile range. The VV-polarized data was also similar to the HH-polarized data in terms of backscattering responses and multi-temporal behavior over the course of the year. The difference between the hinges, i.e., the upper and the lower limit of the values in a given boxplot, were approximately 8 dB for the Lee-filtered data 18 dB for the non-filtered one. Thus, the boxes tended to be much shorter for the former than for the latter, a result that indicated that σ_0 was less likely to vary for images processed with the Lee filter than for the non-filtered one.

Fig. 7 shows the boxplots of the backscattering coefficient of sample plots dominated by coniferous, mixed, and deciduous forests obtained from HH- and VV- polarized Lee-filtered and non-filtered TSX data. These boxplots were used to compare the behavior the σ_0 on 26 January 2009, which represents the leaf-off period, and on 23 July 2008, an exemplary day in the leaf-on period. In both non-filtered and Lee-filtered imagery, similar backscatter characteristics for all three forest types were seen during both the leaf-off and the leaf-on periods. VV-polarized data also tended to have similar backscattering responses to HH-polarized data. Therefore, it was difficult to distinguish between the different types of forest. Since the backscattering coefficient of the non-filtered TSX data were characterized by a large variance, the backscattering coefficient of the Lee-filtered imagery were considered in further statistical analyses.

To describe the covariance structure among many variables in terms

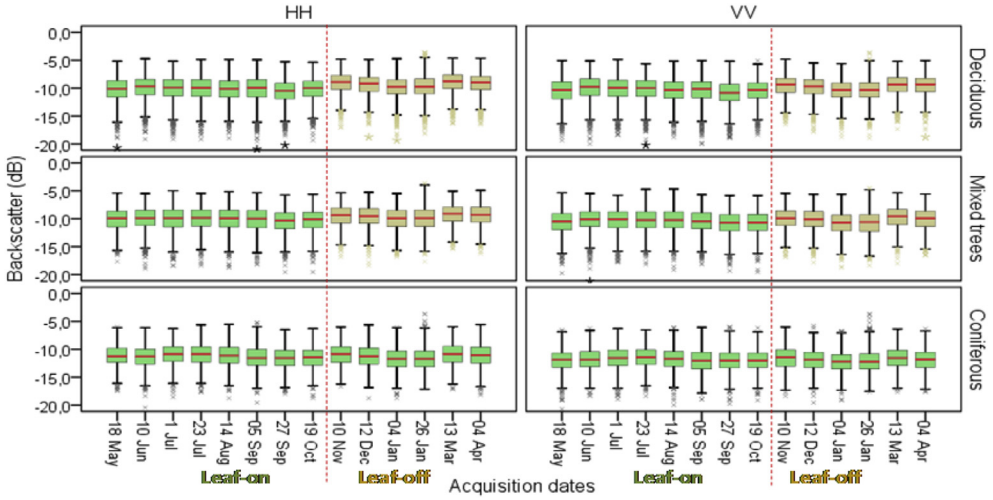

Fig. 6. Boxplots representing the multi-temporal behavior of backscattering coefficient values obtained from dual-co-polarized Lee-filtered TSX images for different types of forest in the sample plots.

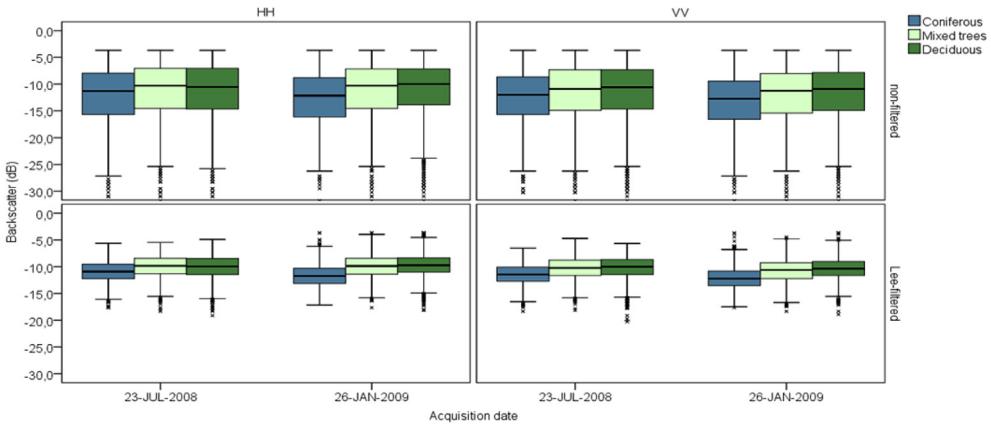

Fig. 7. Boxplots of the backscattering coefficient (dB) of sample plots dominated by coniferous, mixed, or deciduous forest obtained from dual-co-polarized non-filtered and Lee-filtered TSX images that were acquired on 26th January 2009 (leaf-off period) and 23rd July 2008 (leaf-on period).

of a few underlying factors that are not directly observable, Factor Analysis was applied. In this study, this analysis was conducted by grouping the backscattering coefficient of the 14 acquisition times in a way that within-group correlations were large and between-group correlations were small. This step was accomplished by applying the principal components method to the correlation matrix. The number of groups was chosen on the eigenvalues associated with each group, the plot of eigenvalue versus component number, and the cumulative proportion of variance by including additional groups, where every group stands for one axis in metric state space. The axes were interpreted by identifying the common characteristics of metrics. These metrics were computed to discern groups along individual axes and with similar loadings (correlations of metrics with that axis).

Before conducting the EFA on the backscattering coefficient, the Kaiser-Meyer-Olkin (KMO) and Bartlett's tests were applied to check sampling adequacy. The KMO should be greater than 0.5 for a satisfactory Factor Analysis to proceed. Table 4 shows the estimated Kaiser-Meyer-Olkin Measure of Sampling Adequacy (KMO) and Bartlett's Test of Sphericity values for different samples using the Lee-filtered TSX data. As shown in Table 4, the KMO measures were between 0.79 and 0.97. In addition, the significance values of the Bartlett's Test of Sphericity were approximately 0. Since all KMO values were over 0.50 and the significance values were less than 0.05, the samples were adequate and significant. Consequently, the EFA could be conducted.

Correlation matrix was produced for each forest plot to calculate the correlation coefficients between a single variable (one acquisition date) and every other variables considered in this study (other 14 acquisition dates). The factors were extracted based on principle component method and rotated according to the Varimax rotation method. The factor scores were calculated as the weighted sum of all 14 metrics, where the weights were the loadings for that factor. The loadings measured which variables were involved, in which factor pattern, and to what degree. Tables 5–7 show the loadings of the 14 acquisition dates of the HH and VV polarizations in the sample plots. Similarly, Tables 8–11 show the loadings in the entire investigated forest area around Fuhrberger Feld. The loadings larger than 0.4 are shown in these tables.

Table 5 shows the factor loadings of the backscattering coefficient on sample plots dominated by coniferous forest acquired between May 2008 and April 2009 from HH- and VV- polarized TSX images. The loadings results were calculated for the four plot samples (F1, F2, F3, F4) individually and simultaneously. Only one factor was extracted for each field as well as for all fields altogether, and thus no rotation was required. For each investigated case, the extracted factor was accounting for approximately 40% on average for the total variance in the data set and included significant loadings for the σ_0 values of the 14 acquisition times. For HH- and VV-polarized imagery, Factor 1 had indeterminate factor loadings for all acquisition dates. The loadings values for all of the analyzed cases using HH-polarized imagery ranged from 0.5 to 0.68 with an average of 0.62, while those for the VV-polarized imagery ranged from 0.55 to 0.66 with an average of 0.61.

Table 6 shows the factor loadings of the amplitude of backscattering coefficient on sample plots dominated by mixed forest obtained from HH- and VV- polarized Lee-filter TSX data acquired between May 2008 and April 2009. The loadings results were calculated for the four plot samples (F5, F6, F7, F8) separately, and all together. Two factors were extracted for each field and for all together and, consequently, Varimax rotation was able to be applied. For each investigated case, the rotated factors were accounting for approximately 40% on average of the total variance in the data set. For HH- and VV-polarized imagery, Factor 1included significant loadings for acquisition dates during the leaf-on period from May to October. In contrast, Factor 2 1included significant loadings for acquisition dates during the leaf-off period from November to April. Some loadings of factor 2 were less than 0.4 and thus not presented in the table. The loadings values of Factor 1 for all of the samples in the HH-polarized imagery ranged from 0.61 to 0.69 with an average of 0.65, while those in the VV-polarized imagery ranged from 0.55 to 0.69 with an average also of 0.65. The loadings values of Factor 2 for all of the samples in the HH-polarized imagery ranged from 0.48 to 0.84 with an average of 0.64, while those in the VV-polarized imagery ranged from 0.50 to 0.85 with an average also of 0.64.

Table 7 shows the factor loadings of the backscattering coefficient

Table 4
Estimated Kaiser-Meyer-Olkin Measure of Sampling Adequacy (KMO) and Bartlett's Test of Sphericity values for different samples using dual-co-polarized Lee-filtered TSX images.

Forest Type	Sample No.	Kaiser-Meyer-Olkin Measure of Sampling Adequacy	Bartlett's Test of Sphericity		
		KMO	Approx. Chi-Square	Df.	Sig.
Coniferous	F1	0.79	1856.31	378	0
	F2	0.87	2154.92	378	0
	F3	0.94	3359.18	378	0
	F4	0.92	5427.66	378	0
Mixed	F5	0.95	6342.64	378	0
	F6	0.93	5967.06	378	0
	F7	0.96	7426.17	378	0
	F8	0.92	3752.39	378	0
Deciduous	F9	0.97	12452.66	378	0
	F10	0.93	9688.4	378	0
	F11	0.94	8260.72	378	0
	F12	0.86	3949.14	378	0

Table 5
Factor loadings of the backscattering coefficient on sample plots (F1, F2, F3, F4) dominated by coniferous forest obtained from dual-co-polarized Lee-filtered TSX images, which were acquired between March 2008 and January 2009.

Leaf cycle	Acquisition dates	Rotated Component Matrix - HH Polarization					Rotated Component Matrix - VV Polarization				
		F1	F2	F3	F4	All	F1	F2	F3	F4	All
leaf-on	13-MAR-2008	0.523	0.530	0.633	0.516	0.620	0.591	0.582	0.675	0.533	0.551
	04-APR-2008	0.598	0.587	0.690	0.584	0.654	0.498	0.590	0.630	0.515	0.593
leaf-on	18-MAY-2008	0.527	0.591	0.654	0.542	0.585	0.634	0.519	0.688	0.588	0.578
	09-JUN-2008	0.549	0.579	0.739	0.570	0.559	0.564	0.549	0.632	0.545	0.614
	01-JUL-2008	0.514	0.546	0.523	0.639	0.506	0.548	0.533	0.569	0.671	0.587
	23-JUL-2008	0.594	0.512	0.657	0.598	0.593	0.525	0.506	0.652	0.600	0.592
	14-AUG-2008	0.540	0.522	0.609	0.563	0.629	0.580	0.530	0.628	0.578	0.619
	05-SEP-2008	0.544	0.593	0.660	0.610	0.667	0.519	0.578	0.646	0.608	0.660
	27-SEP-2008	0.546	0.523	0.631	0.582	0.603	0.537	0.501	0.623	0.564	0.619
	19-OCT-2008	0.516	0.590	0.641	0.583	0.624	0.556	0.640	0.638	0.599	0.609
leaf-on	10-NOV-2008	0.513	0.597	0.666	0.616	0.682	0.546	0.548	0.679	0.554	0.650
	12-DEC-2008	0.543	0.533	0.671	0.537	0.662	0.590	0.606	0.663	0.519	0.622
	04-JAN-2009	0.659	0.514	0.659	0.650	0.610	0.683	0.509	0.603	0.587	0.648
	26-JAN-2009	0.624	0.563	0.658	0.594	0.677	0.605	0.547	0.676	0.573	0.640

on sample plots dominated by deciduous forest obtained from HH- and VV-polarized Lee-filtered TSX data as above. The loadings results were calculated for the four plot samples (F9, F10, F11, F12) independently, and mutually. Two factors were extracted for each field and for the entire set, and consequently Varimax rotation was able to be applied. For each examined case, the rotated factors were accounting for approximately 40% on average for the total variance in the data set. For HH- and VV-polarized imagery, Factor 1 had significant loadings for acquisition dates during the leaf-on period from May to October. In contrast, Factor 2 incorporated significant loadings for acquisition dates during the leaf-off period from November to April. Some loadings of factor 2 were less than 0.4 and thus not presented in the table. The loadings values of Factor 1 for all samples in the HH-polarized imagery ranged from 0.57 to 0.7 with an average of 0.67, while those in the VV-polarized imagery ranged from 0.65 to 0.71 with an average of 0.68. The loadings values of Factor 2 for all the data of the HH-polarized imagery ranged from 0.41 to 0.86 with an average of 0.58, while those for the VV-polarized imagery ranged from 0.41 to 0.88 with an average of 0.72.

Table 8 shows the factor loadings of the σ_0 in forest areas around Fuhrberger Feld dominated by coniferous forest obtained from same dataset. Only a single factor was extracted for each polarization and thus no rotation was required. For each investigated polarization, the extracted factor accounted for approximately 46% on average for the total variance in the data set and included significant loadings for the backscattering coefficient of the 14 acquisition times. For HH- and VV-polarized imagery, Factor 1 had high factor loadings for all acquisition dates. The loadings values for HH-polarized imagery ranged from 0.64 to 0.71 with an average of 0.68, and similar results were obtained for the VV-polarized imagery.

Table 9 shows the factor loadings of σ_0 in forest areas around Fuhrberger Feld dominated by mixed forest acquired in the same dataset. Two factors were extracted for each polarization, and thus Varimax rotation was applied. For both examined polarizations, the rotated factors accounted for approximately 60% on average of the total variance in the data set. For HH- and VV-polarized imagery, Factor 1 had significant loadings for acquisition dates during the leaf-on period from May to October, similar to the results in Table 6 obtained from the plot samples. Conversely, Factor 2 incorporated significant loadings for acquisition dates during the leaf-off period from November to April. The loadings values of Factor 1 in the HH-polarized imagery ranged from 0.64 to 0.74 with an average of 0.72, and those in the VV-polarized imagery ranged from 0.65 to 0.74 with an average also of 0.72. The loadings values of Factor 2 in HH-polarized imagery ranged from 0.57 to 0.84 with an average of 0.69, while those in the VV-polarized imagery ranged from 0.55 to 0.85 with a mean of 0.67.

Table 10 shows the factor loadings of σ_0 on forest areas around Fuhrberger Feld dominated by deciduous forest acquired from the same dataset. Two factors were extracted also for both polarization and thus Varimax rotation was applied. For each analyzed polarization, the rotated factors accounted for approximately 62% on average of the total variance in the data set. For HH- and VV-polarized imagery, Factor 1 included significant loadings for acquisition dates during the leaf-on period from May to October, which is like the results in Table 7 for the plot samples. By contrast, Factor 2 had significant loadings for acquisition dates during the leaf-off period from November to April. The loadings values of Factor 1 in the HH-polarized imagery ranged from 0.67 to 0.77 with an average of 0.75, while those in the VV-polarized imagery ranged from 0.53 to 0.85 with an average of 0.67. The loadings values of Factor 2 in the HH-polarized imagery ranged from 0.67 to 0.78 with an average of 0.75 too, while those for the VV-polarized imagery ranged from 0.51 to 0.86 with an average of 0.65.

Table 11 shows the factor loadings of σ_0 in the entire forest areas around Fuhrberger Feld dominated by coniferous, mixed and deciduous forest obtained from same dataset. Five factors were extracted for both polarizations and thus Varimax rotation was applied. For each examined polarization, the rotated factors accounted for approximately 57% on average of the total variance in the data set. For HH-polarized imagery, Factor 1 included significant loadings for σ_0 of the coniferous forest for the whole time series. Factors 2 and 3 included significant loadings for σ_0 of the deciduous and mixed forest for the acquisition dates during the leaf-on period from May to October. By contrast, Factors 4 and 5 had significant loadings for σ_0 of the deciduous and mixed forest for the acquisition dates during the leaf-off period from November to April. For VV-polarized imagery, Factor 3 incorporated significant loadings for σ_0 of the coniferous forest for the 14 acquisition times. Factors 1 and 2 included significant loadings σ_0 of the deciduous and mixed forest during the leaf-on period from May to October, while Factors 4 and 5 included significant loadings for σ_0 of the deciduous and mixed forest during the leaf-off period from November to April. For both HH- and VV-polarized imagery, the loadings values of all the rotated Factors were higher than 0.5 with an average of more than 0.65.

The two sample Z-test was carried out to compare the mean backscattering coefficient of coniferous, deciduous and mixed forest, obtained from Lee-filtered dual-co-polarized TSX data, acquired from March 2008 to January 2009. The Kolmogorov-Smirnov test was run initially, and showed that σ_0 values for both HH-, and VV-polarized data were normally distributed, and thus two sample Z-test could be carried out. The TZT was run on the entire acquisition period from March 2008 to January 2009, to compare the variation between forest types with respect to leaf-cycle, acquisition date and acquisition polarization. The results of the TZT are presented in Tables 12–14.

Table 6
Factor loadings of the σ_0 on sample plots (F5, F6, F7, F8) dominated by mixed forest obtained from dual-co-polarized Lee-filtered TSX images, which were acquired between March 2008 and January 2009.

Leaf cycle	Acquisition dates	Rotated Component Matrix - HH Polarization										Rotated Component Matrix - VV Polarization									
		F5		F6		F7		F84		All		F5		F6		F7		F8		All	
		1	2	1	2	1	2	1	2	1	2	1	2	1	2	1	2	1	2	1	2
leaf-off	13-MAR-2008				0.542		0.648		0.527		0.570		0.455		0.413		0.577		0.482		0.536
	04-APR-2008		0.447		0.486		0.484		0.540		0.542						0.442		0.576		0.547
leaf-on	18-MAY-2008	0.572		0.641		0.528		0.639		0.609		0.472		0.712		0.722		0.578		0.632	
	09-JUN-2008	0.592		0.652		0.622		0.626		0.637		0.782		0.636		0.674		0.673		0.698	
	01-JUL-2008	0.618		0.634		0.708		0.750		0.671		0.749		0.624		0.646		0.715		0.694	
	23-JUL-2008	0.617		0.659		0.770		0.589		0.676		0.636		0.627		0.646		0.610		0.626	
	14-AUG-2008	0.657		0.677		0.483		0.565		0.621		0.628		0.619		0.627		0.686		0.638	
	05-SEP-2008	0.634		0.691		0.560		0.701		0.659		0.688		0.743		0.632		0.645		0.682	
	27-SEP-2008	0.727		0.712		0.633		0.686		0.694		0.642		0.664		0.731		0.726		0.696	
	19-OCT-2008	0.629		0.600		0.702		0.633		0.626		0.482		0.545		0.587		0.680		0.550	
leaf-off	10-NOV-2008						0.580		0.451		0.468		0.451		0.423		0.505		0.460		0.500
	12-DEC-2008				0.524		0.574		0.520		0.562				0.554		0.448		0.535		0.581
	04-JAN-2009		0.846		0.862		0.828		0.806		0.843		0.865		0.852		0.863		0.832		0.846
	26-JAN-2009		0.875		0.863		0.796		0.821		0.833		0.833		0.829		0.844		0.838		0.815

Table 7
Factor loadings of the σ_0 on sample plots (F9, F10, F11, F12) dominated by deciduous forest obtained from dual-co-polarized Lee-filtered TSX images, which were acquired between March 2008 and January 2009.

Leaf cycle	Acquisition dates	Rotated Component Matrix - HH Polarization										Rotated Component Matrix - VV Polarization									
		F9		F10		F11		F12		All		F9		F10		F11		F12		All	
		1	2	1	2	1	2	1	2	1	2	1	2	1	2	1	2	1	2	1	2
leaf-off	13-MAR-2008		0.560								0.405										0.418
	04-APR-2008		0.623								0.428		0.453		0.498						0.435
leaf-on	18-MAY-2008	0.683		0.654		0.683		0.609		0.679		0.721		0.656		0.705		0.679		0.694	
	09-JUN-2008	0.785		0.602		0.618		0.651		0.689		0.808		0.680		0.669		0.563		0.707	
	01-JUL-2008	0.767		0.670		0.599		0.534		0.683		0.785		0.648		0.670		0.583		0.688	
	23-JUL-2008	0.734		0.667		0.679		0.624		0.699		0.771		0.655		0.693		0.587		0.693	
	14-AUG-2008	0.726		0.669		0.583		0.492		0.664		0.744		0.631		0.651		0.462		0.658	
	05-SEP-2008	0.748		0.659		0.663		0.621		0.702		0.747		0.685		0.690		0.675		0.706	
	27-SEP-2008	0.677		0.638		0.618		0.594		0.655		0.751		0.611		0.667		0.471		0.662	
	19-OCT-2008	0.583		0.570		0.507		0.461		0.568		0.737		0.577		0.632		0.564		0.651	
leaf-off	10-NOV-2008		0.540								0.437		0.462								
	12-DEC-2008		0.672								0.492		0.495		0.429						0.413
	04-JAN-2009		0.869		0.869		0.871		0.855		0.868		0.875		0.845		0.894		0.857		0.872
	26-JAN-2009		0.875		0.867		0.895		0.854		0.868		0.901		0.849		0.889		0.877		0.883

Table 8
Factor loadings of the backscattering coefficient on forest areas around Fuhrberger Feld dominated by coniferous forest obtained from dual-co-polarized Lee-filtered TSX images, which were acquired between March 2008 and January 2009.

Leaf cycle	Acquisition dates	Component Matrix HH Polarization	Component Matrix VV Polarization
leaf-on	13-MAR-2008	0.643	0.636
	04-APR-2008	0.679	0.671
leaf-on	18-MAY-2008	0.681	0.678
	09-JUN-2008	0.674	0.674
	01-JUL-2008	0.688	0.687
	23-JUL-2008	0.699	0.701
	14-AUG-2008	0.699	0.698
	05-SEP-2008	0.701	0.707
	27-SEP-2008	0.689	0.689
	19-OCT-2008	0.691	0.686
leaf-on	10-NOV-2008	0.666	0.655
	12-DEC-2008	0.673	0.666
	04-JAN-2009	0.709	0.696
	26-JAN-2009	0.680	0.671

Table 9
Factor loadings of the backscattering coefficient on forest areas around Fuhrberger Feld dominated by mixed forest obtained from dual-co-polarized Lee-filtered TSX images, which were acquired between March 2008 and January 2009.

Leaf cycle	Acquisition dates	Rotated Component Matrix - HH Polarization		Rotated Component Matrix - VV Polarization	
		1	2	1	2
leaf-off	13-MAR-2008		0.640		0.586
	04-APR-2008		0.614		0.564
leaf-on	18-MAY-2008	0.717		0.724	
	09-JUN-2008	0.733		0.731	
	01-JUL-2008	0.736		0.737	
	23-JUL-2008	0.731		0.730	
	14-AUG-2008	0.727		0.726	
	05-SEP-2008	0.739		0.737	
	27-SEP-2008	0.714		0.717	
	19-OCT-2008	0.637		0.649	
leaf-off	10-NOV-2008		0.571		0.548
	12-DEC-2008		0.635		0.609
	04-JAN-2009		0.841		0.854
	26-JAN-2009		0.824		0.839

Table 10
Factor loadings of the backscattering coefficient on forest areas around Fuhrberger Feld dominated by deciduous forest obtained from dual-co-polarized Lee-filtered TSX images, which were acquired between March 2008 and January 2009.

Leaf cycle	Acquisition dates	Rotated Component Matrix - HH Polarization		Rotated Component Matrix - VV Polarization	
		1	2	1	2
leaf-off	13-MAR-2008		0.603		0.554
	04-APR-2008		0.602		0.529
leaf-on	18-MAY-2008	0.749		0.745	
	09-JUN-2008	0.768		0.765	
	01-JUL-2008	0.767		0.765	
	23-JUL-2008	0.754		0.758	
	14-AUG-2008	0.749		0.755	
	05-SEP-2008	0.762		0.767	
	27-SEP-2008	0.742		0.738	
	19-OCT-2008	0.667		0.673	
leaf-off	10-NOV-2008		0.526		0.505
	12-DEC-2008		0.623		0.578
	04-JAN-2009		0.848		0.863
	26-JAN-2009		0.821		0.843

Table 12 presents those results of TZT comparing the mean backscattering coefficient of deciduous forest and mixed forest during leaf-off and leaf-on periods. On one hand, for the HH- polarized acquisition, the TZT revealed a statistically significant difference between the deciduous forest and the mixed forest during the leaf-off period ($p < 0.001$), while no statistically significant difference was found between them during the leaf-on period ($p > 0.05$). On the other hand, for the VV- polarized acquisition, the TZT showed a statistically significant difference between the deciduous forest and the mixed forest during both leaf-off and leaf-on periods ($p < 0.001$). Similar tests applied to a comparison between Coniferous forest and deciduous forest determined that the means of these two forest types during both leaf-off and leaf-on periods were statistically different ($p < 0.01$). Similar results were achieved when coniferous forest and mixed forest were compared with each other.

Table 13 shows the results of the TZT comparing the mean backscattering coefficient of the acquisitions taken in leaf-off and leaf-on periods for the coniferous, deciduous and mixed forest. For both HH- and VV-polarized acquisitions, the TZT revealed a statistically significant difference between the leaf-off and leaf-on periods for both the deciduous and mixed forest ($p < 0.001$), while no statistically significant difference was found between these periods for the coniferous forest ($p > 0.05$).

Table 14 demonstrates the results of the TZT comparing the mean backscattering coefficient of deciduous forest and mixed forest on different acquisition dates during leaf-off and leaf-on periods. For the HH-acquisition, the TZT determined that the mean σ_0 of the deciduous forest was not significantly different from the mixed forest during the leaf-on period from May to October ($p > 0.05$). However, means of these two forest types during the leaf-off period from November to April are statistically different ($p < 0.001$). For the VV- polarized acquisition, the TZT revealed that mean the σ_0 of the deciduous forest was not significantly different from the mixed forest during part of the leaf-on period from August to September at the 95% confidence interval ($p > 0.05$), and from May to July at the 90% confidence interval ($0.05 > p > 0.01$). Nevertheless, means of these two forest types during the rest of the acquisition dates from October to April were statistically different ($p < 0.001$).

4. Discussion

Forest pattern plays an essential role in the ground water sustainability through increasing the percentage of the area of mixed forest. As a result, there is a need to have continuous monitoring of forest area in water protection zones to calculate the percentage of available mixed forest. This study evaluated initially the classical maximum likelihood classification method in discriminating between different types of forest. The multi-temporal approach over almost one whole year from March 2008 to January 2009 showed that the use of HH- and VV-polarized imagery acquired during the entire period could effectively distinguish between the class of coniferous forest and the combined class of deciduous and mixed forests. However, poor classification results were obtained from the three-type classifications, since they failed to distinguish between the class of deciduous forest and the class of mixed forest. Therefore, we could not count on the classical classification methods for estimating the area of the mixed forest.

This study then evaluated the potential of Factor Analysis (EFA), as an example for multivariate analysis, and two sample Z-test (TZT), as an example for inferential statistics for forest type differentiation. These statistical tests can be a cost-effective monitoring tool that can be applied to distinguish between various types of forest using TerraSAR–X Spotlight Imagery. The data extracted from both the non-filtered and the Lee-filtered imagery for the 12 forest plots were examined and boxplots were drawn for each forest type using VV- and HH- polarized imagery. The boxplots for the non-filtered TSX data indicate an invariable trend in the median backscattering coefficient and are

Table 11
Factor loadings of the backscattering coefficient on forest areas around Fuhrberger Feld dominated by coniferous, deciduous, and mixed forest obtained from dual-co-polarized Lee-filtered TSX images, which were acquired between March 2008 and January 2009.

Forest Type	Leaf cycle	Acquisition dates	Rotated Component Matrix - HH Polarization					Rotated Component Matrix - VV Polarization				
			1	2	3	4	5	1	2	3	4	5
Coniferous	leaf-on	13-MAR-2008	0.663							0.525		
		04. Apr 08	0.682							0.582		
		18-MAY-2008	0.664							0.656		
		09. Jun 08	0.63							0.666		
		01. Jul 08	0.655							0.648		
		23. Jul 08	0.682							0.658		
		14. Aug 08	0.677							0.652		
		05. Sep 08	0.677							0.662		
		27. Sep 08	0.682							0.656		
		19-OCT-2008	0.683							0.62		
		10. Nov 08	0.664							0.53		
		12-DEC-2008	0.678							0.537		
		04. Jan 09	0.71							0.88		
		26. Jan 09	0.677							0.888		
Deciduous	leaf-off	13-MAR-2008					0.59					0.554
		04. Apr 08					0.588					0.529
	leaf-on	18-MAY-2008		0.758				0.745				
		09. Jun 08		0.776				0.765				
		01. Jul 08		0.776				0.765				
		23. Jul 08		0.764				0.757				
		14. Aug 08		0.758				0.755				
		05. Sep 08		0.771				0.767				
		27. Sep 08		0.752				0.738				
		19-OCT-2008		0.68				0.673				
	leaf-off	10. Nov 08					0.51					0.505
		12-DEC-2008					0.61					0.578
		04. Jan 09					0.841					0.863
		26. Jan 09					0.814					0.843
mixed	leaf-off	13-MAR-2008				0.616					0.573	
		04. Apr 08				0.566					0.537	
	leaf-on	18-MAY-2008			0.741				0.746			
		09. Jun 08			0.744				0.73			
		01. Jul 08			0.747				0.738			
		23. Jul 08			0.734				0.723			
		14. Aug 08			0.744				0.736			
		05. Sep 08			0.752				0.744			
		27. Sep 08			0.732				0.716			
		19-OCT-2008			0.629				0.639			
	leaf-off	10. Nov 08				0.568					0.546	
		12-DEC-2008				0.615					0.613	
		04. Jan 09				0.839					0.849	
		26. Jan 09				0.815					0.832	

characterized by a large variance over the course of entire year, while the Lee-filtered data, indicated similar trends over the course of the year but with less variance than the case of the non-filtered imagery. Therefore, it was difficult to distinguish between the different types of forest. Due to the high variance in the σ_0 for the non-filtered SAR data, only Lee-filtered imagery were used for additional statistical analyses such as EFA and TZT.

The results of the EFA revealed that for each investigated sample plot of the coniferous forest as well as for the plots in total, a single factor was extracted with indeterminate loadings on all acquisition dates, and thus no rotation was required. Similar results were found for areas of coniferous forest in the study area. By contrast, the results of Factor analysis on each investigated sample plot of deciduous forest or the mixed forest as well as the plots combined, two factors were extracted and thus rotation was required. On one hand, for each investigated case, one rotated factor had significant loadings for acquisition dates during the leaf-on period from May to October. On the other hand, the other rotated factor had significant loadings for acquisition dates during the leaf-off period from November to April in most of the investigated cases. Similar results were recorded for regions

Table 12
Comparison between mean backscattering coefficient (σ0) of deciduous forest and mixed forest during leaf-off and leaf-on periods, obtained from HH- and VV-polarized Lee-filter TSX imagery, acquired between March 2008 and January 2009, using two sample Z-test.

Polarization	Leaf Cycle	Forest Type						Z-test	
		Deciduous			mixed			z-score	p-value Sig. (2-tailed)
		N	mean	S.D	N	mean	S.D		
HH	Leaf off	17874	−9.37	1.92	11380	−9.63	2.03	11.00	0
	leaf on	23832	−10.18	2.14	15176	−10.15	2.09	−1.66	0.097
VV	Leaf off	17874	−9.85	1.91	11384	−10.28	2.04	17.81	0
	leaf on	23832	−10.36	2.14	15176	−10.48	2.10	5.46	0

Table 13
Comparison between mean backscattering coefficient (σ0) of leaf-off and leaf-on periods for the coniferous, deciduous and mixed forest, obtained from HH- and VV-polarized Lee-filter TSX imagery, acquired between March 2008 and January 2009 using two sample Z-test.

Polarization	Forest Type	Leaf cycle						Z-test	
		Leaf-off			Leaf-on			z-score	p-value Sig. (2-tailed)
		N	mean	S.D	N	mean	S.D		
HH	deciduous	17874	−9.37	1.92	23832	−10.18	2.14	40.70	0
	mixed	11380	−9.63	2.03	15176	−10.15	2.09	20.10	0
	coniferous	9003	−11.23	2.07	12005	−11.24	2.01	.53	0.596
VV	deciduous	17874	−9.85	1.91	23832	−10.36	2.14	25.48	0
	mixed	11380	−10.28	2.04	15176	−10.48	2.10	7.87	0
	coniferous	9003	−11.86	2.01	12005	−11.80	2.02	−1.95	0.051

of deciduous forest and mixed forest in the study area during the leaf-on period, while better results were achieved during the leaf-off period, as high significant loadings were obtained for all acquisition dates.

The results of the EFA for the backscattering coefficient on the entire forest canopy around Fuhrberger Feld showed five extracted factors for each polarization and thus Varimax rotation was applied. One of the rotated factors showed significant loadings for the coniferous forest during the whole year, while high significant loadings for deciduous forest and mixed forest were observed in two separated factors during the leaf-on period from May to October, in addition to two other factors with high significant loadings during the leaf-off period from November to April for deciduous forest and mixed forest separately.

Based on the above results for EFA tests, extracted or rotated factors can be interpreted as indications of a specific kind of forest canopy. For example, we can identify the regions covered with coniferous forest, where we have one extracted factor with moderate loadings for all the acquisition dates during the whole year. In addition, we can define the regions covered with deciduous forest or mixed forest, where we have two rotated factors, that one of which has significant loadings for all acquisitions during the leaf-on period. Even so, it is not possible from these results to recognize if the investigated region is covered with deciduous forest or mixed forest.

The TZT enabled deciduous forest and mixed forest to be distinguished. The results of the TZT using the HH-polarized imagery revealed no statistically significant difference between the deciduous forest and the mixed forest during the leaf-on period, whereas a statistically significant difference was found between them during the leaf-off period. During the leaf-off period, parts of the mixed forest remain green and do not shed their needle-or scale like leaves, while the deciduous forests in Germany tend to begin shedding their leaves in October, and are characterized by the absence of leaves from November to April. Furthermore, the results of the TZT based on the HH- polarized acquisition, showed no statistically significant difference between the deciduous forest and the mixed forest during the leaf-on period from May to October, in contrast to the leaf-off period. During the leaf-off period from November to April, the TZT results revealed a statistically

Table 14
Comparison between mean backscattering coefficient (σ_0) of deciduous forest and mixed forest on different acquisition dates during leaf-off and leaf-on periods, obtained from HH- and VV- polarized Lee-filter TSX imagery, acquired between March 2008 and January 2009, using two sample Z-test.

Polarization	Leaf Cycle	Acquisition dates	Forest Type						Z-test	
			Deciduous			mixed				
			N	mean	S.D	N	mean	S.D	z-score	p-value Sig. (2-tailed)
HH	Leaf off	13. Mar 08	2979	−8.94	1.82	1897	−9.26	2.07	5.54	0.000
		04. Apr 08	2979	−9.22	1.85	1897	−9.39	1.87	3.04	0.000
	Leaf on	18. Mai 08	2979	−10.25	2.17	1897	−10.13	2.02	−1.88	0.060
		09. Jun 08	2979	−9.89	2.06	1897	−10.00	2.08	1.79	0.074
		01. Jul 08	2979	−10.06	2.16	1897	−10.04	2.14	-.35	0.726
		23. Jul 08	2979	−10.07	2.14	1897	−9.99	2.05	−1.40	0.162
		14. Aug 08	2979	−10.16	2.12	1897	−10.07	2.13	−1.35	0.177
		05. Sep 08	2979	−10.16	2.24	1897	−10.15	2.14	-.06	0.952
		27. Sep 08	2979	−10.55	2.09	1897	−10.49	2.09	−1.02	0.308
		19. Oct 08	2979	−10.20	2.04	1897	−10.30	2.04	1.72	0.085
	Leaf off	10. Nov 08	2979	−9.10	1.81	1897	−9.50	1.91	7.38	0.000
		12. Dec 08	2979	−9.38	1.84	1897	−9.63	1.90	4.63	0.000
		04. Jan 09	2979	−9.88	1.92	1897	−10.08	2.05	3.37	0.000
		26. Jan 09	2979	−9.72	2.08	1897	−9.95	2.22	3.53	0.000
VV	Leaf off	13. Mar 08	2979	−9.49	1.82	1897	−9.82	1.93	5.88	0.000
		04. Apr 08	2979	−9.51	1.81	1897	−10.08	1.98	10.21	0.000
	Leaf on	18. Mai 08	2979	−10.46	2.20	1897	−10.61	2.12	2.27	0.023
		09. Jun 08	2979	−10.06	2.11	1897	−10.21	2.05	2.45	0.014
		01. Jul 08	2979	−10.12	2.12	1897	−10.26	2.08	2.24	0.025
		23. Jul 08	2979	−10.17	2.09	1897	−10.32	2.05	2.35	0.018
		14. Aug 08	2979	−10.44	2.11	1897	−10.35	2.08	−1.56	0.119
		05. Sep 08	2979	−10.54	2.21	1897	−10.44	2.15	−1.60	0.110
		27. Sep 08	2979	−10.89	2.17	1897	−10.83	2.13	-.90	0.368
		19. Oct 08	2979	−10.46	1.98	1897	−10.72	2.09	4.39	0.000
	Leaf off	10. Nov 08	2979	−9.54	1.81	1897	−10.00	1.92	8.29	0.000
		12. Dec 08	2979	−9.80	1.83	1897	−10.18	1.97	6.69	0.000
		04. Jan 09	2979	−10.42	1.90	1897	−10.82	2.06	6.82	0.000
		26. Jan 09	2979	−10.35	2.02	1897	−10.77	2.17	6.70	0.000

significant difference between both forest types due to the fact that parts of the mixed forest usually stay green without losing leaves. For the VV- polarized acquisition, the TZT results verified no significant difference between these two forest types during part of the leaf-on period from May to July at 90% confidence level and from August to September at 95% confidence level, while a statistical significant difference between these two forest types was found for the rest of year. It is noticeable that the mean values of σ_0 for the deciduous forest have slightly higher values than those of the mixed forest during the leaf-off period. As expected, no statistical significant difference for the coniferous forest was found between the leaf-on and the leaf-off periods, where coniferous forest stay green the entire year and do not shed their needle-or scale like leaves. This explained the statistical difference between coniferous forest and both deciduous and mixed forest during both leaf cycles and on every acquisition date.

The above discussion has revealed that results of the TZT for mean σ_0 are affected by both the shape and the presence or absence of leaves. Consequently, the coniferous forest can be identified based on the plots where no statistical significant difference for mean σ_0 exists between leaf-on and leaf-off periods. Furthermore, we can identify the deciduous forest using the HH-polarized acquisitions, where there is no statistical significant difference for mean σ_0 between forest types during the leaf-on period, but a significant difference during leaf-off time with higher values of mean σ_0. With this kind of information, it is possible to distinguish between different types of forest.

In general, forest canopy can usually be dealt as plots. Forest identification based on statistical procedures such as Z-test and Factor analysis for the forest plots in TerraSAR-X imagery as presented in this study opens several ways of driving knowledge about changes in forest distribution. The changes in forest canopy strongly affects not only the ecosystem but also the groundwater quality, especially in water protection zones. The possibility of identifying the percentage of coniferous forest, and the possibility finding the plots where new deciduous trees are replacing the coniferous trees plays an essential role in sustainable groundwater management. Furthermore, the continuous monitoring of the forest with remote sensing data such as TerraSAR-x imagery enables determination of the areas where disasters happen. In the case of fire, for example, the burnt trees usually have no leaves or fall down and thus different values of backscattering coefficient are expected after the disaster. Using TZT for comparing between acquisitions before and after the fire most probably can have a statistically significant difference, especially during the same leaf cycles.

5. Conclusion

This paper has exposed the potential of inferential statistics tests such as two samples Z-test and the multivariate analysis, for example Factor Analysis, for identifying different kinds of forest canopy, based on the backscattering coefficient of the dual-co-polarized TerraSAR-x images of forest plots. This study has found insignificant seasonal variation in the values of backscattering coefficient of the TSX data between plots dominated by coniferous, deciduous and mixed forests. In contrast, EFA results have shown a significant seasonal variation in the factor loadings of these forest plots. It was noticeable that the deciduous forest had two extracted rotated factors, where one of these factors had significant high factor loadings during the leaf-on period, while the other one had significant high loadings during the leaf-off one. Similar results were obtained for the mixed forests. Conversely, the coniferous forest had one extracted factor with more or less similar loadings during the whole time series. This indicates that the loadings were influenced by both the shape and the presence or absence of leaves. Consequently, the results of EFA with regard to loadings can be interpreted as a tracer for a specific kind of forest canopy.

With this kind of information, it was possible to distinguish between coniferous forest against both deciduous forest and mixed forest, however it was not possible to differentiate between deciduous forest and mixed forest. On the contrary, the TZT enabled the former and later forest types to be distinguished. In particular, the TZT results confirmed a statistical significant difference between deciduous forest and coniferous forest during the whole year using both HH- and VV- polarized acquisitions. In addition, the results for HH-polarized acquisitions revealed a statistically significant difference between deciduous forest and the mixed forest during the leaf-off period, while no statistical significant difference was found between them during the leaf-on period. Higher values of mean σ_0 were also observed for the deciduous forest during the leaf-off period. Nevertheless, the results for the VV-polarized acquisition failed to discriminate between them based on leaf cycle, and succeeded partially in showing no significant difference during part of the leaf-on period from August to October with respect to the acquisition dates. Therefore, the results of TZT can be considered as indications of a particular type of forest canopy.

While the emphasis in this study was on the identification of types of forests in the context of managing a ground water protection area, the analysis of σ_0 values obtained from multi-temporal TerraSAR-X by EFA and TZT can also be applied to monitoring forest area, to tracking ecological processes, and to measuring the extent of damage caused by events such as fires or earthquakes. As this research has demonstrated, Factor Analysis and two sample Z-test could be an important tools for researchers and forest managers in monitoring and protecting the forest environment using remote sensing and to the development of sustainable forest management and land use practices.

Acknowledgments

The results presented here have been created using images provided by the *German* Aerospace Center (DLR) to the Institute of Photogrammetry and Geoinformation (IPI) at Leibniz University in Hanover, Germany during a pilot project of DLR TerraSAR Science proposal LAN0011.

Appendix A. Supplementary data

Supplementary data to this article can be found online at https://doi.org/10.1016/j.rsase.2019.100238.

Author contributions

Farghaly conceived and designed the experiments. Sörgel and Elba contributed to data collection; Farghaly performed the experiments and analyzed the data; Urban and Sörgel supervised the research, Urban, Sörgel and Elba contributed to the discussions of the results; Farghaly wrote the paper. All authors have reviewed and approved the final manuscript.

Conflicts of interest

“The authors declare no conflict of interest."

References

Bargiel, D., Herrmann, S., 2011. Multi-temporal land-cover classification of agricultural areas in two European regions with high resolution Spotlight TerraSAR-X data. Rem. Sens. 3 (12), 859–877.

Becker, J., Keienburg, T., Kittel, A., Kretschmann, N., Kruse, E., Mersch, I., Nehlsen, E., Prüter, J., Urban, B., Zimmermann, T., Biebeler, H., Bardt, H., Chrischilles, Mahammadzadeh, M., Striebeck, J., Hrsg, S., 2014. KLIMZUG-NORD - klimaanpassung in der Metropolregion Hamburg. Beispiele für inter- und transdisziplinäre Forschung in Modellgebieten. In: Wege zur Anpassung an den Klimawandel. Institut der deutschen Wirtschaft Köln Medien GmbH, 9783602149322, pp. 85–103.

Becker, N., 2013. Water policy in Israel Context, issues and options. In: Global Issues in Water Policy, vol. 4 Springer, Dordrecht, New York, USA9789400759107, .

BGR, 2009. 50 Years BGR: an Activity Report (1958 - 2008). Federal Institute for Geosciences and Natural Resources (BGR) 0343-8147.

BMEL, 2015. The Forests in Germany Selected Results of the Third National Forest

Inventory. Federal Ministry of Food and Agriculture (BMEL), Berlin, Germany.
DLR, 2007. TerraSAR-X Das Deutsche Radar-Auge im All. The German Radar Eye in Space. Deutschen Zentrum für Luft und Raumfahrt (DLR). (Göttingen, Germany).
Dobson, C.M., Ulaby, F.T., Pierce, L.E., 1995. Land-cover classification and estimation of terrain attributes using synthetic aperture radar. Remote Sens. Environ. 51 (1), 199–214.
DWD, 2015. Zahlen und Fakten zum Klimawandel in Deutschland. Klima-Pressekonferenz Bericht des Deutschen Wetterdienstes am 10 März 2015 in Berlin, Deutscher Wetterdienste (DWD). https://www.dwd.de/DE/presse/pressekonferenzen/DE/2015/PK_10_03-2015/zundf_zur_pk.pdf.
Enercity, 2015. Enercity Wasser. Natürlich aus der Region. Seit über 100 Jahren. Hanover. Enercity Hannover. https://www.enercity.de/infothek/downloads/broschueren/wasser/trinkwasser-enercity.pdf.
Finch, W.H., 2011. A comparison of factor rotation methods for dichotomous data. J. Mod. Appl. Stat. Methods 10 (2), 549–570. https://doi.org/10.22237/jmasm/1320120780.
Fisher Box, J., 1987. Guinness, gosset, Fisher, and small samples. Stat. Sci. 2 (1), 45–52. https://doi.org/10.1214/ss/1177013437. JSTOR 2245613.
Gorsuch, R.L., 1983. Factor Analysis, second ed. Lawrence Erlbaum Associates, Hillsdale, New Jersey.
Haarena, C., Bathkeb, M., 2008. Integrated landscape planning and remuneration of agri-environmental services Results of a case study in the Fuhrberg region of Germany. J. Environ. Manag. 89, 209–221.
Häusler, A., Scherer-Lorenzen, M., 2001. Sustainable Forest Management in Germany: the Ecosystem Approach of the Biodiversity Convention Reconsidered Results of the R +D–Project 800 83 00, vol. 51 BfN –Skripten, Bonn, Germany.
Iizuka, K., Tateishi, R., 2014. Simple relationship analysis between L-band backscattering intensity and the stand characteristics of sugi (cryptomeria japonica) and hinoki (chamaecyparis obtusa) trees. Ars 03 (04), 219–234.
Joshi, N., Mitchard, E., Schumacher, J., Johannsen, V., Saatchi, S., Fensholt, R., 2015. L-band SAR backscatter related to forest cover, height and aboveground biomass at multiple spatial scales across Denmark. Rem. Sens. 7 (4), 4442–4472.
Kaplunovsky, A.S., 2005. Factor analysis in environmental studies. HAIT J. Sci. Eng. B 2 (1–2), 54–94.
Kim, S.J., Kim, J., Kim, K., 2010. Organic carbon efflux from a deciduous forest catchment in Korea. Biogeosciences 7 (4), 1323–1334.
King, M.R., Mody, N.A., 2011. Numerical and Statistical Methods for Bioengineering. Applications in MATLAB. Cambridge: Cambridge University Press, Cambridge, UK.
Klovan, J.E., 1975. R- and Q-Mode Factor Analysis. In: R.B. (Ed.), Concepts in Geostatistics (McCammon. Springer Berlin Heidelberg, Berlin, Heidelberg, pp. 21–69.
Kondratyev, K., Pokrovsky, O., 1979. A factor analysis approach to optimal selection of spectral intervals for multipurpose experiments in remote sensing of the environment and earth resources. Remote Sens. Environ. 8 (1), 3–10.
Kumar, P., Prasad, R., Choudhary, A., Mishra, V.N., Gupta, D.K., Srivastava, P.K., 2017. A statistical significance of differences in classification accuracy of crop types using different classification algorithms. Geocarto Int. 32 (2), 206–224. https://doi.org/10.1080/10106049.2015.1132483.
Kuplich, T.M., Curran, P.J., 1999. Temporal analysis of JERS-1/SAR images over re-generating forests in Brazilian Amazonia. In: IEEE 1999 International Geoscience and Remote Sensing Symposium, vol. 99. IGARSS, pp. 1895–1897.
Liu, C., Ray, S., Hooker, G., Friedl, M., 2012. Functional factor analysis for periodic remote sensing data. Ann. Appl. Stat. 6 (2), 601–624.
Lohmann, P., Sörgel, U., Farghaly, D., 2010. Classification of agricultural sites using time-series of highresolution dual-polarisation TerraSAR – X Spotlight images. In: Imagin (eg) Europe: Proceedings of the 29th Symposium of the European Association of Remote Sensing Laboratories, Chania, Greece (Manakos, I. And Kalaitzidis. IOS Press, Amsterdam, Washington, DC.
Markowski, C.A., Markowski, E.P., 1990. Conditions for the effectiveness of a preliminary test of variance. Am. Statistician 44 (4), 322–326. https://doi.org/10.2307/2684360. JSTOR 2684360.
McRoberts, R.E., Cohen, W.B., Næsset, E., Stehman, S.V., Tomppo, E.O., 2010. Using remotely sensed data to construct and assess forest attribute maps and related spatial products. Scand. J. For. Res. 25 (4), 340–367.
Mulaik, S.A., 2009. Foundations of Factor Analysis. In: Statistics in the Social and Behavioral Sciences Series, second ed. CRC Press - Taylor & Francis Group, Boca Raton, FL, USA9781420099614, .
Oliver, C., Quegan, S., 2004. Understanding Synthetic Aperture Radar Images. SciTech Radar and Defense Series. SciTech Publ., Raleigh, N.C.
Ortiz, S.M., Breidenbach, J., Knuth, R., Kändler, G., 2012. The influence of DEM quality on mapping accuracy of coniferous- and deciduous-dominated forest using TerraSAR X images. Rem. Sens. 4 (12), 661–681.
Ortiz, S., Breidenbach, J., Kändler, G., Koch, B., 2011. Mapping forest types with TerraSAR-X imagery. In: 4th TerraSAR-X Science Team Meeting.
Purkis, S.J., Klemas, V., 2011. Remote Sensing and Global Environmental Change. Wiley-Blackwell, Chichester, West Sussex, UK, Hoboken, N.J.
Richards, J.A., 2009. Remote Sensing with Imaging Radar. Signals and Communication Technology. Springer.
Riitters, K.H., O"Neill, R.V., Hunsaker, C.T., Wickham, J.D., Yankee, D.H., Timmins, S.P., Jones, K.B., Jackson, B.L., 1995. A factor analysis of landscape pattern and structure metrics. Landsc. Ecol. 10 (1), 22–39.
Solberg, S., May, J., Bogren, W., Breidenbach, J., Torp, T., Gizachew, B., 2018. Interferometric SAR DEMs for forest change in Uganda 2000–2012. Rem. Sens. 10 (2), 228.
Syvitski, James P.M., 2007. Principles, Methods and Application of Particle Size Analysis, Digitally Printed Version. Cambridge University Press, Cambridge, New York.
Tavakkoli Sabour, S.M., Lohman, P., Soergel, U., 2008. Monitoring agricultural activities using multi-temporal ASAR ENVISAT data. In: IAPRS XXXVII B7–2. ISPRS, Vienna, Austria, pp. 735–742 2008.
Thompson, B., 2004. Exploratory and Confirmatory Factor Analysis: Understanding Concepts and Applications. American Psychological Association, Washington, DC, USA.
Trendafilov, N.T., 1994. A simple method for procrustean rotation in factor analysis using majorization theory. Multivariate Behav. Res. 29, 385–408.
UNEP, 2011. The Bioenergy and Water Nexus. United Nations Environment Programme - UNEP, Nairobi, Kenya.
Urban, B., Becker, J., Mersch, I., Meyer, W., Rottgardt, E., 2014. Berichte aus den KLIMZUG-NORD Modellgebieten. In: Hrsg, Urban, B., Becker, J., Mersch, I., Meyer, W., Rottgardt, E. (Eds.), Bd. 6, Klimawandel in der Lüneburger Heide – Kulturlandschaften zukunftsfähig gestalten. TuTech Verlag, Hamburg, Germany978-3941492721, .
Venables, W.N., Ripley, B.D., 2002. Modern Applied Statistics with S. In: Statistics and Computing, fourth ed. Springer, New York.
WHO, 2005. Protecting groundwater for health: managing the quality of drinking-water sources. In: Protecting Groundwater for Health: Managing the Quality of Drinking-Water Sources, Online, World Health Organization (WHO).
Wolf, R., 2013. Kurzumtriebsplantagen im Fuhrberger Feld Freisetzung und Verbrauch Klimarelevanter Spurengase und Kohlenstoffakkumulation beim Anbau nachwachsender Rohstoffe. Diplomica Verlag Gmbh, Hamburg, Germany978-3842899728.